

**TUNABLE DIODE LASER SPECTROSCOPY,
NIR OVERTONE AND LIF STUDIES OF
SOME ORGANIC COMPOUNDS**

**Thesis submitted to
COCHIN UNIVERSITY OF SCIENCE AND TECHNOLOGY
for the award of the Degree of
DOCTOR OF PHILOSOPHY**

by
Shaji S.

**DEPARTMENT OF PHYSICS
COCHIN UNIVERSITY OF SCIENCE AND TECHNOLOGY
COCHIN - 682 022, INDIA.**

APRIL 2003




Department of Physics
Cochin University of Science and Technology
Cochin - 682 022, INDIA.

CERTIFICATE

Certified that the work presented in this thesis entitled **“TUNABLE DIODE LASER SPECTROSCOPY, NIR OVERTONE AND LIF STUDIES OF SOME ORGANIC COMPOUNDS”** based on the bonafide research work done by Mr. Shaji. S is an authentic record of research work done by him under my guidance in the Department of Physics, Cochin University of Science and Technology, Cochin 682 022 and has not been included in any other thesis submitted previously for the award of any degree.

Dammam-31451
(Saudi Arabia)
15-03-2003


Dr.T.M.Abdul Rasheed
(Supervising Guide)
Reader, Dept. of Physics
CUSAT, KOCHI-22
Present affiliation:
Department of Physics
King Faisal University
P.B.2114, Dammam-31451
Kingdom of Saudi Arabia

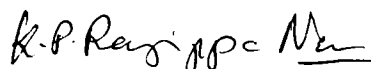


Department of Physics
Cochin University of Science and Technology
Cochin - 682 022, INDIA.

CERTIFICATE

Certified that the work presented in this thesis entitled **“TUNABLE DIODE LASER SPECTROSCOPY, NIR OVERTONE AND LIF STUDIES OF SOME ORGANIC COMPOUNDS”** is based on the bonafide research work done by Mr. Shaji. S under my guidance in the Department of Physics, Cochin University of Science and Technology, Cochin 682 022 and has not been included in any other thesis submitted previously for the award of any degree.

Date: 09-04-2003
Kochi – 22.


Prof. K. P. Rajappan Nair
(Co-Guide)
Dean, Faculty of Science
CUSAT.

Prof. Dr. K.P. RAJAPPAN NAIR
Dean, Faculty of Science
Cochin University of
Science and Technology
Cochin - 682 022, India
Ph : 0484-575588

CONTENTS

	Page
PREFACE	
Chapter I	
TUNABLE DIODE LASER SPECTROSCOPY AND HIGH- RESOLUTION SPECTROSCOPY – A REVIEW	1
Chapter II	
TDLAS EXPERIMENTAL SETUP AND ITS COMPUTER INTERFACING USING LABVIEW	44
Chapter III	
CALIBRATION OF THE TDLAS SETUP USING SPECTRA OF WATER AND METHANOL	62
Chapter IV	
NIR ABSORPTION TECHNIQUES AND VIBRATIONAL OVERTONE SPECTROSCOPY	77
Chapter V	
VIBRATIONAL OVERTONE SPECTRAL ANALYSIS OF CHLOROANILINES, TOLUIDINES AND SOME ALKYL ANILINES	106
Chapter VI	
PULSED LASER INDUCED FLUORESCENCE AND RAMAN STUDIES OF SOME COMPOUNDS	151
SUMMARY AND CONCLUSIONS	173

PREFACE

The detection and analysis of the interaction of light with matter leads to a lot of information on the structure and reactivities of the matter. The invention of lasers, particularly tunable laser sources with high intensity, high spectral monochromaticity, wide tunability and narrow spectral linewidths have opened a class of spectroscopic techniques which allow investigation of the structure of atoms and molecules in much more detail up to the minute details of it. When tunable diode lasers (TDL) were first developed in the mid- 1960's, they found immediate application, as much needed tunable sources for high-resolution infrared laser spectroscopy. The most important application of TDLs to atmospheric measurements has turned out to be their use in conjunction with a long-path cell to provide high sensitivity local measurements. This technique is commonly referred to as TDLAS (tunable diode laser absorption spectroscopy). This technique is very useful in high-resolution spectroscopic studies of atoms and molecules also.

The principle of TDLAS is absorption spectroscopy is by using a single isolated absorption line of the species. As a high-resolution spectroscopic technique it is virtually immune to interferences by other species, and the same instrument can easily be switched from one species to another by changing the laser wavelength and calibration cells. It is easy to construct an instrument that will measure several species simultaneously by multiplexing the outputs of several lasers (commonly up to four) through the multi-pass cell. In recent years, the development of tunable diode lasers in the near infrared region has made it possible to study molecular vibrational overtone bands under high resolution using TDLAS, where the spectral interference from other species is even smaller, as compared to TDLAS in the mid-infrared region. In the present work, we successfully set up and calibrated a high-resolution NIR tunable diode laser spectrometer in a multipass geometry. The experimental setup is interfaced to a PC using LabVIEW software and necessary hardware for data acquisition and control of the laser system. We could reproduce the high resolution second OH overtone spectra of water and methanol, which could thus be used to calibrate the

setup. The setup is further used to record the rotational structure of OH second overtone spectra of a few alcohols.

The vibrational overtone spectroscopic studies of molecules containing X-H (X=C, N, O...) oscillators can yield valuable information, which cannot be obtained by other spectroscopic techniques. The vibrational overtone spectroscopic studies can yield a lot of valuable information, such as the molecular structure, intra- and inter-molecular interactions, radiationless transitions, intra-molecular vibrational relaxations, multiphoton excitations and chemical reactivities. We have studied the liquid phase NIR overtone spectra of some important substituted benzene compounds. The analysis of the CH and NH local mode overtones yielded important structural information about these systems. In an attempt to draw further details on these molecular systems, we have recorded the Nd:YAG laser induced fluorescence and/or Raman spectra of some of the compounds.

The thesis is laid out in six chapters. The first chapter gives a brief review of the area of TDLAS, its applications and high resolution spectroscopic studies. Tunable coherent light sources now have very wide applications in the fields of communication, spectroscopy, biology, medicine etc. Tunable diode lasers with narrow line widths and wide tunability make them ideal light sources for atomic and molecular spectroscopy which require the laser radiation frequency to coincide with the frequency of a definite quantum transition between two energy levels of the atom or molecule. Unique characteristics of laser radiation such as high power density, high monochromaticity and tunability make them ideal sources for high resolution spectroscopy.

The second chapter describes the details of experimental set up used for recording high resolution OH group second overtone using the technique of TDLAS and the computer interfacing of the setup using labVIEW software for experiment control, data acquisition and analysis. Tunable diode laser absorption spectroscopy (TDLAS) is a very important technique for measuring many trace gases with detection sensitivities in the sub-parts-per-billion (ppb) concentration range. This chapter gives a brief description of the experimental setup used in the present work, with specification and details of the components-the laser source,

multipass cell, the balanced photo detector and the neutral density beam splitter. The experimental setup is interfaced with a personal computer using LabVIEW software and necessary hardware components with specifications and details of DAQ – ADC and GPIB PCI cards. Computer program created in LabVIEW is used for the control of the laser system, data acquisition and analysis.

The third chapter describes the successful setting up and calibration of a high-resolution spectrometer using the HITRAN 96 data for water vapor overtone lines and the second overtone band of the OH group in methanol molecule. The high resolution OH second overtone spectrum of ethanol is also recorded using the same experimental setup and the well resolved peaks are assigned. The high resolution spectrum of OH group second overtone in ethanol gives the well resolved spectral lines corresponding to the two different molecular conformers of ethanol.

The fourth chapter is intended for a brief review of the area of vibrational overtone spectroscopy and the local mode model which is used to analyse the overtone transitions in molecules containing X-H (X = C, N, O....) oscillators. The general applications of vibrational overtone spectroscopy, with emphasis on studies of molecular structural details, are also outlined.

The fifth chapter contains the details of the analysis of the NIR vibrational overtone spectra of liquid phase aniline, *ortho*, *meta* and *para* isomers of chloroanilines using local mode model. From the analysis of overtone spectra, we could establish the presence of intramolecular hydrogen bonding in *o*-chloroaniline, confirming the predictions of earlier microwave studies. The NIR vibrational overtone spectra of *ortho*, *meta* and *para* isomers of toluidines are also analyzed using local mode model and the presence electronic and steric effects in *o*-toluidine are confirmed. The analysis of the NIR vibrational overtone spectra of N-methylaniline, N,N-dimethylaniline and N,N-diethylaniline reveals the effect of molecular conformations in the local mode parameters.

The content of the sixth chapter is about a small piece of experimental work done using a pulsed Nd:YAG laser. The pulsed LIF and/or Raman spectra of aniline, *o*-chloroaniline and *m*-chlorotoluene are recorded using a Q-switched Nd:YAG laser-monochromator-CCD arrangement. The characteristic

fluorescence and/or Raman peaks for the aromatic ring and the substituent groups are identified. The observed Raman spectra showed some new lines corresponding to low-lying vibrational states.

The summary and conclusions of the present work are given towards the end of the thesis.

Chapter I

TUNABLE DIODE LASER SPECTROSCOPY AND HIGH-RESOLUTION SPECTROSCOPY – A REVIEW

	Page
1.1 Introduction.....	3
1.2 Applications of laser spectroscopy	4
1.3 Use of a tunable laser	5
1.4 Diode laser spectrometer.....	6
1.5 Tunable diode laser absorption spectroscopy (TDLAS).....	7
1.5.1 Spectroscopic principles of TDLAS-line strengths and shapes	8
1.6 Description of tunable diode laser spectrometer.....	12
1.6.1 Diode laser characteristics, tuning and mode structure.....	12
1.6.2 Optical layout.....	13
1.6.3 Overall experimental layout.....	15
1.6.4 Multipass absorption cell	17
1.6.5 Multi-species operation.....	19
1.6.6 Optical fringes.....	20
1.6.7 Sampling and calibration.....	20
1.6.8 Data processing and experimental control	21
1.6.9 Sensitivity and precision limits	22
1.6.10 Modulation spectroscopy	22
1.6.11 Harmonic detection	23
1.6.12 Signal to noise ratio.....	25
1.6.13 Sweep integration.....	25
1.6.14 Choice of absorption line	26
1.7 Applications of TDLAS for atmospheric measurements	27
1.7.1 Open path measurements	27
1.7.2 Stratospheric measurements.....	28
1.7.3 Flux measurements.....	29
1.7.4 Laser heterodyne measurements	29

Chapter I

1.8 TDLAS as gas sensors and trace gas detection technique	29
1.9 Isotope detection and measurements.....	33
1.10 TDLAS in industrial gas monitoring	34
1.11 TDL based molecular spectroscopy	36
1.12 High resolution overtone spectroscopy – some reported works	37
1.13 The present work.....	39
References	40

Chapter I

TUNABLE DIODE LASER SPECTROSCOPY AND HIGH-RESOLUTION SPECTROSCOPY – A REVIEW

1.1 Introduction

Spectroscopy is an analytic technique concerned with the measurement of the interaction of light with matter usually in the form of absorption or emission of radiant energy. The instruments necessary to make such measurements at the fundamental level and for practical analysis deals with the spectroscopic instrumentation. The interpretation of the interaction of light with matter describes the spectroscopic analysis. A display of the intensity of the emitted or transmitted radiant energy (or some function of the intensity) versus the energy of that light is called a spectrum. Spectra due to the emission of radiant energy are produced as radiation emitted from matter after some form of excitation. The emitted light is collimated by passing through a slit and then separated into components of different energy. Either the transmission through a prism (refraction) or reflection from a ruled grating or a crystalline solid (diffraction) is used for separation of different wavelengths and finally detected by a photodetector. Spectra due to the absorption of radiant energy are produced when radiant energy from a stable source, collimated and separated into its components by a monochromator, passes through the sample whose absorption spectrum is to be measured, and is detected. Instruments, which produce spectra, are commonly known as spectroscopes, spectrometers, spectrographs and spectrophotometers [1].

Interpretation of spectra provides fundamental information on atomic and molecular energy levels, the distribution of species within those levels, the nature of process involving change from one level to another, molecular geometries, chemical bonding and interaction of molecules in solution. At the practical level, comparisons of spectra provide a basis for the determination of qualitative chemical composition and chemical structure, and for quantitative chemical analysis.

Since a quantum transition obeys the relation $E = h\nu$, the change in energy of an ion, atom or molecule associated with absorption or emission of electromagnetic radiation is directly obtained from the measured frequency of the corresponding radiation.

Atoms, ions and molecules absorb or emit characteristically and hence only certain energies of these species are possible. The energy of the photon (quantum of radiant energy) emitted or absorbed corresponds to the difference between two permitted values of the energy of the species, or energy levels. Thus the energy levels may be studied by observing the differences between them. The absorption of radiant energy is accompanied by the promotion of the species from a lower to a higher energy level; the emission of radiant energy is accompanied by falling from a higher to a lower state; and if both processes occur together, the condition is called resonance.

1.2 Applications of laser spectroscopy

1) Investigation of chemical reactions with lasers

The lasers became an important tool for studying elementary chemical processes and for analytical applications. Laser photochemistry is characterized by high selectivity and intensity of the reaction source. The three most important types of reactions in laser-induced chemistry are

- a) Electronically or vibronically excited molecules are produced in a bath of reactants, the activation barriers for a reaction is thus reached or surmounted
- b) Molecules are ionized by single or multi-photon absorption and they either undergo further reactions with other molecules or unimolecularly decay into fragments.
- c) Molecules are dissociated and a high concentration of reactive free radicals are produced by reacting with other molecules.

2) Vibrational relaxation studies

The knowledge of vibrational relaxation of molecules is very important in connection with laser-induced chemistry. When the vibrational energy is stored long enough in the reactant, it leads to a laser initiated process.

- 3) Study of molecular surface interactions with lasers
- 4) Laser investigations in the atmosphere

The laser is an ideal instrument for determining the properties of the atmosphere by absorption and scattering processes. Its high spectral density and low divergence are especially useful for such measurements. Lasers with continuous and discrete tunability can be used to measure specific components selectively.

Normally absorption measurements can be performed with low power diode lasers. A remarkable improvement of the detectivity in absorption measurements becomes possible by a heterodyne technique, where a tunable laser is used as a local oscillator and a photodetector as mixer. A suitable amplifier of narrow bandwidth amplifies the signal at the intermediate frequency. This technique (most advantageous in infra red spectral range) yields an increase in sensitivity of several orders of magnitude, allowing appreciable lengthening of the absorption paths [2].

1.3 Use of a tunable laser

Tunable coherent light sources now have very wide applications in the fields of communication, spectroscopy, medicine, biology etc. Tunable diode lasers with narrow linewidths and wide tunability make them ideal light sources for atomic and molecular spectroscopy, which require the laser radiation frequency to coincide with the frequency of a definite quantum transition between two energy levels of the atom or molecule. The sharpness of the frequency and high power per unit solid angle and unit spectral bandpass in a laser beam make it attractive for infrared spectroscopy at very high resolution. Tunable infrared lasers have been used mainly to measure the energy levels due to the vibration and rotation of the molecules in the gas phase at low pressure. Unique characteristics of laser radiation such as high power density, high monochromaticity and tunability are also making them ideal sources for laser spectroscopy. These properties make them very useful for high resolution spectroscopy. Very accurate values of molecular parameters such as internuclear distances, electric dipole moments, vibrational frequencies and internal force fields can be measured using high resolution techniques. Another use

of laser infrared spectroscopy includes the monitoring of the composition of the atmosphere.

The invention of the laser has brought about a drastic change in the spectroscopy of transient molecules. Tunable diode lasers solved the limitation in wavelength coverage. High resolution spectra of transient molecules allow us not only to confirm the presence of these species in reaction systems, but also to monitor their distributions over quantum states; chemical reactions may often result in selective population of molecules in certain levels. High resolution spectra of free radicals provide extremely reliable means of monitoring these species in various environments like in chemical reactions, radio astronomy, atmospheric studies etc. In these studies, the observed spectrum makes it possible to view selectively a particular species in the presence of many others, and one can thus get very specific information on chemical systems by means of high resolution spectra. Molecular spectroscopy has already contributed much to monitor chemically stable species in the atmosphere and short-lived species such as OH, HO₂, ClO, SH, NO₃ etc. The role of high resolution spectra is very important since they are an indispensable means in unambiguously identifying and monitoring free radicals in various systems and environments. A high resolution molecular spectrum denotes a well resolved rotational structure or it corresponds to rotational transitions of a molecule [3]. Diode laser spectroscopy may be applied to diagnose chemical reaction systems in real time by monitoring the spectra of transient species created or dissipated in systems.

1.4 Diode laser spectrometer

The diode laser consists of a semiconductor p-n junction. When a forward current flows through the p-n junction, laser action is induced by the stimulated carrier-hole recombination emission, with two cleaved facets at the opposite ends of the diode laser as laser mirrors. The strip type double heterostructure has been employed to reduce the threshold current and thus to lower the heat dissipated in the crystal. Either changing the band gap or the index of refraction of the material, both of which are functions of temperature, may tune the oscillation frequency of the diode laser. Therefore the oscillation wavelength may be chosen by adjusting

the temperature of the diode or by varying the current fed to the diode. Although the current is eventually transformed into heat by ohmic loss, it is much more convenient in fine tuning and modulating the oscillation frequency. The oscillation frequency increases with temperature and current.

Several kinds of modulation techniques may be introduced to make the measurement of absorption lines easier with high sensitivity. Chopping the IR beam and detection of signal by a phase sensitive detector (PSD) is the simplest one. Other modulation techniques include Zeeman modulation, Stark modulation, wavelength modulation, frequency modulation etc.

The IR absorption may be recorded in either of the two modes, “spectroscopy” and “kinetics”. In the spectroscopy mode, the computer receives signals for a certain period (gate width) before and after the laser shot and stores the difference between the two signals while the diode laser is continuously swept as usual. In the kinetics mode, the diode laser emission is set to coincide with an absorption line and the computer stores the time variation of the signal intensity averaged for a number of laser shots.

1.5 Tunable diode laser absorption spectroscopy (TDLAS)

The development of semiconductor diode lasers in the near infrared has been spurred by the development of CD players (diode lasers with 0.78 micrometer) and optical fiber communication (diode lasers at 1.3 and 1.55 micrometers). As technology has improved, lasers have been developed for new applications such as pumping of solid state (0.808 micrometer) and fiber (0.98 micrometer) lasers. In addition to wavelength, other important laser parameters are mode stability, current tunability and frequency drift. Long-term frequency stability is one of the most important parameters for the diode lasers used in industrial gas monitors [4].

Over the past few years, the requirement for accurate and precise monitoring of trace gas constituents in the atmosphere has become increasingly important as a direct result of concerns over the cause and effects of atmospheric pollution. The necessity for reliable tools for trace gas monitoring is obvious, but the type of technique depends very much on the particular application being

addressed and the specific trace gas species of interest. High sensitivity laser spectroscopic techniques are needed to detect the very low mixing ratios or concentrations of trace species ranging from several parts per million to sub parts per trillion levels for carbon monoxide, hydroxyl radical etc. When lead-salt tunable diode lasers (TDL) were first developed in the mid- 1960's they found immediate application as tunable sources for high-resolution infrared laser spectroscopy. The most important application of tunable diode lasers to atmospheric measurements has turned out to be their use in conjunction with a long-path cell to provide high sensitivity local measurements. This technique is commonly referred to as tunable diode laser absorption spectroscopy (TDLAS), a general technique for monitoring most atmospheric trace species. The requirement is that the molecule should have an infrared line spectrum, which is resolvable at the Doppler limit. The principle of TDLAS is absorption spectroscopy using a single isolated absorption line of the species. TDLAS has now established itself as one of the leading techniques for atmospheric analysis of trace gas constituents. Operating at infrared wavelengths, most trace gases except nitrogen and oxygen to be monitored via their characteristic vibrational spectra and the high spectral resolution reduces the possibility of interferences from other species. Theoretical studies on the "differential absorption" studies are reported by Byer *et al* [5] and differential absorption technique was first applied to pollution detection by Rothe *et al* [6]. The applications of lead-salt and GaAs based semiconductor tunable diode lasers for atmospheric monitoring are well reviewed by Feher *et al* [7] and Werle [8].

1.5.1 Spectroscopic principles of TDLAS-line strengths and shapes

The intensity of monochromatic radiation of frequency ν transmitted through a cell containing an absorbing species is given by

$$I(\nu) = I_0(\nu) \exp[-\alpha(\nu)L] \quad (1)$$

where I_0 is transmitted intensity in the absence of an absorbing species, L is the optical path-length within the cell, and $\alpha(\nu)$ is the absorption coefficient. $\alpha(\nu)$ is related to the absorption cross-section $\sigma(\nu)$ by:

$$\alpha(\nu) = \sigma(\nu)N \quad (2)$$

where N is the concentration of the absorbing species in molecules per unit volume. The cell absorbance, a , is defined by $a = \alpha(\nu) L$ and the transmittance by $T = I / I_0$.

A given absorption line is characterized by its integrated line strength S

$$S = \int_0^{\infty} \sigma(\nu) d\nu \quad (3)$$

which is independent of pressure (but not of temperature). The line shape depends on sample pressure. At high pressure, collision broadening dominates giving a Lorentzian line shape:

$$\sigma_L(\nu) = \frac{S}{\pi} \frac{\gamma_L}{[(\nu - \nu_0)^2 + \gamma_L^2]} \quad (4)$$

where γ_L is the half width at half maximum (HWHM), of the line shape and ν_0 is the line-centre frequency. γ_L varies with P and T approximately according to:

$$\gamma_L = \gamma_{L_0} \left(\frac{P}{P_0} \right) \left(\frac{T_0}{T} \right)^{1/2} \quad (5)$$

where γ_{L_0} is the value of γ_L at S.T.P (T_0, P_0)

As the sample pressure is reduced the pressure broadened linewidth decreases until, at pressures below a few mbar, Doppler broadening dominates and the line shape becomes Gaussian:

$$\sigma_D(\nu) = \frac{S}{\gamma_D} \left[\frac{\ln 2}{\pi} \right]^{1/2} \exp \left[-\frac{(\nu - \nu_0)^2 \ln 2}{\gamma_D^2} \right] \quad (6)$$

where γ_D is the Doppler HWHM given by:

$$\gamma_D = \left[\frac{2kT (\ln 2)}{M'} \right]^{1/2} \frac{\nu_0}{c} \quad (7)$$

where M' is the molecular mass and c is the velocity of light.

For TDLAS the optimum sampling pressure is a compromise between sensitivity (best at high pressure) and selectivity (best at low pressure).

Even for strongly absorbing species, typical line-strengths are such that, an atmospheric concentration of 1 ppbv produces an absorption of only 1 part in 10^7 over a 10 cm path-length. TDLAS overcomes this problem firstly by using a multi-pass cell to give path-lengths of 100 m or more. Such cells achieve the long path

Chapter I

by using mirrors to fold the optical path, giving typically 100 passes of a 1 m base-length cell. Various types of modulation spectroscopy techniques are employed in which the diode-laser wavelength is modulated over the absorption linewidth at frequencies of anywhere between 100 Hz and 2 GHz. These modulation techniques allow absorptions as low as 1 part in 10^5 to be measured with a 1 Hz bandwidth.

TDLAS is used in a continuous sampling mode in which air is continually drawn through the multi-pass cell at a pressure of about 30 mbar. Operating at reduced pressure narrows the absorption lines avoiding possible interferences from other species and also reduces the range over which the laser needs to be modulated, which in turn reduces the effects of laser noise. The main features of TDLAS are as follows:

- As a high resolution spectroscopic technique it is virtually immune to interferences by other species - a problem that plagues most competing methods. This ability to provide unambiguous measurements leads to the use of TDLAS as a reference technique against other similar methods.
- The same instrument can easily be converted from one species detection to another by changing the laser and calibration cells. Similarly it is easy to measure several species simultaneously using the same instrument by multiplexing the outputs of several lasers (commonly up to four) through the multi-pass cell. It is a general technique.
- It offers automated measurements at time-constants of a minute or so. It offers *in-situ* monitoring within a very short time with very high sensitivity.

The easily collimated and steered laser beam is ideal for *in-situ*, remote monitoring over an open path thus by-passing many of the problems associated with sampling such as wall losses, condensation or chemical conversions. Multipass cells are commonly employed to increase the absorption pathlength. High sensitivities thus enable fast response measurements of less than 1 second, which is the requirement for measuring rapidly fluctuating concentrations.

TDLAS instruments are complex and expensive, and they require operators with good skills and expertise. The diode lasers themselves can be unreliable and each laser is unique, leading to the need to calibrate the instrument whenever a new laser is installed. Commercially available tunable diode lasers are divided into two classes: lead-salt based tunable diode lasers operate in the mid infrared region approximately from 3–30 micrometers and GaAs based lasers from approximately 0.6–4 micrometers. Operation in the mid IR allows access to most fundamental vibrational bands of the molecules and, combined with long pathlength and harmonic detection, monitoring at the ppb level and below is possible. In the near infrared, overtones and combination bands of molecules can be accessed which are often two to three orders of magnitude weaker than the fundamental bands, yet sub-ppm level sensitivities can still be attained with TDLAS.

The main application of lead-salt based diode lasers has been high resolution infrared spectroscopy of both stable molecules and transient species such as free radicals and ions. GaAs lasers have been developed for different reasons: the shorter wavelength devices are used in compact disc players, bar code scanners and optical guidance systems, the longer wavelength devices (especially at around 1.3 and 1.5 μm for optical fiber communications. Their applications to atmospheric monitoring has been limited due to the lack of spectral coverage and lower sensitivities associated with overtone and combination band transitions but has advantages such as room temperature operation, cost and high power are making them a viable alternative to the lead salt diode lasers for the purpose of atmospheric monitoring. Additionally they can be easily coupled to optical fibres, which is ideal for monitoring remote and possibly dangerous locations without the need for complicated optical arrangements.

Two other uses of TDLs in atmospheric measurements are long-path monitoring and heterodyne spectroscopy. Long-path monitoring replaces the folded path in the multi-pass cell with an open-path, through the atmosphere, to a retro-reflector and back. This gives a path-averaged value of the species concentration, which for some purposes can be an advantage. In heterodyne spectroscopy the diode laser is used as a local oscillator in a heterodyne receiver looking at solar radiation. This allows atmospheric column contents of species to be determined.

1.6 Description of tunable diode laser spectrometer

1.6.1 Diode laser characteristics, tuning and mode structure

The semiconductor laser chip is a rectangular block of sizes a few hundred micrometer, with a thin active layer of nearly 0.3 micrometer. In most of the laser diodes (except the external cavity versions) the cleaved facets of the laser chip acts as resonator mirrors as mentioned earlier. On increasing the injection current, the power increases and the laser works as an inefficient LED. When the diode starts lasing at a threshold current, the power increases rapidly with current. The wavelength tuning can be achieved by altering the temperature or the injection current of the diode, which results in change in refractive index and cavity length. On increasing the temperature or current, the emitted wavelength in lead salt based diode lasers increases, where as it decreases in GaAs-based diodes.

Lead-salt tunable diode lasers are similar in principle to the more familiar GaAs semiconductor lasers used widely in communications. The simplest form of laser consists of a crystal of a lead-salt semiconductor such as $\text{Pb}_{1-x}\text{Sn}_x\text{Se}$ on which a p-n junction is formed by diffusion of a salt of different stoichiometry into the top surface. The crystal is cleaved to a chip about 300 μm long with front and rear faces about 100 μm square. These front and rear facets form the laser cavity and do not need any reflective coating, as the Fresnel reflection is sufficiently strong. If electrodes are deposited on the top and bottom surfaces and a current of a few hundred milli ampere passed through the junction, lasing action takes place at a wavelength determined by the semiconductor energy gap. This energy gap is temperature dependent and a typical laser can be temperature tuned over about 100 cm^{-1} .

Most of the diodes are manufactured from complex ternary or quaternary compounds of group III–group V elements (GaAs based), group IV–group VI elements (containing different lead salts) or less importantly from group II–group VI elements. The simplest lead salt diode design is the homostructure diode with one n-type and one p-type semiconductor layer, where as in double heterostructure diodes, an n (or p) type semiconductor diode is sandwiched between two layers of opposite material. Another new development is the appearance of PbEuSeTe/PbTe buried heterostructure diode lasers, in which

differently doped layers are deposited by molecular beam epitaxy (MBE). The GaAs based diodes (GaAlAs, InGaAs and InGaAsP) emit laser light in the near infrared region. Most of these have a double heterojunction design. A very promising development in laser production is the strained quantum-well laser. A quantum-well laser is a layer so thin (<20 nm) that carriers are confined to quantum states. Additional lattice mismatches help to reduce threshold current and increase power up to 300 mW. These lasers also have a wider scanning range from 6 nm – 1.55 μm . TDLs are tuned by varying the temperature of the active region. This can be done either by varying the temperature of the cold stage on which the diode is mounted or by varying the laser drive current, which varies the Ohmic heating of the active region.

Single mode operation of the diode laser is another problem to be solved. Two solutions have been successfully used to solve this mode structure problem by incorporating a grating into the semiconductor structure and the diodes are operated near the maximum specified drive current to diminish all but the dominating mode.

- Laser output is single-mode at low drive current and then becomes increasingly multi-mode at higher currents.
- Although the power per mode shows some increase as current increases, the main effect of increased drive current is an increase in the number of modes.
- An individual mode tunes over about 2 cm^{-1} with power first increasing then decreasing with drive current.

There are some wavelengths that are not accessible at all. This can sometimes be remedied by choosing a different combination of base temperature and drive current but frequently the only solution is to use a different laser.

1.6.2 Optical layout

A typical optical arrangement is briefly described; the strongly divergent laser beam is focused, collimated and split into two or three different beams. Most of the laser power is used in the sample beam to monitor the trace gas interest in either in a multipass cell or in an open arrangement. A second beam is passed through a reference cell for wavelength stabilization and the third beam is passed

Chapter I

through a concentration calibration cell. The invisible infrared beam is normally traced by sending the output of a helium neon laser along the same optical path to aid in alignment, whereas infrared viewers can be used in the near infrared arrangements.

Multipass cells are used for increased absorption and pathlength. A monochromator is only required for multimode lasers where a single mode must be selected from all the others oscillating simultaneously to prevent absorption interferences. High resolution monochromators are not required for this purpose as the mode separation is usually of the order of several wavenumbers.

In general, each beam has a separate detector. For the mid infrared, cryogenically cooled photoconductive or photovoltaic detectors, such as mercury cadmium telluride (HgCdTe or MCT) or indium antimonide (InSb) are most commonly used. Commercially available HgCdTe detectors have high sensitivity and high responsivity in the mid infrared. In the near infrared, much less expensive PIN photodiodes or avalanche germanium, silicon or GaAs photodiodes operating at room temperature are preferred.

The corresponding electronic arrangement consists of a computer that drives the temperature and current controllers. Each of the pre-amplified detector signal is passed to a phase sensitive detector referenced at the wavelength modulated frequency, f . The sample signal is demodulated at $2f$ (second harmonic detection) and the signal is processed in a computer. As the second harmonic signal is proportional to the concentration of the trace gas being monitored one possibility is to lock the laser wavelength to the line center and to continuously monitor the peak height above the background level but this is susceptible to background drift. An alternative is to lock the laser to the line center and introduce a slow DC ramp into the feedback loop allowing one to scan from one edge of the line to the other.

The spectroscopic basis of diode laser monitoring is the same as for classical infrared spectroscopy with non-laser sources where the amount of light absorbed by the sample gas are given by the Beer – Lambert law, is recorded as a function of wave number. The resultant lineshape is dependant on pressure. The choice of the absorption line to monitor is important one and several factors must be taken into consideration. The selected line must be well separated from other

absorptions, both of the same species and of other species, to prevent interferences. This is easier when monitoring at reduced pressure in multipass cells, but problems can arise at higher pressures due to the extensive absorptions of the atmospheric water vapor. A strong line must be selected for increased sensitivity. The identification of the line can be useful for concentration determination, if the line is sufficiently strong to observe in direct absorption. Other information such as line strength, line center wavenumber, linewidth and pressure broadening parameters can be obtained on a wide range of trace gas species of atmospheric interest from databases such as HITRAN [9, 10, 11] or GEISA [12]. A final consideration in the choice of an absorption peak is that the diode laser must tune across the whole line in a single mode.

An absorption spectrum is easily obtained with a diode laser spectrometer by scanning the laser wavelength over an absorption feature and measuring the decrease in laser power, usually with the aid of amplitude modulation with a chopper.

1.6.3 Overall experimental layout

The beam from the TDL housed in the cold head is first collimated and then directed by a sequence of mirrors through the multi-pass White cell and onto the cooled detector as specified earlier. Part of the beam is split off and directed through a line-locking cell and also to a scanning Fabry-Perot interferometer that is used to give an on-line display of the laser mode-structure. A calibration cell can be inserted into the main beam under computer control. A visible He-Ne laser or diode laser beam is combined with the invisible infrared beam to assist in alignment (fig.1.1).

The most important requirement is to minimize optical fringes. Precautions that will reduce the chances of etalon formation include the use of reflective optics where possible, wedging and angling of all windows and anti-reflection coating window and lens surfaces. Similar precautions will also help avoid feedback of scattered or reflected radiation into the laser. Accurate alignment of the TDLAS optical system is important in avoiding optical fringing, and is difficult to achieve due to the invisibility of the beam. Riedel [13] and Fried *et al* [14] have discussed the various useful alignment techniques and tools that are in use.

TUNABLE DIODE LASER SPECTROMETRY

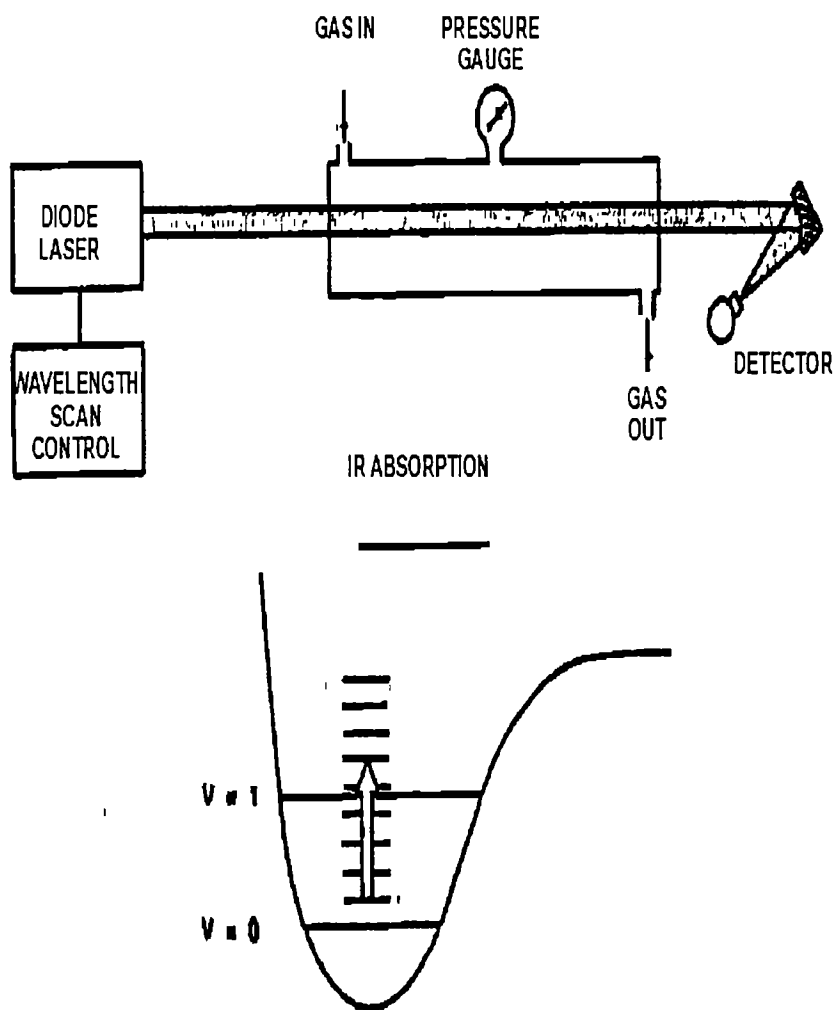


Fig.1.1. Schematic representation of a TDLA spectrometer

1.6.4 Multipass absorption cell

From the Beer – Lambert law, increasing the pathlength increases absorbance and thus sensitivity. In some cases it is possible to achieve sensitivities in the ppb range in a 1 m absorption cell but more typically several hundred meters pathlengths are required. In order to increase the pathlength in a cell, two arrangements have been applied: White cells and Herriott cells. The limiting factors in the pathlength are the optical surface qualities and reflectivity of the mirrors and in practical applications a few hundred meters are commonly used. In the White cell arrangement [15] the major factor affecting sensitivity is interference fringes, resulting from two images of the entrance focus partially overlapping at the exit [16]. One of the most serious shortcomings of the traditional White cells is that astigmatism limits the attainable pathlength. Herriott cell is more straightforward as it uses a simpler mirror design and the adjustment is also easier. The same number of passes can be accommodated in smaller Herriott cells by using astigmatic mirrors so that the reflections form a Lissajous pattern [17].

1.6.4.a White cell

As the name implies, the original design of multipass absorption cell was given by White [15], but a slightly modified design due to Bernstein and Herzberg (18) is commonly used in TDLAS instruments. A typical cell of this type would have a 1 m mirror separation, a volume of 10 l and a usable path-length of 100 m.

1.6.4.b Herriott cell

The Herriott cell [19, 20] consists of two spherical mirrors separated by nearly their radius of curvature. The optical beam is injected through a hole in one mirror and is reflected back and forth a number of times before exiting from the same hole. Unlike the White cell, the beam remains essentially collimated throughout its traversals of the cell. In the original design the beam traces out elliptical paths on the two mirrors, however this does not give optimum use of the mirror area and thus a modified arrangement using slightly astigmatic mirrors normally used.

A further advantage of the Herriott cell over the White cell is that it is easy to align, since the output beam direction is insensitive to changes in the mirror alignment. Unlike the White cell a Herriott cell can support several independent optical paths, each with a separate entrance and exit hole in the input mirror [21].

This allows multi-species measurements with independent optical channels. There are also other absorption cell designs, like the Welsh cell with four mirrors, plane mirrors multipass cells and Perry cell, which is a two mirror arrangement like a Herriott cell but with the images on both mirrors forming a parabola instead of an ellipse.

The choice of material for the sampling system and multipass cells must be a consideration for polar molecules that easily adsorb onto surfaces (NH_3 , H_2O , HNO_3 , H_2O_2 etc) as well as reactive species (HF-Glass, SO_2 -Stainless steel). These effects can be somewhat reduced by high pumping speeds. The optimum pressure in the measurement is dependent on the arrangement and is the result of two factors: pressure broadening and the increase of the amount of sample on increasing the pressure. Values of around 10–100 torr usually present a reasonable compromise. For measuring the changes in concentration in a multipass cell, the response time of the gas handling system has to be considered which is dependent on pump speed, measurement pressure, dimensions adsorption properties, and it can be as much as several seconds.

The design requirements for the multi-pass cell are as follows:

Long path-length: Long total path-length to give high sensitivity

Compact design: The multi-pass cell is often the largest component and can determine the overall dimensions of the instrument.

Low volume: This is needed to give a fast response time for flux measurements and is also useful in lower bandwidth measurements since it allows sample and background spectra to be alternated more rapidly which in turn helps to reduce the effects of optical fringes also.

High overall transmission: This is particularly important in modulation spectroscopy systems that are usually detector or shot noise limited.

Freedom from optical fringing: The optical fringes in the multi-pass cell arise when the output beam from the cell contains some radiation that has traversed a smaller number of passes than the main beam.

Ability to easily vary the number of passes: The higher the number of passes, the greater the path-length and hence the higher the instrument sensitivity. However a high number of passes increases the amplitude of optical fringes and also decreases the overall transmission and hence the power of the signal. The ability to optimize

the number of passes is thus important for any system and is particularly important in frequency modulation systems where this optimum number of passes will vary with the power of the laser being used.

Freedom from optical aberrations: This is important, firstly in avoiding optical fringes and secondly in ensuring that the beam can be focused to a spot smaller than the detector element.

Lack of memory effects: Lack of memory effects due to adsorption of the monitored species on the internal surfaces. This is mainly a problem with polar molecules such as HNO_3 and NH_3 . Use of glass and Teflon construction helps to minimize the problem and metals should be avoided.

1.6.5 Multi-species operation

In practical applications it is often necessary to monitor several different gases simultaneously. The gases must have strong absorptions over a narrow wavelength range to record their spectra within one laser mode. A solution to this is to operate the laser in different modes for different species or even to have several lasers with the beam passed through the absorption path alternately [22]. This method is called time multiplexing and its major disadvantage is the low time resolution of the order of minutes.

Because of the limited tuning range of an individual laser, multi-species operation usually requires a separate laser for each species. In the most common approach the collimated beams from these lasers are sequentially directed along the optical path through the instrument by either a rotating selecting mirror on a galvanometer drive or by individual "pop-up" mirrors for each laser. A different approach is wavelength multiplexing where two laser beams are combined. They are detected with two detectors each of which is only sensitive to one of the wavelengths.

If a Herriott cell is used as the multi-pass cell then its ability to provide several independent optical paths allows truly simultaneous measurements of several species by using separate optical channels for each. In such a system only the sampling system, Herriott cell, and data acquisition system are common to each species-measurement. The four-species ALIAS [21] and the proposed two-species ARGUS [22] instruments use these systems.

1.6.6 Optical fringes

Most TDLAS systems are limited in sensitivity not by laser or detector noise but by optical fringes superimposed on the measured spectrum. These result from unwanted etalons formed by reflections and scattering in the optical system and they appear in the form of an approximately sinusoidal variation of the background signal. This is true both for the direct absorption signal and for the various orders of modulation spectra [23]. These fringes can be reduced by careful optical design and adjustment, but it is usually difficult to reduce the fringe amplitude to a level much below that equivalent to an absorbance of 10^{-4} [24]. In order to achieve sensitivities in the 10^{-5} to 10^{-6} range some method of reducing the effect of the fringes must be found. These techniques can be categorized as follows: (i) mechanical modulation or dithering of the etalon spacing (ii) modified modulation schemes (iii) background subtraction and (iv) post-detection signal processing.

1.6.7 Sampling and calibration

1.6.7.a Sampling system

A high-speed rotary pump sucks air through the multi-pass cell at reduced pressure. A valve on the cell inlet controls this pressure, which is normally servo-controlled to maintain a fixed cell pressure. Polar species such as HNO_3 , HCl and NH_3 are readily adsorbed onto the surfaces of the inlet system and multi-pass cell. This leads to memory effects due to subsequent out gassing, which can persist for days after high concentrations have been sampled. Metals give the worst adsorption problems. PTFE (polytetrafluoroethylene) and glass are the preferred materials for most species and these materials need to be used for the whole of the inlet system including the valves. The multi-pass cell also needs to be of glass or lined with PTFE. Other measures like high throughput and trace heating of the inlet tubing [25] help to reduce adsorption problems.

1.6.7.b. Calibration methods

The best and most direct calibration method is to attach calibrant and zero air sources to the instrument inlet. This method has the advantage of calibrating the entire signal processing chain and also corrects for any loss of species due to surface adsorption (to the extent that this loss is proportional to concentration). In

general oven-stabilized permeation sources are preferred although dilution of standard gas mixtures can be used. For polar species calibration concentrations should be comparable with levels being measured because adsorption losses can be non-linear. Ideally zero air should be obtained by scrubbing from the ambient air only the species being monitored. In this way the background spectrum will contain any interferences from other atmospheric species, and these will then be subtracted off the sample spectrum. The zero air should contain levels of the monitored species well below the required detection limit since all measurements will be relative to this zero air level. Alternatively the level can be established in a separate experiment and a correction applied. Because of the inherent linearity of the TDLAS technique a single point calibration is sufficient.

Direct calibration can be time consuming especially for polar species with long equilibrium times. Because of this it is often convenient to use a sealed calibration cell as a transfer standard. This cell contains a sufficient concentration of the species being measured to give a strong signal when inserted into the optical path between the multi-pass cell and the detector (but low enough to still be in the linear response regime). The cell is filled with buffer gas to the same pressure as the multi-pass cell so that the lineshape is the same. This procedure corrects for most instrumental drifts without requiring frequent primary calibrations. In principle TDLAS measurements can be calibrated absolutely using the known absorption line strength and HWHM.

1.6.8 Data processing and experimental control

Whilst no two TDLAS systems are alike, the data processing and experimental control system is typical and serves to illustrate the principles. The laser frequency is ramped through the absorption line at 100 Hz and the resulting second harmonic spectra are averaged in the microprocessor-controlled signal-averager. On completion of the desired number of scans the averaged spectrum is transferred to the PC for further processing.

1.6.9 Sensitivity and precision limits

1.6.9.a Sensitivity

Sensitivities in the sub-ppb range have been achieved for many trace gases with lead salt diode lasers. In the near infrared, ppm and sub-ppm sensitivities can be demonstrated.

A TDLAS system can be operated either with the laser wavelength fixed at the point of maximum harmonic signal (often at line-centre) or with the laser repetitively scanning through the line and building up a spectrum by accumulating the scans in a signal averager. The first method theoretically gives the highest sensitivity for a given bandwidth because it gives maximum duty factor on the point of maximum signal. However unless fast response is needed (e.g. for flux measurements) the second method has overwhelming advantages because it avoids various systematic errors, which can affect the fixed wavelength technique. These include residual etalon fringes and a residual amplitude modulation (RAM) offsets which drift with time, and interferences from nearby absorption lines of other species. Scanning over the line also gives increased confidence in the measurement because the characteristic feature of the measured species is clearly seen and unwanted spectral features due to interfering species or etalon fringes can be identified.

1.6.9.b Precision and Accuracy

For measurements of trace species, sensitivity is usually more important than accuracy, and the 10 - 20 % accuracy of most systems is normally adequate. However when monitoring the more abundant long-lived species such as CO, CH₄, and CO₂ high accuracy is often needed [14]. TDLAS accuracy depends firstly on the calibration procedure and secondly on instrument drift between calibrations. Calibration usually involves injecting a calibration mixture and also a zero air sample into the instrument inlet.

1.6.10 Modulation spectroscopy

The modulation technique employed in the majority of the applications is wavelength modulation spectroscopy (WMS, also called derivative spectroscopy). The laser wavelength is modulated by rapidly varying the drive current at a frequency f (typically up to several kHz), while being slowly tuned across the

absorption line. The crucial difference is that for FMS the modulation frequency is equal to or greater than the absorption linewidth whereas for WMS the modulation frequency is much less than the linewidth. Thus FMS uses modulation frequencies of around 500 MHz and WMS frequencies of around 50 kHz. A phase sensitive detector at the modulation frequency or the harmonics of this then demodulates the resulting signal. Detection is usually done at the first or second harmonics of the modulation signal (hence harmonic detection), which is called '1f' or '2f' detection respectively. Unfortunately, modulating the wavelength rapidly over several absorption linewidths also results in RAM due to the variation of laser power with current.

The benefits of modulation spectroscopy in TDLAS are firstly, it produces a signal, which is directly proportional to the species concentration, rather than the small change in a large signal that occurs with a conventional absorption measurement, and this reduces drift. Secondly it allows the signal to be detected at a frequency at which the laser noise (one of the two main factors limiting sensitivity) is much reduced.

1.6.11 Harmonic detection

Figure 1.2 illustrates the direct, first, and second harmonic absorption line shapes. As shown, second harmonic detection produces a zero baseline signal, thus eliminating the necessity of measuring small differences between two large intensities, I and I_0 , as is the case for direct absorption.

Further advantages of second harmonic detection over direct absorption are:

- (1) the elimination of a strongly sloping background often present in direct absorption
- (2) reduced susceptibility to low frequency noise due to the kHz detection regime and
- (3) enhanced discrimination against signals that do not have a strong wavelength dependence such as the broad absorption tails of ambient H₂O vapor. Employing second harmonic detection, minimum detectable absorbances ($\ln \frac{I_0}{I}$) of 10^{-5} to 10^{-6} are frequently obtained in TDLAS systems using total pathlengths around 100 m. This corresponds to

minimum detectable concentrations ranging between a few parts-per-trillion (pptv) to parts-per-billion (ppbv), depending upon the absorption cross section. Unlike direct absorption, many instrument and experiment-dependent factors must be taken into account when deducing absolute concentrations from the measured second harmonic response. As a result, accurate quantitative analysis employing second harmonic detection is most frequently accomplished using calibration standards.

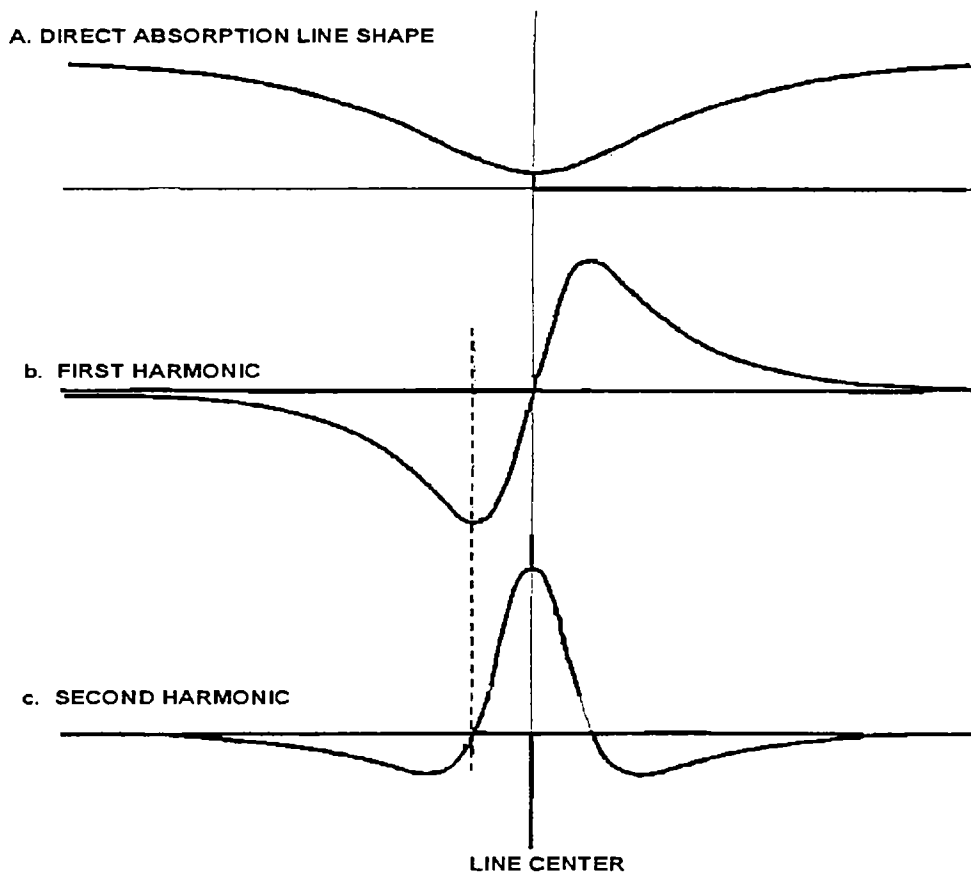


Figure 1.2 Direct, first and second harmonic line shapes

1.6.12 Signal to noise ratio

The noise is due to several factors like the signal independent thermal noise, the detector shot noise from the incident photons and laser excess noise caused by laser mode competition and stray optical feedback. Mechanical vibrations also may cause noise. The largest influence on noise in diode laser monitoring systems is Fabry – Perot interference fringes or “etaloning” caused by reflection off optical surfaces in the beam such as monochromator slits or cell windows, the fringe spacing being equal to the free spectral range of the etalon. Placing optical components at an angle, by careful optical alignment and the use of antireflection coatings can reduce their magnitude.

In modulation spectroscopy the *signal* is directly proportional to the laser power, incident on the detector, in the mode being absorbed. The *noise* arises from four sources: detector shot noise, detector thermal noise, laser excess-noise and RAM offset noise. We consider these in turn.

Detector shot noise corresponds to the photon noise on the laser power incident on the detector (P). The noise power is proportional to \sqrt{P} and has a white noise frequency spectrum.

Detector thermal noise is the signal-independent noise of the detector and preamplifier and depends on the type of detector used. This noise also has a white noise spectrum.

Laser excess-noise is the laser noise within the measurement bandwidth centered on the detection frequency. This noise is laser dependent and is influenced by mode competition and by optical feedback to the laser due to scattering from components in the optical system. The frequency at which the laser excess-noise reduces to below the shot noise is laser dependent.

RAM offset noise. The RAM offset carrying the low frequency laser excess-noise through to the mixer or lock-in amplifier output causes it.

1.6.13 Sweep integration

Some TDLAS measurements have used sweep integration of the direct absorption spectrum instead of modulation spectroscopy. In the sweep integration, the absorption line is scanned over repeatedly many times and the signal averaged to produce a direct absorption signal. In this technique the output from the detector

measuring the transmitted radiation is fed directly into a signal averager [26, 27]. The laser wavelength is not modulated but is instead swept repeatedly across the absorption line of the species being detected. A direct absorption spectrum of the species is thus built up. Sweep integration has been shown to be more stable than harmonic methods due to rapid baseline subtraction for systems under harsh environmental conditions and has a strictly linear response. It has also claimed an order of magnitude more than “2f” detection although it has not been used as widely.

1.6.14 Choice of absorption line

Several factors are to be considered while choosing the absorption line. A strong line is required for trace gas monitoring, to give high sensitivity in the experiment. Because the tuning range of a diode laser is not always continuous, a particular absorption line might not be accessible. It is important to choose a wavelength with several strong lines within the tuning range of the laser (typically 100 cm^{-1}) so that there is a high probability that at least one strong line will always be accessible. The line should, if possible be isolated from other lines of the same species, but this is not an absolute requirement and can prove difficult to achieve for the more complex molecules. The line should also be isolated from interfering lines due either to other trace species or to the more abundant atmospheric constituents such as H_2O , CO_2 or O_3 . H_2O causes the most problems because it absorbs over a large part of the infrared region and it has a relatively high and variable concentration.

Because TDLAS operates at reduced pressure it is not restricted in wavelength to the so-called atmospheric windows such as $3.4\text{-}5\ \mu\text{m}$ and $8\text{-}13\ \mu\text{m}$. However when operating outside these window regions it is not always possible to arrange for the absorption due to the tails of strong H_2O or CO_2 lines to be small compared to the absorption due to the line being measured. The line being measured can be easily instrumentally distinguished from the slow variation with wavelength of the absorption due to the wings of the strong lines.

The task of choosing the operating wavelength is made easier by the existence of spectral-lines databases of which the most popular is the HITRAN compilation [9-11]. The database is available on magnetic tape, PC-format floppy

disks, and CD ROM together with software to produce spectral plots for any combination of species and at any temperature and pressure. This currently covers a total of 709,000 transitions over a frequency range of 0-23,000 cm^{-1} and includes data on the following species (although not on all bands of each species): H_2O , CO_2 , O_3 , N_2O , CO , CH_4 , O_2 , NO , SO_2 , NO_2 , NH_3 , HNO_3 , OH , HF , HCl , HBr , HI , ClO , OCS , HCHO , HOCl , N_2 , HCN , CH_3Cl , H_2O_2 , C_2H_2 , C_2H_6 , PH_3 , COF_2 , SF_6 , H_2S . For each line the data includes wavenumber, line strength, Lorentzian half width and lower state energy.

1.7 Applications of TDLAS for atmospheric measurements

The aim of diode laser trace gas monitoring is to establish absolute concentrations. These can be measured directly from the absorbance and the lineshape information using published line strengths and widths [10] at a given pressure and pathlength. For harmonic detection, it is also necessary to relate the harmonic lineshape to the normal absorption lineshape, which can be done either by mathematical treatment using the experimental modulation depth or by determining the proportionality constant between the measured absorbance of an arbitrary amount and the second harmonic signal. Absolute concentration can be obtained indirectly by comparing with known concentrations, which can either be purchased commercially or can be determined for a similar concentration by wet chemistry or gas chromatography.

TDLAS has been used for atmospheric measurements of CH_4 [28] CO [29], HCl [30], HCHO [31], H_2O_2 [28, 31], H_2O [32,33], HNO_3 [34], NO [34], NO_2 [25, 31, 34], N_2O [35], OCS [14], and SO_2 [34, 36]. With the single exception of one of the H_2O measurements [32], which used sweep integration, all the above measurements used second-harmonic wavelength modulation spectroscopy.

Some representative applications of TDLAS to atmospheric measurements are

1.7.1 Open path measurements

Open-path or long-path monitoring, in which the multi-pass cell is replaced with an open atmospheric path to a remote retro-reflector and back, was the first application of lead-salt lasers to atmospheric monitoring [37, 38]. The technique has the great advantage that there are no sampling problems, also in some

applications the path-averaged concentration which this method gives is more useful than the point measurement provided by conventional TDLAS. However, there are also several disadvantages like the measurement at atmospheric pressure produces wider absorption lines which lead to interference problems due to nearby lines of other atmospheric species, variation of laser power with greater modulation, greater noise, difficulty in getting zero air baseline or back ground spectrum, less sensitivity etc. Despite these problems open-path measurements have produced useful measurements.

An interesting example of the application of long-open-path monitoring to stratospheric measurements is found in the BLISS system [39-41], which was developed at the Jet Propulsion Laboratory (NASA, U.S.A). The system has made many flights and species measured include NO, NO₂, O₃, CH₄, H₂O, CO₂, HCl, HNO₃, and N₂O [40 - 42]. In open path measurement the detector is either situated some way from the laser source or a retro reflector is used which returns the beam to the detector, near the source. Unlike multipass cells, open path monitoring provides unique, *in-situ*, direct information on gas concentrations over large areas. Unfortunately new problems arise such as pressure broadening, which seriously limit the sensitivity, as well as weather effects, scattering on dust particles, and atmospheric turbulence. The aim of the retro reflector is to return the laser beam parallel to the incoming beam. The most often used design is the corner-cube with three mirrors mounted perpendicularly.

1.7.2 Stratospheric measurements

Whilst TDLAS has mainly been used for tropospheric measurements interest in its use in the stratosphere is increasing. Recently instruments using multi-pass cells have been developed for use on stratospheric research aircraft such as the NASA ER-2. ATLAS [35] is a conventional single-species instrument for the ER-2, which has measured nitrous oxide as a tracer species during the Antarctic AAOE experiment [43, 44] and the arctic AASE expedition. ALIAS [21] is a more radical design which is mounted in an un-pressurized external pod of the ER-2. It has a compact optical layout using a Herriott cell with four independent optical channels, giving it the capability of simultaneous four-species measurements.

1.7.3 Flux measurements

Accurate gas fluxes can be determined using the method of eddy correlation. In this, the three components of the wind velocity are correlated with fast concentration measurements to yield the net flux of the gas normal to the surface. The wind velocity can be measured with three axis sonic anemometers and the gas concentrations with lead salt or GaAs type diode lasers.

1.7.4 Laser heterodyne measurements

Heterodyne radiometers using TDLs as the local oscillator can be used to probe the atmosphere by measuring the spectra of the sun, moon, or planets. Column contents of atmospheric species can be determined from their absorption of the solar, or other spectrum. Instruments of this type have been used to measure N_2O , O_3 , CH_4 , and CO_2 [45 – 47].

1.8 TDLAS as gas sensors and trace gas detection technique

Laser optical sensors in the near and mid infrared spectral region are now at the threshold of routine applications in gas analysis and increasingly these sensors are transformed to industrial and monitoring applications wherever sensitive, selective and fast analysis is required. With increasing complexity of the process, online gas analysis is becoming a key issue in automated control of various industrial applications such as combustion diagnostics, investigation of aero-engines and automobile exhaust measurements. Other challenges are online analysis of high purity process gases, medical diagnostics and monitoring of agricultural and industrial emissions. The need to meet increasingly stringent environmental and legislative requirements has also led to the development of analyzers to measure the concentrations of a variety of gases based on near and mid infrared absorption spectroscopy [8].

The features of diode laser spectroscopy rendering it such a valuable technique for gas analysis is: it is specific and as a high resolution spectroscopic technique, it is virtually immune to interference by other species – a problem that plagues most competing methods. This ability to provide unambiguous measurements leads to the use of TDLAS as a reference technique against which other methods are often compared. It is a technique universally acceptable to all

smaller IR active molecules and the same instrument can easily be converted from one species to another by changing the laser and the calibration gases. The time resolution of TDLAS measurements can be traded off against sensitivity and this allows very fast measurements with millisecond time resolution. In order to improve sensitivity, various types of direct and modulation spectroscopy have been employed. These techniques allow absorption as low as one part in 10^6 to be measured within a 1 Hz bandwidth. In combination with optical multipass cells, this is equivalent to detection limits of around 20 pptv for the most strongly absorbing species and better than 1 ppbv for almost all species of interest [8].

Werle *et al* [48] describes spectroscopic gas analyzers based on indium-phosphide, antimonide and lead-salt diode lasers. In this paper, the currently available semiconductor lasers for spectroscopy in the near infrared and mid infrared regions based on direct band-to-band transitions as gallium arsenide, indium-phosphide, antimonides and lead salt containing compounds are discussed with main features of different tunable diode laser absorption spectrometers for trace gas analysis. Measurements of atmospheric carbon dioxide with a room temperature 2 μm indium-phosphide laser, applications of antimonide lasers for methane and formaldehyde sensing in the 3–4 μm range and a fast chemical sensor for methane flux measurements based on lead salt diode lasers operating near 7.8 μm are also presented. Vicet *et al* [49] reported trace gas detection using antimonide based quantum well diode lasers. Widely tunable GaInAsSb/AlGaAsSb quantum well (QW) lasers have been grown by molecular beam epitaxy (MBE) on GaSb substrates. Their emission wavelength from 2.0 – 2.5 μm make them suitable for detection of many gas species in the wavelength range, which corresponds to an atmospheric transmission window. Using these devices an experimental setup for open path detection has been developed.

Trace gas detection is of great interest in industrial process control and pollution monitoring. Gas detection systems based on TDLAS provides that the lasers emit at a single frequency and are able to work at room temperature in continuous wave (cw) regime. In order to improve the sensitivity of the TDLAS measurement techniques such as heterodyne detection, wavelength (2f – WMS) and frequency (FMS) modulation spectroscopy are used [50] in combination with multipass cells increasing the absorption path. Many atmospheric pollutants as well

as some gaseous species involved in industrial process have strong absorption lines in the spectral region between 2.0–2.5 μm . The 2.3 μm window is especially interesting for gas analysis because it corresponds to a transmission window of the atmosphere where gas traces can be measured without the interfering effect of water vapor absorption. The advantage of this spectral region compared with longer wavelengths is the possibility to develop high quality semiconductor lasers and detectors that are able to operate at room temperature.

A novel single frequency stabilized Fabry – Perot (SFP) laser diode with an emission wavelength at 1590 nm for H_2S gas sensing is reported by Weldon *et al* [51]. The application of this device to spectroscopic based H_2S sensing is demonstrated by targeting absorption lines in the wavelength range $1588 \leq \lambda \leq 1591$ nm. Using wavelength modulation spectroscopy (WMS) a low detection limit of 120 ppm $\text{mHz}^{1/2}$ was estimated while targeting the absorption line at 1590.08 nm. The results demonstrate the potential of the stabilized FP laser diode at this wavelength as a tunable, single frequency source for spectroscopic based gas sensing. The application of a multi-laser tunable diode laser absorption spectrometer for atmospheric trace gas measurements at sub-ppbv levels is reported by Kormann *et al* [52]. This paper describes the application of a three-laser tunable diode laser absorption spectrometer (TDLAS) called “tracer in-situ TDLAS for atmospheric research (TRISTAR) to measure nitrogen dioxide (NO_2), formaldehyde (HCHO) and hydrogen peroxide (H_2O_2).

A portable diode laser based sensor for NH_3 detection using vibrational overtone spectroscopy at 1.53 μm is reported by Claps *et al* [53]. Use of fiber coupled optical elements makes such a trace gas sensor rugged and easy to align. On-line data acquisition and processing requiring less than 30 sec can be performed with a laptop PC running labVIEW software. The gas sensor is primarily used for NH_3 concentration measurements with a sensitivity of 0.7 parts per million. The feasibility of simultaneous, real –time measurements of NH_3 and CO_2 concentrations is also reported.

The measurements of CO , CO_2 , OH and H_2O in room temperature and combustion gases by use of a broadly current tuned InGaAsP diode laser is reported by Upschulte *et al* [54]. This paper reports a new laser technology that achieve nearly 100 nm quasi-continuous tuning with only injection current control

in a four section grating coupler sampled reflector laser is used to detect CO and CO₂ simultaneously in the room temperature gas mixtures. The same grating coupler sampled reflector laser is used to perform *in-situ* measurements of CO, H₂O and OH in the exhaust gases of a CH₄ air flame. A diode laser sensor is applied to monitor CO, CO₂ and CH₄ in combustion gases with absorption spectroscopy and fast extraction sampling techniques is reported by Mihalcea *et al* [55]. Species concentrations above a laminar, premixed, methane – air flame are determined from measured absorption in a fast flow multipass cell containing probe sampled combustion gases; good agreement is found with calculated and chemical equilibrium values.

Two tunable infrared laser differential absorption spectroscopy (TILDAS) technique is used to measure the N₂O emission levels of on-road motion vehicles exhausts by Jimenez *et al* [56]. They have used two different TILDAS based techniques to measure the N₂O/CO₂ emission ratios of on-road motor vehicles. Average N₂O/CO₂ emission ratios for each TILDAS technique are comparable and their distributions are similar, even though the measurement circumstances are quite different.

The principal gas sensor technologies are based on absorption spectroscopy of fundamental bands in the 3–25 μm spectral region and NIR vibrational overtone and combination bands from 1–3 μm. Common radiation sources include continuous wave (CW) diode lasers (GaAs based, antimonide based and lead salt based), parametric frequency conversion devices (difference frequency generation and optical parametric oscillators) gas lasers (CO and CO₂) and quantum cascade lasers. Telecommunication distributed feedback (DFB) diode lasers are ideally suited for overtone spectroscopy of molecules with chemical bonds such as C-H, O-H and N-H in the NIR region (0.78–2.5 μm). Overtone spectroscopy exhibits absorption line strengths that are typically approximately one to two orders of magnitude weaker than those of fundamental vibrations in the mid IR. To obtain the required sensitivity in the NIR, longer absorption pathlengths and optical balancing of laser noise are required. For this purpose, a compact multipass cell configured for a 36 m total optical pathlength and an auto balance detection technique is used [57]. Other groups have used cavity-enhanced spectroscopy to monitor ro-vibrational overtone and combination band transition [58, 59].

The spectrum of the weakly bound complex Ar-CH₄ in the 7 μm region is discovered, analyzed and compared with a spectrum predicted by *ab initio* calculations by Wangler *et al* [60]. Probing a supersonic gas expansion with a tunable diode laser did the measurements. Several bands of Ar-CH₄ associated with different ro-vibrational transitions of the ν₄ vibration of CH₄ are recorded and analyzed in the spectral region 1295–1330 cm⁻¹. The experimental results show close agreement with the *ab initio* calculations.

1.9 Isotope detection and measurements

Tunable diode lasers are used in isotope separation processes also. Lithium isotope separation with TDL is reported by Olivares *et al* [61]. A laser isotope separation study of lithium has been performed with two-step excitation involving UV laser radiation and a visible tunable diode laser. The method yields a high degree of selectivity by tuning the narrow linewidth diode laser to the D1 or D2 levels of the lithium atom. Selective laser excitation is simplified by the use of the tunable diode laser and the overall approach benefits from the applications of a compact mass selector that includes a precision magnetic sector and an ion beam that is designed specifically for light atoms such as lithium.

High precision isotopic ratio measurement system for methane by using a near infrared diode laser absorption spectroscopy is reported by Yamamoto *et al* [62]. They demonstrate that the absorption spectroscopic method could be applied to a precise δD (an index of ¹²CH₃D/¹²CH₄) and δ¹³C (an index of ¹³CH₄/¹²CH₄) analysis for methane samples of natural isotopic abundance. The measurements are performed on choosing an appropriate absorption line pair whose absorption coefficients have nearly the same temperature dependences. This minimizes the temperature effects. They measured ¹²CH₃D/¹²CH₄ ratio by using near-infrared external cavity diode lasers and a new type of multipass cell. The δD value can be determined from the ¹²CH₃D/¹²CH₄ signal – intensity ratio with a fine correction by taking into account of the interference of ¹³CH₄ lines. Similarly the ¹³δC value is determined from the ¹³CH₄ /¹²CH₄ signal intensity ratio, which is measured by using distributed-feedback laser and a modified Herriott-type cell and corrected for the abundance ¹²CH₃D.

In absorption spectroscopy, in contrast different isotopic molecular species can be distinguished easily irrespective of their masses if appropriate absorption lines are selected. Then the abundance ratio is determined by comparing the ratio of the absorbances of the selected absorption lines in the same sample gas with that in the standard gas of known isotopic composition. There are related works for isotope analyses by spectroscopic methods using lead salt diode laser in the mid infrared [63], a DFB (Distributed feed back) single mode laser in NIR [64], a 3.3 μm He-Ne laser [65], a colour center laser [66] a quantum cascade laser [67] in 8 μm region and FTIR spectrometer.

1.10 TDLAS in industrial gas monitoring

Gas monitoring in the process industry using diode laser spectroscopy is reported by Linnerad *et al* [68]. Gas monitors for industrial applications must have high reliability and require little maintenance. Monitors for *in-situ* measurements using tunable diode laser absorption spectroscopy in the near infrared can meet these requirements. Over the last few decades there has been increasing concern about man made pollution of the atmosphere. The dilution of pollutants in the atmosphere makes the concentrations very low, often below 1 ppb, and therefore difficult to measure.

TDLAS is one of the emerging techniques used in pollution and trace gas detection. In recent years new techniques has emerged such as Fourier Transform Infrared (FTIR), Differential optical absorption spectroscopy (DOAS), Laser Induced Fluorescence (LIF) and tunable diode laser absorption spectroscopy (TDLAS). Tunable diode lasers (TDL) have line widths of only a few MHz or less and are therefore well suited for high resolution spectroscopy. In the near infrared (NIR, 0.8–3 micrometers) we have the first and second overtones of the rotational/vibrational modes of the trace gases and there are commercial semiconductor lasers available that operates at room temperatures.

Due to short response time, industrial TDLAS monitors are ideal as process control tools in processes requiring a fast response, and they are also well suited for continuous emission monitoring of gases such as HCl and HF where the

maximum permissible emission levels are in the low ppm range. Some typical examples are presented below

- 1) Process control
 - a) O₂ measurement
 - b) NH₃ measurement
 - c) CO measurement
 - d) H₂S measurement
- 2) Emission monitoring
 - a) CO, NO, NO₂, SO₂
 - b) HF, HCl, NH
- 3) Measurement of O₂, CO and HCl from a waste incinerator
- 4) Measurement of HF in a primary aluminium smelter
- 5) Measurement of NH₃ at a coal fired power plant with SCR abatement system.

Sandstrom *et al* [69] reported TDLAS application for simultaneous contact free measurement and monitoring of the oxygen concentration as well as the gas temperature in a reheating furnace. During the production, the tunable diode laser spectrometer measured *in-situ* across the preheating zone and the soaking zone in the furnace. The oxygen concentration and gas temperature in the furnace environment were simultaneously monitored and instantaneous variations in these parameters could be easily recorded and subsequently correlated to actual changes in the process. Compared with the conventional measurement methods, TDLAS technique have much shorter response time and hence it can be used for energy savings as well as product quality improvements by controlling the burners in the reheating furnace.

As already explained, frequency modulation, baseline reduction methods, line locking, reduction in interference fringes, reduction in random noise and choice of integration time, usage of optical fibers, diode laser optoacoustic trace gas monitoring, heterodyne measurements etc are some of the advanced techniques used in trace gas detection using TDLAS.

1.11 TDL based molecular spectroscopy

Spectroscopy in the infrared, visible and ultraviolet regions serves qualitative and quantitative purposes. The quantitative analysis of the material is done through the radiation that the material absorbs or emits. Qualitative analysis is made possible by the fingerprint nature of the spectra: they are highly characteristic of the material concerned. Quantitative analysis can be carried out in cases where relative intensities are accurately measurable. The quantitative analysis in these regions is a very powerful and accurate tool for the investigation of atomic and molecular structure. This includes not only the determination of molecular geometry in ground electronic state but also how molecules behave when they vibrate and rotate and how both atoms and molecules change when they are in excited electronic states. Low-resolution spectra is used for analytical purposes, where as high resolution spectra is used for obtaining more and more accurate structural information.

Microwave and millimeter wave spectroscopy are intrinsically high resolution techniques because of the highly monochromatic nature of the sources and the very small linewidths of the transitions involved. The development of continuously tunable backward wave oscillators, tunable lasers and tunable diode lasers are useful in high resolution studies in other regions also [70].

High-resolution spectroscopy requires the narrow-bandwidth excitation sources that are only achievable with lasers. Studies in the visible spectral region typically use a tunable dye laser and studies in the near ultraviolet and near infrared are becoming more common as frequency doubling and wave-mixing methods improve. Mid infrared and Near-infrared tunable diode lasers are also used for high-resolution vibrational spectroscopy.

Super high-resolution studies also require cooling of the molecules to remove spectral congestion and to reduce the Doppler width of the transitions. Gas-phase studies use free-jet expansions or molecular beams to cool molecules to very low temperatures. The major application of TDLAS is high resolution recording of vibrational rotational spectra of molecules in the gas phase [71]. The major uses are summarized below.

Chapter I

- i. Investigation and analysis of fundamental and vibrational-rotational bands of chemically stable molecules, line assignments, determination of precise spectroscopic constants and molecular structure
- ii. Study of rotational fine structure of molecular spectra
- iii. Investigation of individual line parameters- profiles, intensities widths and also coefficients of broadening and shifts
- iv. Spectroscopy of transient species, in particular, free radicals and molecular ions
- v. Investigation of absorption by molecules in excited states
- vi. Study of dynamic molecular process

Tunable diode laser absorption method is used to study the fine structures in many molecules corresponding to interactions between different forms of molecular motion (electronic, vibrational and rotational). The molecules whose fine structures are studied using lead salt diode lasers include H₂, CO, NO, HCl, LiF, CO₂, N₂O, H₂S, OCS, O₃, NH₃, C₂H₂, CH₄, CF₄, CCl₄, SiF₄, HCOOH, HNO₃, CH₃CN, C₄H₂, SF₆, C₂H₆, C₆H₅Cl, C₈H₈ etc., [71].

1.12 High resolution overtone spectroscopy – some reported works

With the recent developments in high resolution FTIR spectrometers, tunable diode laser spectrometers and other high sensitivity laser based techniques like photothermal methods, NIR overtone spectral analysis have now become an important tool for molecular structural studies and for applications like trace gas monitoring.

The local mode effects on the high resolution overtone spectra of H₂S near 12500 cm⁻¹ are reported by Vaittinen *et al* [72]. The overtone spectrum is studied by intracavity laser absorption spectroscopy in the wavenumber region 12270 – 12670 cm⁻¹. The rovibrational analysis has provided upper state rotational parameters for the three interacting vibrational states. A local mode type behavior is evidenced by the values of rotational parameters.

Becucci *et al* [73] studied the high resolution photothermal spectra of pyridine S₀ – S₁ electronic transition. Rotational profile measurement for several vibronic bands revealed severe homogeneous broadening, with linewidths of the

order of 3 – 5 GHz. The rotational constants of pyridine in the excited state S_1 vibronic levels were extracted by a band contour analysis and the values obtained are in good agreement with results from *ab initio* calculations.

Held *et al* [74] studied the high resolution FTIR spectroscopy first overtone of N-H stretch and the fundamental of C-H stretch in gas phase pyrrole. The first overtone N-H stretch is rotationally analyzed using an asymmetric top model and was found to exhibit two separate perturbations. These perturbations produce line splitting and anomalous intensity patterns in the spectrum. The C-H fundamental stretches are also analyzed. A combined high resolution and theoretical study of the rovibrational spectrum of hydroxylamine is carried out by Luckhaus *et al* [75]. They reported the ro-vibrational spectrum of hydroxylamine (NH_2OH) recorded by interferometric Fourier transform spectroscopy with a resolution up to 0.004 cm^{-1} close to the Doppler limit at room temperature, in the spectral range of 800 cm^{-1} up to the visible region. A detailed rotational analysis of all the fundamentals and numerous overtones up to 10500 cm^{-1} are also done.

Photoacoustic spectroscopy is used in high resolution vibrational overtone studies by Douketis *et al* [76]. The high resolution vibrational overtone spectrum of H_2O_2 vapor between 7400 and 7600 Å is recorded under both bulk gas and supersonic beam conditions. An absorption band corresponding to a $\Delta V = 4$ of O-H stretch is observed in this spectral region. Rotational analysis indicated that it is a hybrid band with mainly parallel character. Spectral linewidths are found to be Doppler limited in all cases.

The photoacoustic spectra of stannane with its rotations and local modes is reported by Zhan *et al* [77]. The fifth and the seventh stretching vibrational overtone bands of a monoisotopic stannane sample have been recorded with Doppler limited resolution using intracavity photoacoustic technique using a titanium:sapphire ring laser. The rotational fine structures of these bands have been analyzed with the symmetric top energy formula and a spherical top Hamiltonian and about 200 rotation-vibration transitions have been assigned for both the systems.

High resolution infrared emission spectrum of sodium monofluoride is recorded with a high resolution Fourier transform spectrometer and reported by Muntianu *et al* [78]. They observed a total of 1131 vibration – rotation transitions

from the $v=1 \rightarrow 0$ to $v=9 \rightarrow 8$ vibrational bands and assigned. The high resolution spectral analysis of $^{13}\text{CH}_3\text{OH}$ in the excited torsional states are reported by Mukhopadhyay *et al* [79]. They did a theoretical analysis of ^{13}C substituted methanol to include a large number of spectral lines with the help of microwave and Fourier transform for infrared spectral lines involving up to the second excited torsional state ($n=2$) in the ground vibrational state and the effective Hamiltonian parameters were determined.

Long path length, high resolution Fourier transform spectrometer measurements for water which covered the near infrared, visible and near ultra violet regions are reported by Carleer *et al* [80]. Transitions in the range 13100 – 21400 cm^{-1} are analyzed using line lists computed using first principle calculations. The newly observed 15 overtone and combination bands of water and the energy levels for these were presented. High resolution spectra of H_2^{16}O vapor covering the region 11610 – 12861 cm^{-1} are reported by Toth [81]. The line positions and strengths of 933 lines which include vibration – rotation transitions were reported. New water vapor line parameters in the 26000 – 13000 cm^{-1} region with a high resolution Fourier transform spectrometer combined with a long path absorption cell are reported by Coheur *et al* [82]. Naus *et al* [83] reported the high resolution cavity ring down spectrum of water vapor in the range 555 – 604 nm. The spectrum contained 1830 lines calibrated against iodine standard with an accuracy of 0.01 cm^{-1} .

1.13 The present work

We have setup a narrow band near infrared tunable diode laser based absorption spectrometer. The spectrometer is automated by interfacing with LabVIEW software and is successfully used for recording the rotationally resolved second OH overtone spectra of some alcohols. We could reproduce the reported rotational structures of OH second overtone bands of water and methanol, which are thus used for the calibration of the spectrometer. The details of the experimental configuration, spectral calibration and spectral measurements are described in detail in the following chapters.

References

- [1] S.P Parker, “*Spectroscopy Source Book*”, Mc-Graw Hill Book Company, 1987.
- [2] F.T.Arecchi, F.Strumia and H.Walther (ed.), “*Applications of laser spectroscopy*” – Herbert Walther from *Advances in laser spectroscopy*, Plenum Press, New York and London, 1981.
- [3] E.Hirota, “*High resolution spectroscopy of transient molecules*”, Springer series in Chemical Physics, 40 Springer-Verlag, 1985.
- [4] I.Linnerad and P.Kaspersen, T. Jaeger; *Appl. Phys. B.*, 67 (1998) 297.
- [5] R.L.Byer and M.Garburg, *Appl. Opt.*, 12, (1973) 1496.
- [6] K.W.Rothe, U.Brinkmann and H.Walther; *Appl. Phys.*, 3 (1974) 114.
- [7] M.Feher and P.A Martin; *Spectrochim. Acta. A*, 51 (1995) 1579.
- [8] P.Werle; *Spectrochim. Acta. A*, 54 (1998) 197.
- [9] www.hitran.com
- [10] L.S.Rothman, R.H.Tipping, C.P.Rinsland, M.A.H.Smith, D.C.Benner, V.M.Devi, J.M.Flaud and C.Camy-Peyret, *J. Quant. Spectrosc. Radiat. Transfer.*, 48 (1992) 469.
- [11] L.S.Rothman, *Atmospheric propagation and remote sensing II* in A.Kohnle, W.B.Miller (Eds.), *SPIE*, 1968 (1993) 687.
- [12] N.Husson, B.Bonnet, N.A.Scott and A.Chedin; *J. Quant. Spectrosc. Radiat. Transfer.*, 48 (1992) 509.
- [13] W.J.Riedel, *Measurements of atmospheric gases*, *Proc. SPIE*, 1433 (1991) 179.
- [14] A.Fried, J.R.Drummond, B.Henry and J.Fox; *Appl. Opt.*, 30 (1991) 1916.
- [15] J.U.White; *J. Opt. Soc. Am.*, 32 (1942) 285.
- [16] J Reid, M.El-Sherbiny, B.K.Garside and E.A Ballik; *Appl. Opt.*, 19 (1980) 3349.
- [17] D.R.Worsnop, D.D.Nelson and M.S.Zahniser; *SPIE*, 1715 (1992) 18.
- [18] H.J.Bernstein and G.Herzberg; *J. Chem. Phys.*, 16 (1948) 30.
- [19] D.R.Herriott and H.J.Schulte; *Appl. Opt.*, 4 (1965) 883.
- [20] W.R.Trutna and R.L.Byer; *Appl. Opt.*, 19 (1980) 301.
- [21] C.R.Webster, R.D.May, C.A.Trimble, R.G.Chave and J.Kendall; *Appl. Opt.*, 33 (1994) 454.
- [22] H.J.Kramer; “*Observation of the Earth and its environment, Survey of missions and sensors*”, Springer-Verlag, Berlin, 1994.

- [23] C.R.Webster; *J. Opt. Soc. Am. B*, 2 (1985) 1464.
- [24] D.S.Bomse, A.C.Stanton and J.A.Silver; *Appl. Opt.*, 31 (1992) 718.
- [25] H.I.Schiff, D.R.Karecki and G.W.Harris; *J. Geophys. Res.*, 95 D (1990) 10147.
- [26] D.E.Jennings; *Appl. Opt.*, 19 (1980) 2695.
- [27] D.T.Cassidy and J.Reid; *Appl. Opt.*, 21 (1982) 2527.
- [28] G.I.Mackay, D.R.Karecki and H.I.Schiff; *Proc. SPIE.*, 1433 (1991) 104.
- [29] A.Fried, B.Henry, D.D.Parrish, J.R.Carpenter and M.P.Buhr; *Atmos. Env.*, 25A (1991) 2277.
- [30] A.Fried, R.Sams and W.W.Berg; *Appl. Opt.*, 23 (1984) 1867.
- [31] G.W.Harris, D.Klemp, T.Zenker, J.P.Burrows and B Mathieu; *J. Atmos. Chem.*, 15 (1992) 315.
- [32] J.A.Silver and A.C.Stanton; *Appl. Opt.*, 26 (1987) 2558.
- [33] A.Fried, B.Henry and J.R.Drummond; *Appl. Opt.*, 32 (1993) 821.
- [34] G.Schmidke, W.Kohn, U.Klocke, M.Knothe, W.J.Reidel and H.Wolf; *Appl. Opt.*, 28 (1989) 3665.
- [35] J.Podoske and M.Loewenstein; *Appl. Opt.*, 32 (1993) 5324.
- [36] J.Reid, J.Shewchun, B.S.Garside and A.E.Ballik; *Appl. Opt.*, 17 (1978) 300.
- [37] R.S.Eng, A.W.Mantz and T.R.Todd; *Appl. Opt.*, 18 (1979) 3438.
- [38] D.T.Cassidy and J.Reid; *Appl. Opt.*, 21 (1982) 1185.
- [39] R.T.Menzies, C.R.Webster and E.D.Hinkley; *Appl. Opt.*, 22 (1983) 2655.
- [40] C.R.Webster and R.D.May; *J. Geophys. Res.*, 92 D (1987) 11931.
- [41] R.D.May and C.R.Webster; *J. Geophys. Res.*, 94 D (1989) 16343.
- [42] C.R.Webster and R.D.May; *Geophys. Res. Lett.*, 19 (1992) 45.
- [43] J.R.Podolske, M.Loewenstein, S.E.Strahan and K.R.Chan; *J. Geophys. Res.*, 94D (1989) 16767.
- [44] M.Loewenstein, J.R.Podolske, K.R.Chan and S.E.Strahan; *J. Geophys. Res.*, 94D (1989) 11589.
- [45] M.A.Frerking and D.J.Muelner; *Appl. Opt.*, 16 (1977) 526.
- [46] D.Glenar, T.Kostiuk, D.E.Jennings, D.Buhl and M.J.Mumma; *Appl. Opt.*, 21 (1982) 253.
- [47] H.Fukunishi, S.Okano, M.Taguchi and T.Ohnuma; *Appl. Opt.*, 29 (1990) 2722.
- [48] P.Werle, K.Maurer, R.Kormann, R.Mucke, F.D'Amato, T.Lancia and A.Popov; *Spectrochim. Acta A.*, 58 (2002) 2361.

- [49] A.Vicet, D.A.Yarekha, A.Perona, Y.Rouillard, S.Gaillard and A.N.Baranov; *Spectrochim. Acta. A.*, 58 (2002) 2405.
- [50] F.K.Tittel, D.G.Lancaster and D.Richter; *Laser Phys.*, 10(2000) 348.
- [51] V.Weldon, K.Boylan, B.Corbett, D.McDonald and J.O’Gorman; *Spectrochim. Acta. A.*, 58 (2002) 2433.
- [52] R.Kormann, H.Fischer, C.Gurk, F.Helleis, Th.Klupfel; K.Kowalski, R.Konigstedt, U.Parchatka and V.Wagner; *Spectrochim. Acta. A*, 58 (2002) 2489.
- [53] R.Claps, F.V.Englich, D.P.Leleux, D.Richter, F.K.Tittel and R.F.Curl; *Appl. Opt.* 40 (2001) 4387.
- [54] B.L.Upschulte, D.M.Sonnenfroh and M.G.Allen; *Appl. Opt.*, 38 (1999) 1506.
- [55] R.M.Mihalcea, D.S.Baer and R.K.Hanson; *Appl. Opt.*, 36 (1997) 8745.
- [56] J.L.Jimenez, J.B.McManus, J.H.Shorter, D.D.Nelson, M.S.Zahniser, M.Koplow, G.J.McRac and C.E.Kolb; *Chemosphere – Global Change Science.*, 2 (2000) 397.
- [57] P.C.D. Hobbs, *Appl. Opt.*, 36 (1997) 903.
- [58] Y.He and B.J.Orr; *Chem. Phys. Lett.* 319 (2000) 131.
- [59] R.Peters, G.Berden, A.Apituley and G.Meijer; *Appl. Phys. B.*, 71 (2000) 231.
- [60] M.Wangler, D.A.Roth, V.M.Krivtsun, I.Pak, G.Winnewisser, M.Geleijns, P.E.S.Wormer, and A.van der Avoird, *Spectrochim. Acta. A.*, 58 (2002) 2499.
- [61] I.E.Olivares, A.E.Duarte, E.A.Saravia and F.J.Duarte; *Appl. Opt.*, 41 (2002) 2973.
- [62] K.Yamamoto and N.Yoshida; *Spectrochim. Acta. A.*, 58 (2002) 2699.
- [63] J.F.Becker, T.B.Sauke and M.Loewenstein; *Appl. Opt.*, 31 (1992) 1921.
- [64] K.Uehara; *Appl. Phys. B*, 67 (1998) 517.
- [65] P.L.Kababian, M.S.Zahnister and C.E.Kolb; *Appl. Opt.*, 35 (1996) 1942.
- [66] E.R.Th. Kerstel, R.van Trigt, N.Dam and H.A.J.Meijer; *Anal. Chem.*, 71 (1999) 5297.
- [67] A.A.Kostemv, R.F.Curl and F.K.Tittel, *Opt. Lett.*, 24 (1999) 1762.
- [68] I.Linnera, P Kaspersen and T. Jaeger; *Appl. Phys. B*; 67 (1998) 297.
- [69] L.Sandstrom and D.Malmberg; *Spectrochim. Acta. A.*, 58 (2002) 2449.
- [70] J. M. Hollas, “*High resolution spectroscopy*”, second edition, John Wiley and Sons, Chinchester, U.K. 1998.

- [71] V.S.Letokhov, "*Laser Analytical Spectrochemistry*", Adam Hilger, Bristol, 1986.
- [72] O.Vaittinen, L.Biennier, A.Campargue, J.M.Flaud and L.Halonen; *J. Mol. Spectrosc.*, 184 (1997) 288.
- [73] M.Becucci, N.M.Lakin, G.Pietraperzia, P.R.Salvi, E.Castellucci and E.R.Th.Kerstel; *J. Chem. Phys.*, 107 (1997) 10399.
- [74] A.Held and M.Herman; *Chem. Phys.*, 190 (1995) 407.
- [75] D.Luckhaus, *J. Chem. Phys.*, 106 (1997) 8409.
- [76] C.Douketis and J.P.Reilly; *J. Chem. Phys.* 91 (1989) 5239.
- [77] X.Zhan, M.Halonen, L.Halonen, H.Burger and O.Polanz; *J. Chem. Phys.*; 102 (1995) 3911.
- [78] A.Muntianu, B.Guo and P.F.Bernath; *J. Mol. Spectrosc.*, 176 (1996) 274.
- [79] I.Mukhopadhyay, Y.Duan, X.T.Wu and K.Takagi; *Spectrochim. Acta. A*, 56 (1999) 19.
- [80] M.Carleer, A.Jenouvrier, A.C.Vandaek, M.F.Merienne, R.Colin, N.F.Zobov, O.L.Polansky, J.Tennyson and V.A.Savin; *J. Chem. Phys.*, 111 (1999) 2444.
- [81] R.A.Toth; *J. Mol. Spectrosc.*, 166 (1994) 176.
- [82] P.F.Coheur, S.Fally, M.Carleer, C.Clerbaux, R.Colin, A. Jenouvrier, M.F.Merienne, C.Hermans and A.C.Vandaele; *J. Quant. Spectrosc. Radiat. Trans.*, 74 (2002) 493.
- [83] H.Naus, W.Ubachs, P.F.Levelt, O.L.Polansky, N.F.Zobov and J.Tennyson; *J. Mol. Spectrosc.*, 205 (2001) 117.

Chapter II

TDLAS EXPERIMENTAL SETUP AND ITS COMPUTER INTERFACING USING LABVIEW

	Page
2.1 Introduction.....	45
2.2 Near Infrared Tunable diode laser based high resolution spectrometer....	45
2.2.1 The New Focus Model 6321 Velocity Tunable Diode Laser	47
2.2.2 Neutral density filter	49
2.2.3 Multipass cell	49
2.2.4 Nirvana autobalanced photo receiver.....	51
2.2.5 Sample container	54
2.2.6 Vacuum system	55
2.3 Computer Interface for the experimental setup.....	55
2.3.1 LabVIEW	55
2.3.2 Virtual Instrumentation (VI)	57
2.3.3 Icon/Connector.....	57
2.3.4 PCI-6023E.....	58
2.3.5 CB-68LP	60
2.3.6 PCI-GPIB for Windows.....	60
References.....	61

Chapter II

TDLAS EXPERIMENTAL SETUP AND ITS COMPUTER INTERFACING USING LABVIEW

2.1 Introduction

Tunable diode laser absorption (TDLA) technique is a versatile tool for carrying out high resolution molecular spectroscopy of fundamental and overtone transitions. This technique is very useful for detecting many trace gases with sensitivities in the sub-parts-per-billion (ppb) concentration range. In the present work, a high resolution NIR tunable diode laser based spectrometer is set up and it is used for recording the highly resolved rotational structure of the second overtone spectra of OH group in some compounds. This chapter gives the details of the experimental lay out, brief descriptions of the specifications of various components used in the experiment and the experimental procedure. The details of computer interface of the experiment, using LabVIEW, and program developed for control, operation and data acquisition along with the specification and details of DAQ-ADC and GPIB PCI cards are also included. The experimental setup is calibrated using the water vapor absorption spectral lines and the HITRAN 96 database.

2.2 Near infrared tunable diode laser based high resolution spectrometer

The main components of the tunable diode laser high resolution spectrometer are:

- a) A diode laser which is tunable in the wavelength range 936 – 976 nm with a tunability of the order of 0.01 nm in single mode (linewidth <300 kHz for 50 ms or <5 MHz for 5 s) with a constant power mode or not
- b) A neutral density beam splitter with variable split ratio
- c) A multipass cell with a maximum path length of 36 m
- d) Nirvana Photodetector that gives a balanced detection with logarithmic output
- e) Vacuum system for evacuation of the multipass cell, and to work at the required sample pressure

The entire setup is mounted on an indigenously made vibration free table, with granite top and shock absorber legs, which provides the required vibration isolation for the high resolution experiment.

A block diagram of the experimental setup is given in Fig.2.1.

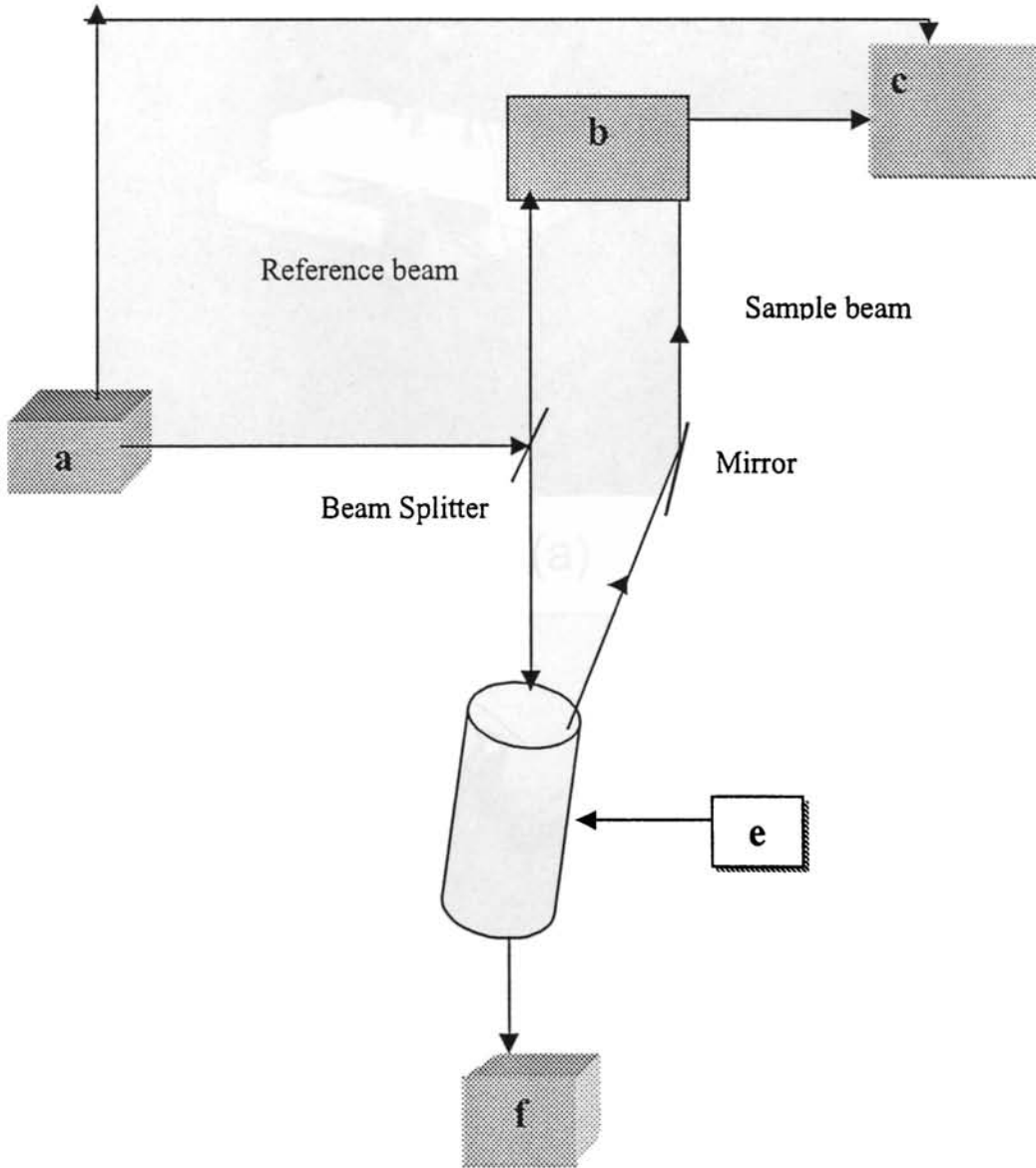
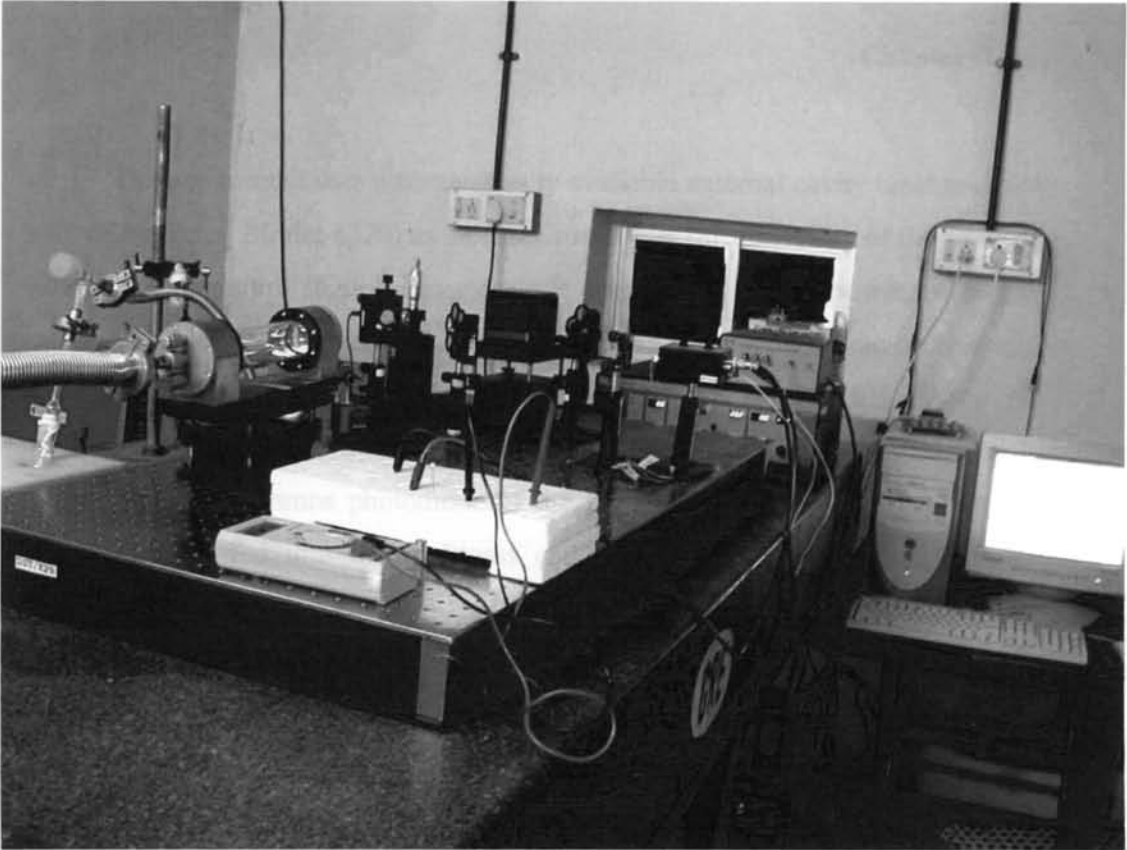
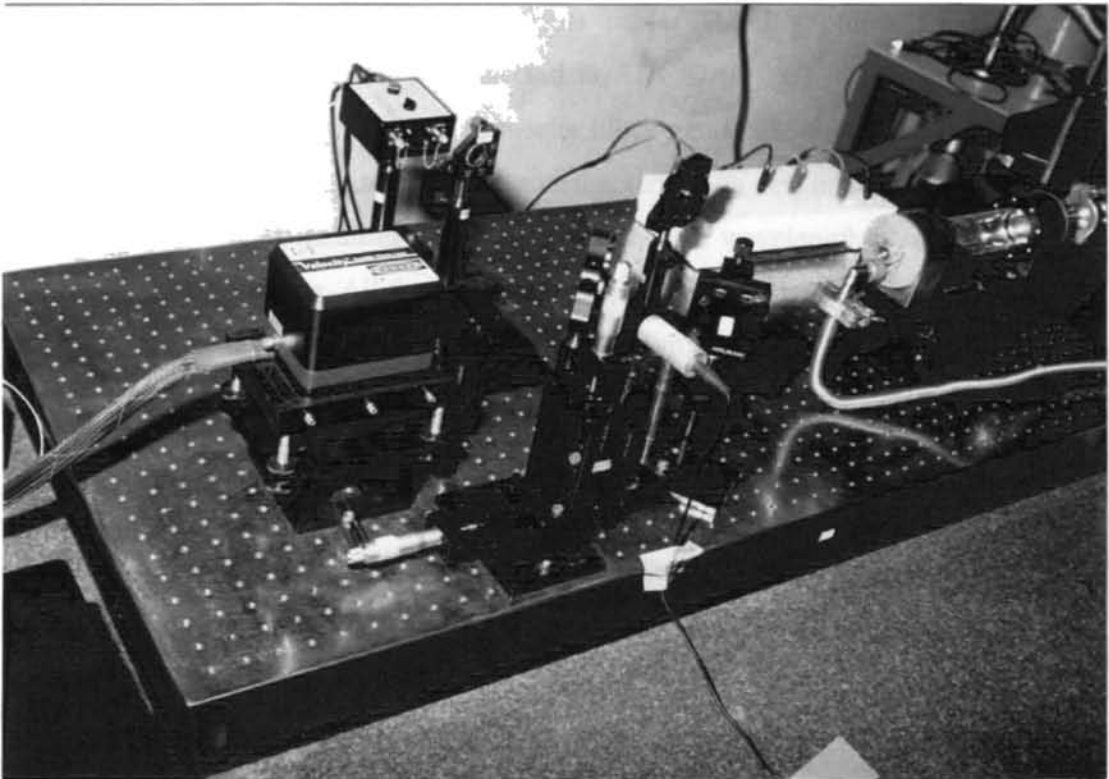


*Fig.2.1. Schematic representation of the experimental setup
a-Tunable diode laser, b-photodetector, c-computer,
d-multipass cell, e- sample holder, f-vacuum system*



(a)



(b)

Experimental setup for TDLAS

The experiment uses a commercially available external cavity tunable diode laser (New focus, Model 6320) as the laser source. Its fine tunability of the order of 0.01 nm, temperature stability, single mode operation, constant power mode etc. makes it an ideal laser source for high resolution spectrometer. It can be operated in single mode at a constant power of 3–4 mW is found suitable for most of the measurements. The laser beam is split into two – one reference beam which falls directly on the reference photodiode of the photodetector and the other –signal beam which is fed into the multipass cell which contains the sample whose spectrum to be recorded in gas phase (water, methanol, ethanol, isopropanol etc.). A rotary pump is used to evacuate the multipass cell below atmospheric pressure. The beam emerging from the multipass cell at a slightly different angle with the incident beam is deflected using a mirror and is focused onto the signal photodiode of the balanced photodetector.

The laser controller has both IEEE – 488 and RS-232 communication ports. Hence it is interfaced to the PC through IEEE – 488 ports using a PCI GPIB (National Instruments, U.S.A) and a GPIB cable. The log output from the photodetector is analog and it is connected to ADC/DAQ PCI 6023E (National Instruments, U.S.A) using CB68LP connector block and R 6868 64 pin connector cable. The multipass cell is evacuated and the sample is fed into it. When the sample pressure becomes steady, the tunable diode laser wavelength is scanned in the region 936 – 976 nm. All the scan parameters such as scan speed, wavelength range, power etc can be set using the program done in LabVIEW. The output data can be obtained in Microsoft Excel data (*.xls format). The finer details of the components of the setup are given below.

2.2.1 The New Focus Model 6321 velocity tunable diode laser

The Model 6321 is an external cavity tunable diode laser operating in the wavelength range of 936 nm – 976 nm with a tunability of 0.01 nm as mentioned earlier. It is a stable, narrow linewidth (<300 kHz for 50 ms or <5 MHz for 5 s) source. It can be operated manually from the front panel of the controller or remotely using a computer control. Digital control facilitates remote operation and computer interfacing compatible with RS-232 and GPIB (IEEE-488) addressing.

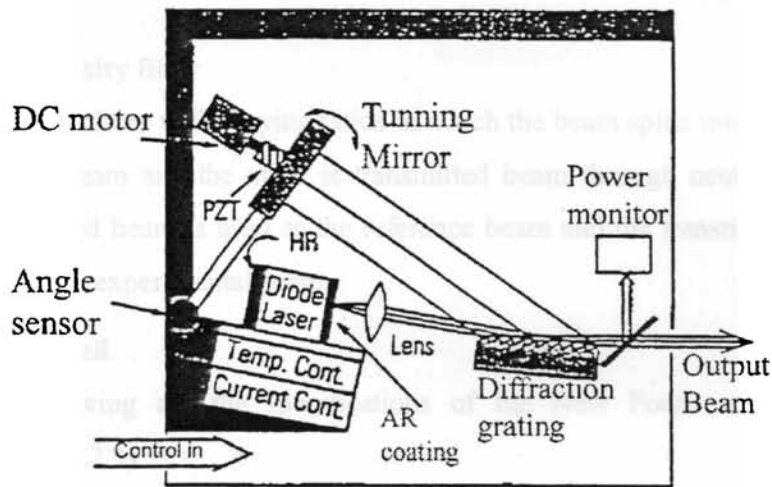


Fig.2.2 Laser cavity

Diffraction grating is used for wavelength selection in the laser. For single mode operation, a narrow grating spectral filter is used. The laser controller is to provide a stable, low noise power source for diode laser, set the temperature in the laser head, command wavelength scanning and provide all readouts of relevant parameters like scan speed, optical power, current etc.

A laser diode is used as the gain medium. One end of the diode laser has a high reflectivity coating, which acts as an end mirror of external cavity (fig.2.2). The other end of the diode has an antireflection coating. The diode laser is bonded to a temperature sensor and a thermoelectric cooling block, which maintains the diode temperature constant to within one milliKelvin. A lens collimates the laser beam radiating from the diode before striking a high quality diffraction grating. The grating is precisely aligned and its position is fixed with respect to the diode. From the diffraction grating, a fraction of the beam is directed to the tuning mirror. The position of the mirror determines the wavelength of the laser. The tuning mirror is mounted on a stiff arm. An angle sensor near the pivot point of the arm provides the data for wavelength readout. The other end of the arm is moved by a DC motor driven screw and a piezoelectric transducer (PZT). The DC motor makes coarse wavelength changes while PZT is used for mirror scale movements, which correspond to sub angstrom wavelength tuning position. A small fraction of the output beam is directed to a power monitor [1].

2.2.2 Neutral density filter

As beam splitter with varying ratios in which the beam splits into two – one is the reflected beam and the other is transmitted beam through neutral density filter. The reflected beam is used as the reference beam and the transmitted beam as the signal in the experimental setup.

2.2.3 Multipass cell

The following are the specifications of the New Focus model 5611 multipass cell (fig.2.3)

Optical path length	– 36 m
Number of passes	– 182
Mirror separation	– 20 cm
Cell volume	– 0.3 litres
Pressure	– 1 – 760 torr
Mirrors	– protected silver coating
Reflectivity (3 – 10 micrometer)	- > 99%
Reflectivity (1 – 3 micrometer)	- > 98 %

Mirrors are made from nickel-plated Aluminium substrates with a protected silver coating. Light enters and exits the cell through front window assembly. The input and output beam travel in the horizontal plane, cross at the front mirror surface and make an angle of 3 to 6 degrees with respect to the cell axis [2].

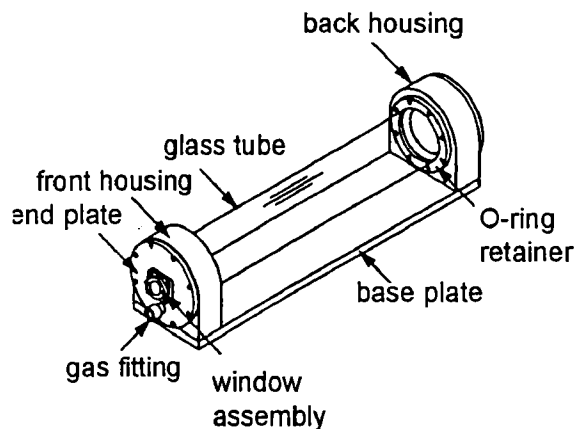


Fig.2.3. Multipass cell

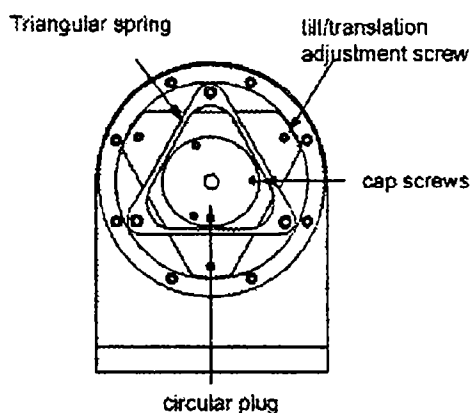


Fig.2.4. Rear end of multipass cell

Base plate: Anodized Aluminium with three slots for mounting on optical table with 1" hole spacing. At either end of the base plate, a housing is attached by two 0.25 -20 cap screws. Two alignment pins allow the housings to be removed and reattached to the base plate without upsetting the mirror alignment.

Glass tube: Glass tube is made of borosilicate glass and is sealed to the housings with an O-ring that is held in the place by anodized Aluminium O ring retainer. O-rings are made of Viton fluoroelastomer from Dupont Dow Elastomers.

Housings: Two housings are made of Nickel-coated Aluminium. Each housing has a circular endplate attached to it with 8 screws. An 'O' ring seated in the housing forms a seal between the housing and the plate. A total of three couplings for uses such as flowing gas through the cell or monitoring cell pressure etc. The cell cannot be operated above atmospheric pressure. The back plate of the cell is equipped with a safety relief valve to prevent over pressure.

Mirrors: The mirrors are made of Nickel-plated Aluminium substrate that is polished into the desired torroidal shape. A protected silver coating is deposited onto this surface. Operating temperature is 10 – 40 °C

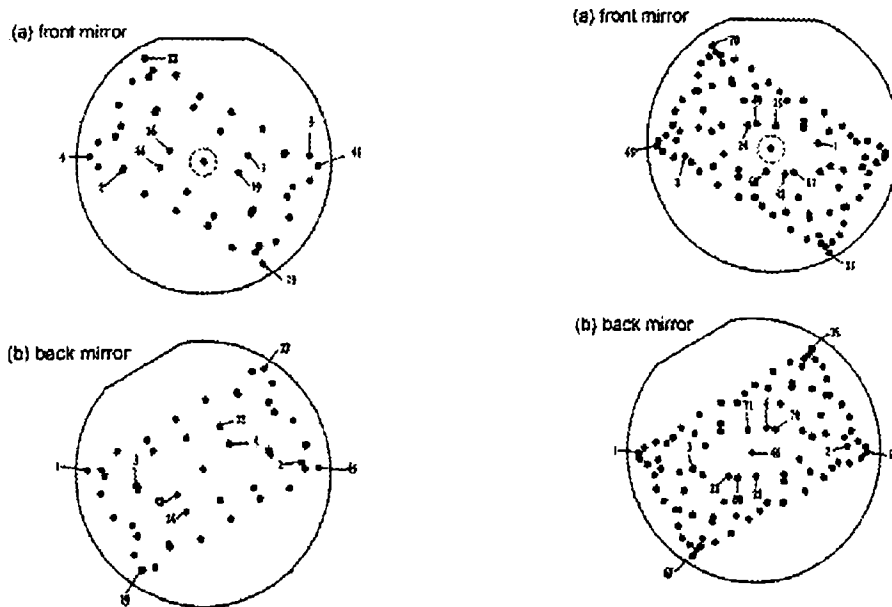


Fig.2.5. Pattern of beam spots for the 90-pass and 180-pass configuration

2.2.4 Nirvana autobalanced photo receiver

The specifications of the MODEL 2017 Nirvana auto balanced photo receiver (fig.2.6-2.8) are

Wavelength range	- 800 – 1700 nm
Detector type	- InGaAs PIN
Detector diameter	- 1 mm
Output impedance	- 100 Ohm
Maximum pulse power	- 10 mW
CW saturation power	- 0.5 mW
Optical input	- Fibre coupled (FC) and free space
Power requirements	- ± 15 V DC, < 300 mA

It is designed for use in a dual beam setup; one invariant reference path and one signal path, which contains the multipass cell with sample.

Front panel: It consists of two photodiodes as inputs. One is designated the reference photodiode REF and the other is signal photodiode SIGNAL [3].

Top panel: The top panel of the Nirvana photodetector have four different output options namely, SIG/BAL/AutoBAL/10X. In the SIG position, the

Chapter II

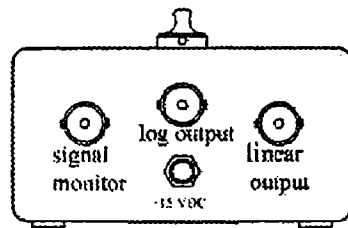
photodetector gives an output voltage proportional to the received signal optical power. In the BAL position, the photodetector does the traditional balanced detection and the output voltage is proportional to the difference between received signal and reference optical powers. In the AutoBAL position, the photodetector does the auto-balanced detection, zero DC voltage, and noise suppressed AC signal proportional to received signal optical power. In the 10X position, the photodetector functions auto balanced detection with higher gain; same as AutoBAL settings, but with output voltage increases 10 times.

Loop bandwidth – knob controls the cutoff frequency of electronic gain compensation in auto balanced operation. Optimal setting is 100.

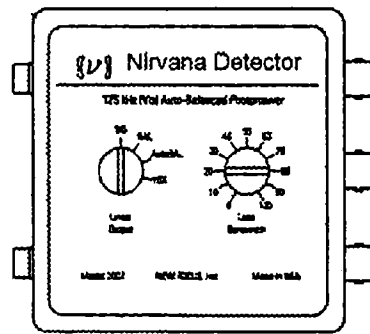
Back panel – Input ± 15 V DC.

Signal monitor BNC directly monitors the optical beam on the signal photodiode. The linear output BNC monitors the balanced output voltage. The output of LOGOUTPUT BNC depends on the top panel linear output knob setting. When it is turned to either AutoBAL or 10X, the log output voltage is

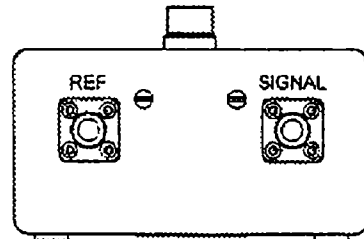
$$\text{LOGOUTPUT} \cong -\ln\left[\left(\frac{P_{ref}}{P_{sig}} - 1\right)\right]$$



Nirvana Back Panel



Nirvana Top panel



Nirvana Front Panel

Fig.2.6. Nirvana photodetector

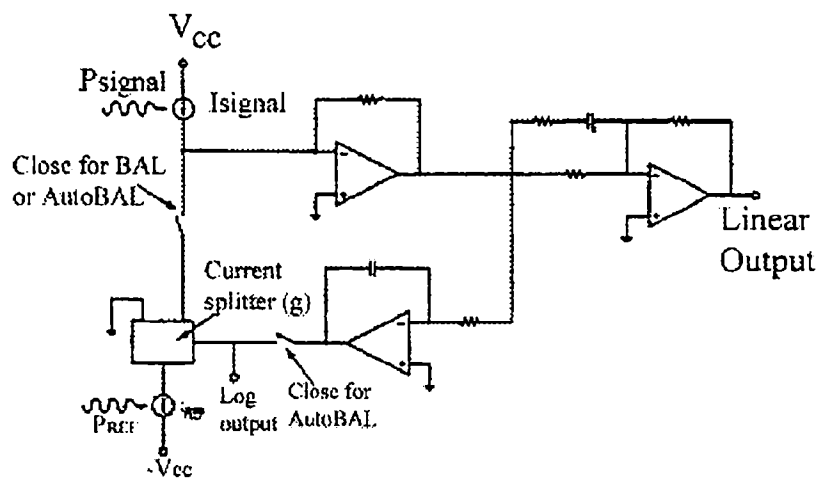


Fig.2.7. Schematic diagram of Nirvana photodetector

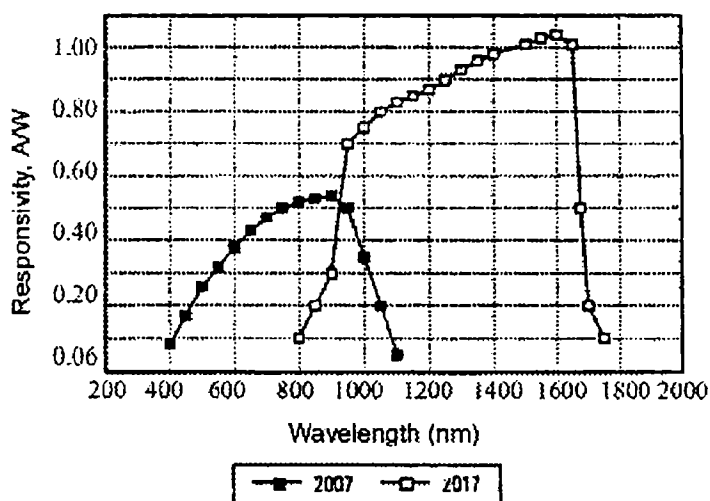


Fig.2.8. Typical photodiode responsivity

2.2.5 Sample container

A sample container with fine needle valve is used for the regulated flow of the sample to the multipass cell. High purity spectroscopic grade liquid samples are taken in the sample container connected to the sample inlet of the multipass cell. Once evacuated, at low pressure the vapours of the sample taken in the container will be fed into the multipass cell. The sample flow can be regulated using the needle valve.

2.2.6 Vacuum system

A rotary vacuum system, which is sufficient for the present experiment, is used to evacuate the multipass cell and for sample gas feeding. The multipass cell is evacuated continuously while recording the spectra.

2.3 Computer Interface for the experimental setup

2.3.1 LabVIEW (Laboratory Virtual Instrument Engineering Workbench)

Manually noting down hundreds of data for hours from an analytical instrument without any errors is a very difficult job. This is often time consuming, laborious and the measurements are prone to errors. The time and effort that is lost for this exercise will restrict the number of points, repetitions and accuracy of an experiment. Since the advent of personal computers, automation of analytic instruments for data acquisition and analysis of the obtained data have become much more simple, efficient and accurate.

The LabVIEW software is used successfully for interfacing and data acquisition in many experimental setups. The following are some of the reported laser absorption experimental setups interfaced using LabVIEW. Claps *et al* [4] have successfully used LabVIEW in ammonia detection by use of near infrared diode laser based overtone spectroscopy. They have used LabVIEW software running in a laptop PC for the online data acquisition and processing requiring less than 30 seconds.

The data acquisition and analysis using LabVIEW is made use in the laser based absorption sensors for trace gas monitoring in a spacecraft habitat by Titel *et al* [5]. The data is digitized and transformed to a laptop computer by use of a 16-bit A/D card (NI DAQ (ARI) AI – 16XE-50). It is also successfully used in room temperature mid-infrared laser sensor for trace gas detection by Topfer *et al* [6].

LabVIEW is also used in open path trace gas detection of ammonia based on cavity enhanced absorption spectroscopy by Peeters *et al* [7]. The Photodetector (New Focus, Nirvana 2017) is connected to an analog input of a multiplexer (National Instruments, BNC 2090). The data is transferred to a personnel computer via a data acquisition card (National Instruments, PCI-MIO-E 16) using LabVIEW based data acquisition software.

Chapter II

With the introduction of digital controllers and programmable test equipment, the need arose for a standard, high-speed interface for communication between instruments and controllers from various vendors. In 1975, the Institute of Electrical and Electronic Engineers (IEEE) published ANSI/IEEE Standard 488. IEEE Standard Digital Interface for Programmable Instrumentation contained the electrical, mechanical, and functional specifications of an interfacing system. In 1990, the IEEE 488.2 specification included the Standard Commands for Programmable Instrumentation (SCPI) document. SCPI defines specific commands that each instrument must obey irrespective of the different vendors or manufactures. Thus, SCPI guarantees complete system compatibility and configurability among these instruments. It is no longer necessary to learn a different command set for each instrument in an SCPI-compliant system, and it is easy to replace an instrument from one vendor with an instrument from another. This bus is now used worldwide and is known by three names:

- General Purpose Interface Bus (GPIB)
- Hewlett-Packard Interface Bus (HP-IB)
- IEEE 488 Bus

National Instruments (USA) launched the software called LabVIEW based on G programming which has since become an industry standard benchmark for virtual instrumentation programming. LabVIEW is a powerful instrumentation and analysis programming language based on G (the graphical programming language) for personal computers running under different operating platforms for controlling instruments and acquiring data. LabVIEW supports IEEE 488(GPIB), RS 232/422, VXI and Plug in data acquisition (DAQ) boards. LabVIEW departs from the sequential nature of traditional programming languages and features a graphical programming environment with all tools needed for data acquisition, analysis and presentation are in the form of Icons. LabVIEW has an instrument library with drivers for hundreds of instruments, which simplifies the instrument control applications. For analyzing data the analysis library contains functions for linear algebra, array arithmetic, regression, signal processing and signal generation. Because of the graphical nature in LabVIEW, it is inherently a data presentation package. LabVIEW can present the acquired data or analyzed data in the form of

charts, graphs and also in the form of tables. Thus making it easy to understand the material properties under study.

2.3.2 Virtual instrumentation (VI)

LabVIEW programs are called virtual instrumentation (VI). LabVIEW made the concept of the virtual instrumentation (VI) a practical reality. The objective in virtual instrumentation is to use a general-purpose computer to imitate real instruments with their controls and displays but with the added versatility that comes with the software. The programs in LabVIEW are called VI. All VI has three main parts, the Front Panel, Block Diagram and the Icon/connector. The front panel is used for setting input values and viewing outputs. Because the front panel is analogous to the front panel of the real instrument the inputs are called controls and the outputs are called indicators. A variety of controls and indicators such as knobs, switches, buttons, charts and graphs make the front panel a replica of the front panel of the real instrument.

Each front panel has an accompanying block diagram, which contains the graphical program and source code of VI. Block diagram is built using the graphical programming language G. The components of the block diagram represent program nodes, for example, for loops, case structures and arithmetic functions. These components are wired together to define the flow of data within in the block diagram. Once all the components in the block diagram are wired, then the VI can be run or can be converted as a sub VI of another program [9].

2.3.3 Icon/Connector

Icon connector is used to turn a VI into an object (sub VI) that can be used as a subVI in the block diagram of others VIs. The icon graphically represents the VI in the block diagram of other VIs. The connector terminals determine where one must wire the inputs and outputs on the Icon. The terminals correspond to the controls and indicators on the front panel.

The device driver for 6321 New Focus Velocity Tunable Diode Laser is downloaded from National Instruments website through Internet and is completely modified as per our requirements. An instrument driver is a set of high-level functions for controlling a GPIB, VXI or serial instrument. The instrument driver functions handle the instrument command syntax, I/O interface protocol and data

Chapter II

parsing. These drivers can be optimized or modified to work with different instruments.

Complete automation and analysis is fulfilled with the modification of the downloaded device drivers according to our requirements. So modifications are done in order to automate the data acquisition from the instrument, analyse it and then store the data in .xls (Microsoft Excel) format. The laser parameters including the current, laser power and scan parameters like wavelength range, scan speed etc can be set using the modified device driver program. This program is so modified that after complete data acquisition and analysis the spectrum is shown in graphs in the required format. The saved data file can also be opened using Microsoft excel and the spectrum can be plotted using graphical packages like origin or sigma plot for further analysis.

2.3.4 PCI-6023E

The National Instruments PCI-6023E is a low-cost data acquisition board that uses E Series technology to deliver high-performance, reliable data acquisition capabilities in a wide range of applications. We can get sampling rate up to 200 kS/s and 12-bit resolution on 16 single-ended analog inputs [8]. The channels marked ACH 0 – ACH 15 are the single ended analog inputs and AIGND is the ground. These channels with ground can be used for 8 differential input channels. We have used channel 9 (Pins 66 and 67) for the single ended analog input from the autobalanced photodetector.

- 8 digital I/O lines; two 24-bit counters
- NI-DAQ driver software is used to simplify configuration and measurements. The pin configuration and details of the PCI-6023 E are shown in Fig.2.9.

I/O Connector

Figure shows the pin assignments for the 68-pin I/O connector on the PCI-6023E and PCI-6024E.

ACH8	34	68	ACH0
ACH1	33	67	AIGND
AIGND	32	66	ACH9
ACH10	31	65	ACH2
ACH3	30	64	AIGND
AIGND	29	63	ACH11
ACH4	28	62	AISENSE
AIGND	27	61	ACH12
ACH13	26	60	ACH5
ACH6	25	59	AIGND
AIGND	24	58	ACH14
ACH15	23	57	ACH7
DAC0OUT [†]	22	56	AIGND
DAC1OUT [†]	21	55	AGND
RESERVED	20	54	AGND
DIO4	19	53	DGND
DGND	18	52	DIO0
DIO1	17	51	DIO5
DIO6	16	50	DGND
DGND	15	49	DIO2
+5 V	14	48	DIO7
DGND	13	47	DIO3
DGND	12	46	SCANCLK
PF10/TRIG1	11	45	EXTSTROBE*
PF11/TRIG2	10	44	DGND
DGND	9	43	PF12/CONVERT*
+5 V	8	42	PF13/GPCTR1_SOURCE
DGND	7	41	PF14/GPCTR1_GATE
PF15/UPDATE*	6	40	GPCTR1_OUT
PF16/WFTRIG	5	39	DGND
DGND	4	38	PF17/STARTSCAN
PF19/GPCTR0_GATE	3	37	PF18/GPCTR0_SOURCE
GPCTR0_OUT	2	36	DGND
FREQ_OUT	1	35	DGND

[†] Not available on the PCI-6023E

Fig.2.9. Pin assignments in PCI- 6023 E

2.3.5 CB-68LP

It is the connector block used to connect the analog output from the photodetector to the DAQ PCI 6023E.

R 6868 Connector Cable is used to take connection from CB-68LP to the PCI 6023E DAQ-ADC.

2.3.6 PCI-GPIB for Windows

The PCI-GPIB is a high-performance Plug and Play IEEE 488 interface for PCs and workstations equipped with PCI expansion slots. We can use the PCI-GPIB in PCs running Windows 2000/NT/Me/9x, Power Macs, Sun Ultra Workstations, and DEC Alpha Workstations.

The PCI – GPIB and DAQ – ADC PCI 6023 E are installed in a Pentium PC working in Windows 98 operating system in which the LabVIEW 6 is installed. The laser controller is connected to the PCI-GPIB using the GPIB cable and a GPIB address is set for the laser controller. The analog output of the Nirvana photodetector is connected to one of the single input channels of the CB68 LP Connector block. The R6868 68 pin cable is used to connect the CB68 LP connector block to the PCI – 6023E DAQ-ADC.

The LabVIEW driver for New Focus Model 6321 tunable diode laser is downloaded from the National Instruments website (www.ni.com) and is modified according to our requirements. The power on/off of the laser, modulation current, laser power output and scan parameters like scan speed, wavelength scanning range, the output detector type whether it is a power meter or DAQ, linear/log output etc can be set using the modified program. The output data can be stored in *.xls (Microsoft excel) format.

References

- [1] Model 6300 The Velocity Tunable Diode Laser, User's manual, New Focus Inc., U.S.A.
- [2] Models 5611 and 5612 Multipass Cell, User's manual, New Focus Inc., U.S.A.
- [3] Model 2007 and 2017 Nirvana Auto-balanced Photoreceivers, User's manual, New Focus Inc., U.S.A.
- [4] R.Claps, F .V Englich, D.P.Leleux, D.Richter, F.K.Tittel and R.F.Curl; *Appl. Opt.*, 40 (2001) 4387.
- [5] F.K.Titel, D.G.Lancaster, D.Richter, R.F.Curl and J.C.Graf; *29th International Conference on Environmental Systems*, Paper number 99ES-02, Denver, July 1999.
- [6] T.Topfer, K.P.Petrov, Y. Mine, D.Jundt, R.F.Curl and F.K.Tittel; *Appl. Opt.*, 36 (1997) 8042.
- [7] R.Peeters, G.Berden, A.Apituley and G.Meijer; *Appl. Phys. B. Lasers and Optics*, 71 (2000) 231.
- [8] www.ni.com
- [9] C.J.Mathai; "*Preparation of some plasma polymerized thin films and evaluation of their structural, optical and electrical properties*", Ph.D Thesis; Cochin University of Science and Technology, 2002.

Chapter III

**CALIBRATION OF THE TDLAS SETUP USING SPECTRA
OF WATER AND METHANOL**

	Page
3.1 Introduction.....	63
3.2 Spectrum of water vapor and HITRAN.....	63
3.3 Earlier OH overtone measurements in alcohols.....	65
3.4 TDLA spectrometer Calibration Techniques.....	66
3.5 Calibration of analytical signal.....	67
3.6 Experimental considerations.....	67
3.7 Calibration of the setup using spectra of water vapor and methanol.....	69
3.8 Spectrum of ethanol (C ₂ H ₅ OH).....	72
3.9 Conclusion.....	74
References.....	75

Chapter III

CALIBRATION OF THE TDLAS SETUP USING SPECTRA
OF WATER AND METHANOL

3.1 Introduction

This chapter describes the successful setting up and calibration of the TDL high resolution spectrometer using the HITRAN data for H₂O and the second overtone band of the -OH group in methanol molecule. The high resolution second overtone spectrum of -OH group in ethanol is recorded and the observed peaks are assigned. To our knowledge, this is the first high resolution study of the said transition in ethanol.

3.2 Spectrum of water vapor and HITRAN

The spectroscopic studies of water molecule, both theoretical and experimental, are very well reviewed by Bernath [1]. The experimental data obtained in water spectra are included in the database editions HITRAN 86 [2], HITRAN 92 [3] and HITRAN 96 [4] and the details are available from the website of HITRAN [5].

The theoretical studies of water molecule include the *ab initio* studies and water line assignments by Polansky *et al* [6], and the self-consistent field configuration interaction (SCF-CI) studies by Xie *et al* [7]. The vibrational fundamental and overtone band intensities of H₂O are calculated by Kjaergaard *et al* [8]. The experimental studies include the water vapor line parameters in 26000 – 13000 cm⁻¹ region using a combined high resolution Fourier transform spectrometer with a long path absorption cell by Coheur *et al* [9].

The pressure broadening coefficients for rotational transitions of H₂O in the 380 – 600 cm⁻¹ range, recorded using a Bruker IFS 120 high resolution spectrometer, is reported by Steyert *et al* [10]. The near infrared, visible and near ultraviolet overtone spectrum of water is reported by Carleer *et al* [11], who used a novel long pathlength high resolution Fourier transform spectrometer for the measurements. The spectrum covers the near infrared, visible and near ultraviolet

regions and contained water transitions belonging to all polyads from 3ν to 8ν . Transitions in the range $13100 - 21400 \text{ cm}^{-1}$ are analyzed based on line lists computed using variational first principle calculations, and 2286 new spectral lines were assigned to H_2O transitions. The analysis lead to the first assignment of fifteen new overtone and combination bands and the mapping of the corresponding energy levels in water. This work suggested that local mode (rather than normal mode) vibrational assignments are more appropriate for the vibrational states of water in the polyads 4ν and above.

A novel infrared diode laser spectrometer, used to measure H_2O spectra in the range $7165 - 7168 \text{ cm}^{-1}$ for atmosphere application is employed by Parvitte *et al* [12]. They used a near infrared diode laser spectrometer to measure H_2O line intensities near $1.39 \mu\text{m}$. A temperature stabilized White cell was used to perform measurements between room temperature and $60 \text{ }^\circ\text{C}$.

The method of pulsed cavity ring down spectroscopy is employed to record the water vapor absorption spectrum in the wavelength range $555 - 604 \text{ nm}$ by Naus *et al* [13]. They used an Nd: YAG laser-pumped tunable pulsed dye laser with a bandwidth of 0.05 cm^{-1} . The spectra consisted of 1830 lines calibrated against the iodine standard with an accuracy of 0.01 cm^{-1} . The visible and near ultraviolet ro-vibrational spectrum of HOD, recorded from $\text{H}_2\text{O}/\text{D}_2\text{O}$ vapor mixture, is reported by Janouvrier *et al* [14]. They used a Fourier Transform spectrometer/long path cell setup in the wave number range $16300 - 22800 \text{ cm}^{-1}$ for the experiment.

Temperature measurements in flames using water molecule overtone spectra are carried out by Cheskis *et al* [15]. They recorded the overtone absorption spectra of water molecules using a Ti: Sapphire laser-based intracavity absorption spectroscopy (ICLAS) setup. Atmospheric pressure methane/air or hydrogen/air flame is placed in the cavity of the Ti: Sapphire laser. Though the flame occupied only a small portion of the cavity, substantial changes in water spectrum are observed and new lines appeared. This suggests the possibility of measuring temperature in flames using an ICLAS spectrum of water.

Measurements of H_2^{16}O line positions and strengths in the region $11610 - 12861 \text{ cm}^{-1}$ with resolved rotational structure, using a high resolution Fourier

transform spectrometer, are reported by Toth [16]. Most of these water line measurements are included in HITRAN database.

Buntine *et al* [17] recorded the vibrational overtone excitation in water using laser induced grating spectroscopy, leading to a calculation of OH stretching band intensities of water dimer and trimer. Other related works in water molecules and OH stretching includes that by Low *et al* [18] and Vander Wal *et al* [19], who studied the spectra, on selectively breaking the OH bond in HOD. The OH stretching spectrum of liquid water with a random network model interpretation is reported by Belch *et al* [20] and an improved analysis of the OH stretching spectrum of amorphous solid water by Nelson *et al* [21]. An experimental and theoretical study of the bond selected photo dissociation of HOD is reported by Vander Wal *et al* [22].

3.3 Earlier OH overtone measurements in alcohols

The intensities for several OH vibrational overtone bands of vapor phase methanol, ethanol and isopropanol, are measured by Phillips *et al* [23]. Vibrational overtones of gaseous alcohols are reported by Fang *et al* [24], who measured the overtone absorption spectra of gaseous 1-propanol, 2-propanol and *tert* butyl alcohol using ICL- PAS and FTIR spectroscopy.

A temperature study of vibrational overtones in gas phase ethanol with its molecular conformers is studied by Fang *et al* [25]. The vibrational overtone spectra for ethanol vapor in the region 10150 – 19900 cm^{-1} , was measured by ICL-PAS technique. The OH overtones are composed of two sub-bands, which are assigned as the transitions of two conformers of OH bond in the *trans* or *gauche* position with respect to the methyl group. From the temperature dependence of the OH overtone intensity, the enthalpy difference between the conformers is determined to be 0.7 kcal/mole. Experimental and *ab initio* investigations for the OH overtone vibration of ethanol are reported by Weibel *et al* [26]. The intracavity dye laser photoacoustic absorption spectra of ethanol, ethanol (1, 1-d₂) and ethanol (2, 2, 2-d₃) are reported for the region 16550 – 16700 cm^{-1} that contains the OH fourth overtone vibrations. The distinct absorption bands are assigned as due to the *trans* and *gauche* conformational isomers. Absorption spectra of gas phase

methanol ($10150 - 19900 \text{ cm}^{-1}$) and methanol -d ($10150 - 17600 \text{ cm}^{-1}$), measured using intracavity dye laser photoacoustic spectroscopy are reported by Fang *et al* [27]. The prominent features in the spectra are assigned as OH, OD and CH overtones within the local mode model of loosely coupled anharmonic vibrations. Relatively less intense peaks are assigned as combinations involving a local mode overtone and lower frequency motions in the molecules.

3.4 TDLA spectrometer calibration techniques

According to Beer's law, the signal due to absorption is linearly proportional to the number of absorbing molecules and the power of the laser beam for small optical depths. Several methods are employed to determine the frequency of laser light. The major techniques are outlined below [28].

- (1) Using Michleson scanning interferometer and by counting the number of interference maxima [29,30]
- (2) Method of internal standard in which the frequency is determined from a value of absorption linewidth under Doppler limited conditions [31]
- (3) Calibration with a Fabry-Perrot etalon and reference lines
- (4) Optical heterodyne techniques, when the frequency stabilized CO_2 or CO laser is used as a local oscillator

The simplest method is that in which the laser frequency dependence on tuning parameter is determined by measurement of Fabry-Perrot etalon transmission spectrum and the absolute calibration of this dependence are performed using frequency calibration standards [32-34].

The important aspects in wave number calibration can be summarized as below.

- i. The reproducibility of the entire tuning curve from scan to scan could not be worse than $1 \times 10^{-4} \text{ cm}^{-1}$ and the producer of spectra recording over a single mode frequency range takes only a few seconds. The acquisition should in the sweep integration method. The bandwidths of detectors and amplifiers used, should not higher than 1 MHz
- ii. Digital data recording and processing with the help of microcomputers is advantageous [35]. Baseline correction would be made using subtraction or dividing the transmission spectra of the studied gases and the etalon point by

point by the background one. Analog or digital filtering is also effective for background elimination

- iii. To exclude systematic errors a set of spectral recordings (background, reference gas, the studied gas and fringes of the Fabry-Perrot etalon) should be made more than once at different tuning parameters.

3.5 Calibration of analytical signal

The important problem for qualitative analysis is to establish the functional dependence of a gas analyzer signal on the concentration of molecules detected and to calibrate this dependence. A very sharp spectral line of a TDL ensures the validity of Beer's law. The linear dependence exists not only if the direct transmission signal is detected but also when harmonic integration or correlation methods are used. The non-linearity may be caused by optical effects such as a parasitic etalon fringes, baseline slope, interference absorption lines or by molecular process such as adsorption on cell walls or chemical reaction in the mixture. The calibration in ppb range in the optical absorption method can be performed using standard mixtures with high concentrations. This can be achieved by placing a short cell containing a calibrated mixture with relatively higher concentration, in the laser beam sequentially with the multipass cell. Because the absorption is linearly proportional to the concentration path length product this method enables to simulate an absorption signal equivalent to that from mixtures with extremely low concentration [36].

3.6 Experimental considerations

Scanning the laser wavelength range and detecting the signal accomplish the recording of absorption spectra using the TDL set up. However, there are several conditions to be satisfied in the experimental arrangement. The first condition is laser should be operated in a single mode. Operating the laser at low power and mounting the laser on a vibration free table can achieve this goal.

The laser beam from the TDL source is allowed to split into two using a neutral density filter, which is adjusted to allow 40% transmittance. The reflected beam from the filter is considered as the reference beam and is focused to the

reference photodiode of the Nirvana autobalanced photoreceiver. The transmitted beam is passed into the multipass cell where the sample is fed at a low pressure of ~ 0.02 m bar. The multipass cell is aligned properly to get maximum number of passes. This is done by noting the number of spots obtained in the cell with the visible diode laser (red) beam kept aligned to trace the path of the NIR diode laser beam.

The recording of the high resolution spectra using the TDLAS setup is accomplished by scanning the tunable diode laser wavelength at an increment of 0.01 or 0.02 nm and recording the autobalanced output from the Nirvana photodetector. The spectrum can be recorded manually using an X-Y recorder. In this case, the output voltage corresponding to the wavelength from the back panel of the laser controller is along X axis and the log output (autobalanced) from the photodetector along Y axis. In the present work, the setup is interfaced to the PC successfully and a program is developed in LabVIEW for the operation, control and data acquisition. Hence we can obtain the spectral data in the computer itself (wavelength vs. voltage that is proportional to absorbance). However, there are several experimental requirements to be satisfied to obtain a good spectrum.

After switching on the power of the laser controller, the diode temperature is set to 20 °C, and is kept for warm up for about 30 minutes. Then the diode laser is switched on and the modulation current is increased so that the laser power increases (< 80 mA). The laser power is set at a constant value normally between 3 – 4 mW so that the laser will operate in single mode also. Sometimes, at higher power, multimode operation of the laser may occur. The multipass cell has to be evacuated fully to avoid signal distortions due to atmospheric water vapor or presence of other gases. The multipass cell is connected to the vacuum pump using a flexible alloy tube 1.25 m in length. The working of vacuum pump may also induce vibrations on the multipass cell. To avoid this, the tube connecting them is fixed to vibration arresting clamps. The sample to be fed into the cell is taken in a round bottom flask and is connected to one of the nozzles of the multipass cell using a flow controller and a bend tube.

The multipass cell is evacuated to rotary vacuum. The sample-feeding knob is slowly opened so that the sample (water, methanol, ethanol etc.) is fed slowly into the multipass cell, allowing the sample pressure to increase gradually. The

wavelength scanning can be started when the pressure becomes steady between 0.1 – 0.05 mbar. The power supply of the Nirvana photodetector ($\pm 15V$) is now fed, and we can check the strength of the reference beam, signal beam and the balanced output by changing the control knob on top of the photodetector in balance mode. The strength of the reference beam should be at least twice that of the signal beam. This condition is to be ensured every time before taking the autobalanced output. If the signal strength is more, then it is to be decreased by slowly adjusting the focusing lens or by changing the ratio of the neutral density beam splitter. At this condition, change the knob to autobalance. The output of the photodetector is connected to the A/D converter.

The scan parameters are set in the program and it is run to start wavelength scanning. When the wavelength scanning is finished, save the spectral data in Microsoft Excel format. This data can be used for plotting the spectrum as wavelength versus absorbance and for further analysis of the spectrum.

3.7 Calibration of the setup using spectra of water vapor and methanol

The calibration of the set up is done using the HITRAN 96 database for water vapour and –OH second overtone in methanol. We have recorded the absorption spectra of water vapour and methanol in the region 10300 cm^{-1} to 10650 cm^{-1} . The experimentally observed peak positions are respectively compared with the HITRAN 96 database for water vapor and the methanol spectrum reported earlier by Fang *et al* [27].

The experimental procedure is as follows: The water sample is taken in the sample container. The laser diode temperature is set to $20\text{ }^{\circ}\text{C}$ and kept for half an hour for warm up for thermal stability. Then the laser is switched on and the current adjusted for a moderate power. Then the signal output voltage and reference voltages are checked using the linear output BNC and the beam splitting ratio is adjusted such that the reference input power is twice the strength of the signal input. The signal input power can be adjusted either by adjusting the focusing lens used in the path of the signal beam or by changing the number of passes in the multipass cell by tilting its alignment very slowly. A constant power mode is selected for laser output so that the beam is under single mode. Then the

laser parameters (start wavelength, end wavelength, scan speed etc) are set using the software. The data can be saved in Microsoft excel format (.xls) or text data (.txt). The experimental conditions used for recording the spectrum of water vapor is given below.

Sample - water
Constant power - 3.4 mW
Scan speed - 0.05 nm/sec
Pressure - 0.2 mbar
Log output from photodetector

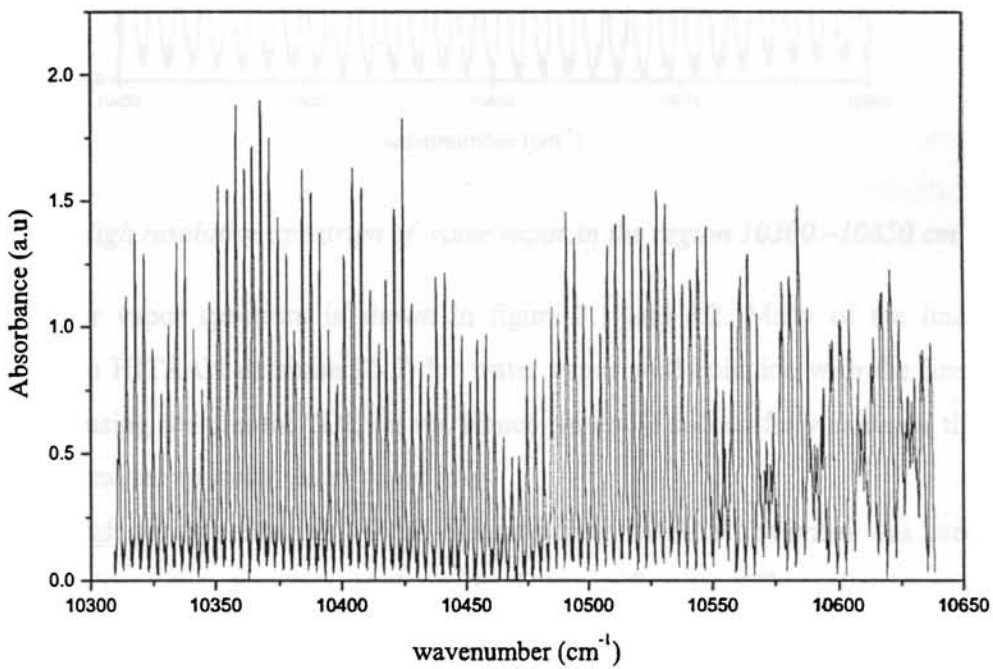


Fig.3.1. High resolution spectrum of water vapor in the region 10300 – 10650 cm⁻¹

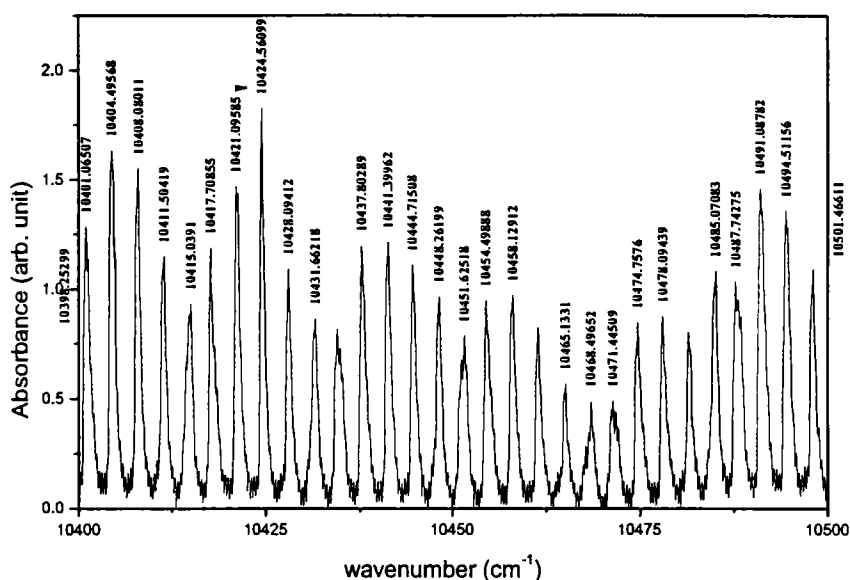


Fig.3.2. High resolution spectrum of water vapor in the region 10300 –10650 cm⁻¹

The water vapor spectrum is shown in figure 3.1 and 3.2. Many of the lines reported in HITRAN database [2-5] for water vapor well coincide with the lines observed using the present TDL set up. Hence we could successfully calibrate the experimental set up using water vapor lines.

High purity methanol (>99%) obtained from MERCK, Mumbai was used for recording the spectrum without further purification. The experimental parameters are given below.

Laser Power - 2.8 mW
 Scan Speed - 0.02 nm/sec
 Temperature - 26°C
 Pressure - 0.02 mbar

The conspicuous peaks obtained agree fairly well with the values reported by Fang *et al* [27], for the $\Delta V=3$ region of the -OH group in methanol. The spectrum obtained by Fang *et al* using photoacoustic technique shows P, Q, R branch heads at frequencies 10515 cm⁻¹, 10531 cm⁻¹, 10546 cm⁻¹ respectively. Eappen *et al* [37], have reported the well-resolved high resolution spectra of these bands.

3.8 Spectrum of ethanol (C_2H_5OH)

We have successfully recorded the high resolution spectra of $-OH$ second overtone in ethanol (fig.3.3). High purity ethanol (>99%) obtained from MERCK, Mumbai was used for recording the spectrum without further purification. The experimental parameters are given below.

Laser Power - 2.7 mW
Scan Speed - 0.02 nm/sec
Temperature - 26°C
Pressure - 0.05 mbar

The gas phase spectrum of ethanol in this region was recorded earlier by Fang *et al* [25] using intracavity photoacoustic spectroscopy. They could obtain two sub bands for each $-OH$ overtone corresponding to the *trans* or *gauche* conformers of ethanol. With the limited spectral resolution of their experiment, they could get only the P, Q and R band positions corresponding to the *trans* conformer. The present high resolution experiment gives the well-resolved rotational structure of these bands. These transitions can be used as signature lines of ethanol molecule in this spectral range. The experimental results in comparison with the reported values are given in Table.3.1. To the best of our knowledge, this is the first high resolution study of ethanol OH overtone band in the said spectral region

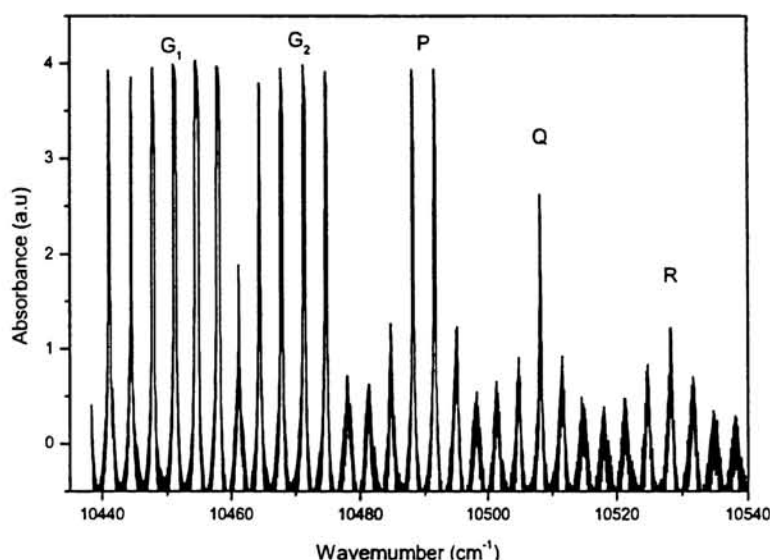


Fig.3.3. High resolution spectrum of ethanol with the P, Q and R branches of the $\Delta V=3$ OH overtone band in ethanol

Table 3.1

V	Description	Experimental (cm ⁻¹)	Reported (cm ⁻¹)
		10441.11	
		10444.52	
	G ₁	10447.89	
		10451.19	10450
OH (3ν ₁) <i>gauche</i>		10454.54	
		10457.86	
		10461.2	
		10464.465	
	G ₂	10467.85	10469
		10471.4	
		10474.74	
OH (3ν ₁) <i>trans</i>	P	10484.71	
		10488.02	10502
		10491.56	
		10495.16	
	Q	10504.91	10514
		10508.16	
		10511.51	
	R	10524.83	10525
		10528.19	
		10531.75	

Table 3.1 Comparison of Experimental Results of the ethanol spectrum with the reported values.

3.9 Conclusion

We have successfully calibrated the tunable high resolution spectrometer using the water vapor spectrum and HITRAN database. The spectrum recorded for methanol also shows very good agreement with the earlier reported results. The -OH second overtone spectrum of ethanol is recorded successfully and the absorption spectral lines corresponding to both the *trans* and *gauche* conformers of ethanol molecule are obtained.

References

- [1] P.F.Bernath, *Phys. Chem. Chem. Phys.*, 2 (2002) 1501.
- [2] L.S.Rothman, R.R.Gamache, A.Goldman, L.R.Brown, R.A.Toth, H.M.Pickett, R.L.Poynter, J.M.Flaud, C.Camy-Peyret, A.Barbe, N.Hasson, C.P.Rinsland and M.A.H.Smith, *Appl. Opt.*, 26 (1987) 4058.
- [3] L.S.Rothman, R.H.Tipping, C.P.Rinsland, M.A.H.Smith, D.C.Benner, V.M.Devi, J.M.Flaud, C.Camy-Peyret, A.Perrin, A.Goldman, S.T.Massie, L.R.Brown and R.A.Toth; *J. Quant. Spectrosc. Radiat. Trans.*, 48 (1992) 469.
- [4] L.S.Rothman, C.P.Rinsland, A.Goldman, S.T.Massie, D.P.Edwards, J.M.Flaud, A.Perrin, C.Camy-Peyret, V.Dana, J.Y.Mandin, J.Schroeder, A.McCann, R.R.Gamache, R.B.Watson, K.Yoshino, K.V.Chance, K.W.Jucks, L.R.Brown, V.Nemtichinov and P.Varanasi; *J. Quant. Spectrosc. Radiat. Trans.*, 60 (1998) 665.
- [5] <http://www.hitran.com>
- [6] O.L.Polansky, J.Tennysion and N.F. Zobov; *Spectrochim. Acta A.*, 55 (1999) 659.
- [7] D.Xie, and G.Yan; *Chem. Phys. Lett.*, 248 (1996) 409
- [8] H.G.Kjaergaard, B.R.Henry, H.Wei, S.Lefebvre, T.Carrington Jr., O.S.Mortensen and M.L.Sage; *J. Chem. Phys.*, 100 (1994) 6228.
- [9] P.F.Coheur, S.Fally, M.Carleer, C.Clerbaux, R.Colin, A. Jenouvrier, M.F.Merienne, C.Hermans and A.C.Vandaele; *J. Quant. Spectrosc. Radiat. Trans.*, 74 (2002) 493.
- [10] D.W.Steyert, W.F.Wang, J.M.Sirota, N.M.Donahue and D.C.Reuter; *J. Quant. Spectrosc. Radiat. Trans.*, 72 (2002) 775.
- [11] M.Carleer, A.Jenouvrier, A.C.Vandaele, M.F.Merienne, R.Colin, N.F.Zobov, O.L.Polansky, J.Tennysion and V.A.Savin; *J. Chem. Phys.*, 111 (1999) 2444.
- [12] B.Parvitte, V.Zeninari, I.Pouchet and G.Durry, *J. Quant. Spectrosc. Radiat. Trans.*, 72 (2002) 493.
- [13] H.Naus, W.Ubachs, P.F.Levelt, O.L.Polansky, N.F.Zobov and J.Tennysion; *J. Mol. Spectrosc.*, 205 (2001) 117.
- [14] A.Janouvrier, M.F.Merienne, M.Carleer, R.Colin, A.C.Vandaele, P.F.Bernath, O.L.Polansky and J.Tennysion, *J. Mol. Spectrosc.*, 209 (2001) 165.

- [15] S.Cheskis, A.Kachanov, M.Chenevier and F.Stockel; *Appl. Phys. B*, 64 (1997) 713.
- [16] R.A.Toth; *J. Mol. Spectrosc.*, 166 (1994) 176.
- [17] M.A.Buntine, D.W.Chandler and C.C.Hayden; *J. Chem. Phys.*, 102 (1995) 2718.
- [18] G.R.Low and H.G.Kjaergaard; *J. Chem. Phys.*, 110 (1999) 9104.
- [19] R.L.Vander Wal, J.L.Scott and F.F.Crim; *J. Chem. Phys.*, 92 (1990) 803.
- [20] A.C.Belch and S.A.Rice; *J. Chem. Phys.*, 78 (1983) 4817.
- [21] G.Nelson and S.A.Rice; *J. Chem. Phys.*, 78 (1983) 4824.
- [22] R.L.Vander Wal, J.L.Scott, F.F.Crim, K.Weide and R.Schinke; *J. Chem. Phys.*, 4 (1991) 3548.
- [23] J.A.Phillips, J.J.Orlando, G.S.Tyndall and V.Vaida; *Chem. Phys. Lett.*, 296 (1998) 377.
- [24] H.L.Fang and D.A.C.Compton; *J. Phys. Chem.*, 92 (1988) 6518.
- [25] H.L.Fang and R.L.Swofford; *Chem. Phys. Lett.*, 105 (1984) 5.
- [26] J.D.Weibel, C.F.Jackels and R.L.Swofford; *J. Chem. Phys.*, 117 (2002) 4245.
- [27] H.L.Fang, D.M.Meister and R.L.Swofford; *J. Phys. Chem.*, 88 (1984) 405.
- [28] V.S.Letokhov; “*Laser Analytical Spectrochemistry*”, Adam Hilger, Bristol Publication, 1986.
- [29] K.Nagai, K.Kawaguchi, C.Yamada, K. Hyakawa, Y.Takagi, E.Hirota; *J. Mol. Spectra.*, 80 (1980) 197.
- [30] M.V. Shubin; *Sov. J. Opt. Technology.*, 12 (1983) 46.
- [31] T.Y.Chang, R.N.Morris and E.S.Yeung; *Appl. Spect.*, 35 (1981) 587.
- [32] J.Kauppinen, K.Jolma and Horneman; *Appl. Opt.*, 21 (1982) 3332.
- [33] K.Jolma, J.Kauppinen and Horneman; *J. Mol. Spect.*, 101 (1983) 300.
- [34] K.Jolma, J.Kauppinen and Horneman; *J. Mol. Spect.*, 101 (1983) 278.
- [35] P.B.Davis, P.A.Hamilton, W.Lewis Bevan and M.Okumura; *J. Phys. E. Sci. Instr.*, 16 (1983) 289.
- [36] J.Reid, J.Shewchun, B.K.Garside and E.A.Ballik; *Appl. Opt.*, 17 (1978) 300.
- [37] S.M.Eappen, S.Shaji, T.M.A.Rasheed and K.P.R.Nair; (Paper accepted for publication in *J. Quant. Spectrosc. Radiat. Trans.*)

Chapter IV

**NIR ABSORPTION TECHNIQUES AND VIBRATIONAL
OVERTONE SPECTROSCOPY**

	Page
4.1 Introduction	78
4.2 NIR spectroscopy	78
4.3 Normal modes of vibration	81
4.4 Vibrational spectroscopy.....	81
4.5 Vibrational and rotational transitions of diatomic molecules	82
4.6 Vibrational overtone excitation of polyatomic molecules in the ground electronic state.....	84
4.6.1 Theoretical description of higher excited vibrational levels – the Local Mode Model.....	84
4.6.2 Refinements in local mode model.....	89
4.7 Molecular structural details studied by overtone spectroscopy-a survey	90
4.8 Intensity aspects in overtone spectra.....	100
References.....	102

Chapter IV

NIR ABSORPTION TECHNIQUES AND VIBRATIONAL OVERTONE SPECTROSCOPY

4.1 Introduction

This chapter gives a brief review of the techniques used to measure near infrared (NIR) absorption, vibrational overtone transitions in molecules containing X-H (X = C, N, O..) oscillators, and the applications of vibrational overtone spectroscopy in molecular structural analysis.

4.2 NIR spectroscopy

NIR occupies the wavelength range 800-2500 nm of the electromagnetic spectrum. The absorption bands in this region correspond to overtones and combinations of the fundamental vibrational transitions. NIR offers a number of advantages for quantitative analysis even though the much-reduced number of absorption bands in this region limits its use in structural studies. The inherent instrumental advantages of NIR are that, since the emission maximum of the source is close to the region of interest, a high energy throughput and low stray radiation result. This, combined with the availability of sensitive solid state detectors, leads to a signal to noise ratio, which is typically 10000:1. Low cost and robust materials such as glass or quartz are transparent to NIR radiation and are therefore available for optical components and cells. The detectors have response times measured in microseconds and hence extremely rapid analyses are possible. However, probably the most important advantage arises from the fact that absorptivities for NIR bands are lower by at least an order of magnitude for each successive overtone. Therefore, moderately concentrated samples and more convenient path lengths compared with mid-IR may be used. This means that quantitative NIR transmission spectra of intractable materials such as plastics or protein fibres may be obtained, possibly without sample preparation or destruction of the samples. The absorptivities of solvents, including water, are sufficiently low as to cease to pose a serious problem in the NIR.

Chapter IV

Near infrared photometry is widely used in industry for on-line process measurement. NIR spectroscopy can be a workhorse technique for materials analysis in industries such as agriculture, pharmaceuticals, chemicals and polymers. A near-infrared spectrum represents combination bands and overtone bands that are harmonics of absorption frequencies in the mid-infrared. Near-infrared absorption includes a combination-band region immediately adjacent to the mid-infrared and overtone regions.

All four near-infrared regions contain "echoes" of the fundamental mid-infrared absorptions. For example, vibrations in the mid-infrared due to the C-H stretches will produce four distinct bands in each of the overtone and combination regions. As the bands become more removed from the fundamental frequencies they become more widely separated from their neighbors, more broadened and are dramatically reduced in intensity. Because near-infrared bands are much less intense, more amount of the sample can be used to produce a spectrum; this may reduce or eliminate the sample preparation activities. In addition, long path lengths and the ability to sample through glass in the near-infrared allows samples to be measured in common media such as culture tubes, cuvettes and reaction bottles. This is unlike mid-infrared region where very small amounts of a sample produce a strong spectrum; thus sample preparation techniques must be employed to limit the amount of the sample that interacts with the beam.

Generally, only vibrations involving hydrogen (C-H, O-H and N-H...) show measurable absorbance in the NIR region, and the corresponding absorbance values are much smaller than those of the mid-infrared bands for the same vibrations. NIR absorbance of a material depends primarily on its chemical composition and structure. Like the mid-infrared, combination bands and overtone bands correspond to the frequencies of vibrations between the bonds of the atoms making up the material. Because each different material is a unique combination of atoms, no two compounds produce the exact same near-infrared spectrum. Therefore, near-infrared spectroscopy can result in a positive identification (qualitative analysis) of each different material. In addition, the size of the peaks in the spectrum is a direct indication of the amount of material present. With modern software algorithms, near infrared is an excellent tool for quantitative analysis. NIR instruments can provide accurate, fast, reliable, non-contact measurements

Chapter IV

of critical process stream composition parameters. NIR is one of the few reliable on-line technologies that can make a non-destructive measurement of individual chemical constituents of a process sample. These on-line measurements can be useful or essential for real-time process and quality control systems.

NIR instruments can analyze most solids using NIR reflectance and most liquids and gases using NIR transmission. In transmission, the NIR light passes through the sample (liquids or gases) before it is detected. For opaque samples, including most solids, reflectance geometry is used which detects the light reflected from the sample.

NIR spectroscopy offers a practical alternative to time consuming, solvent intensive wet-testing methods and liquid chromatography techniques. NIR is ideal for quick and reliable raw material identification while also being a powerful analysis tool capable of accurate multi-component quantitative analysis. NIR is also ideal for process monitoring due to various sampling techniques and fiber optic sampling.

Strengths of NIR includes

Robust instrumentation: Spectroscopically, the NIR spectral region is very convenient for on-line instrumentation design. NIR light works well with conventional optical and optoelectronic materials. Halogen bulbs are very bright NIR sources, optical glass is transparent to NIR light and lead sulphide (PbS) is a sensitive, stable and inexpensive NIR detector.

Easy sample handling: Process NIR instrumentation is non-contact and non-destructive. No sample preparation is required. For transmission measurements, NIR instruments typically use a relatively long pathlength to maintain good sensitivity. The long pathlength makes NIR sample handling relatively easy.

Advantages of NIR include:

- No sample preparation
- Can sample through glass and packaging materials
- Nondestructive measurements
- Fast, sample throughput accurate, reliable analysis
- Reduced costs
- Time saving (can analyze 10 times more samples in a day)

Chapter IV

- Remote sampling with low cost fiber optics

In the present work, we used a Hitachi-3410 UV-Vis-NIR spectrophotometer for recording the near infrared absorption spectra of some liquid phase organic compounds. The spectrophotometer uses a tungsten lamp as the NIR source and a PbS (lead sulphide) cell as the NIR detector. It is a double beam spectrometer in which a grating is used for wavelength separation. A quartz cuvette with 1 cm path length is used as sample cell. These investigations have revealed many structural details of the molecules studied, the details of which are discussed in the next chapter.

4.3 Normal modes of vibration

The complex vibrations of a molecule are the superposition of relatively simple vibrations called the *normal modes of vibration*. Each normal mode of vibration has a fixed frequency. It is easy to calculate the expected number of normal modes for a molecule made up of N atoms. A linear molecule with N atoms has $3N-5$ normal modes of vibration and a non-linear molecule has $3N-6$ normal modes of vibration. The symmetries of the normal modes can be classified by group theory.

4.4 Vibrational spectroscopy

There are two types of spectroscopy that involve vibrational transitions. - Infrared spectroscopy and Raman Spectroscopy. Infrared spectroscopic transitions between vibrational energy levels of a molecule occur due to change in dipole moment induced by the absorption of infrared (IR) radiation. Raman scattering occurs when the vibrational transitions take place due to the change in polarizability during vibration.

At room temperature almost all molecules are in their lowest vibrational energy levels with quantum number $V = 0$. For each normal mode, the most probable vibrational transition is from this level to the next highest level ($V = 0 \rightarrow 1$). The strong IR or Raman bands resulting from these transitions are called fundamental bands. Other transitions to higher excited states ($V = 0 \rightarrow 2$, for

Chapter IV

instance) result in overtone bands. Overtone bands are much weaker than fundamental bands.

4.5 Vibrational and rotational transitions of diatomic molecules

High-resolution gas-phase IR spectra show information about the vibrational and rotational behavior of heteronuclear diatomic molecules. Vibrational transitions may be modeled by the harmonic oscillator when the bond length is near R_e (fig.4.1). In this region, the potential energy can be expressed as:

$$E = \frac{1}{2} k (R - R_e)^2 \quad (1)$$

where k is the force constant of the bond. The Schrödinger equation for a particle undergoing harmonic motion can be modified to give an equation to calculate the allowed vibrational energy levels:

$$E(v) = (v + \frac{1}{2}) h\nu \quad (2)$$

where 'h' is Planck's constant, ν is the vibrational frequency, and the vibrational quantum number $v = 0, 1, 2, \dots$

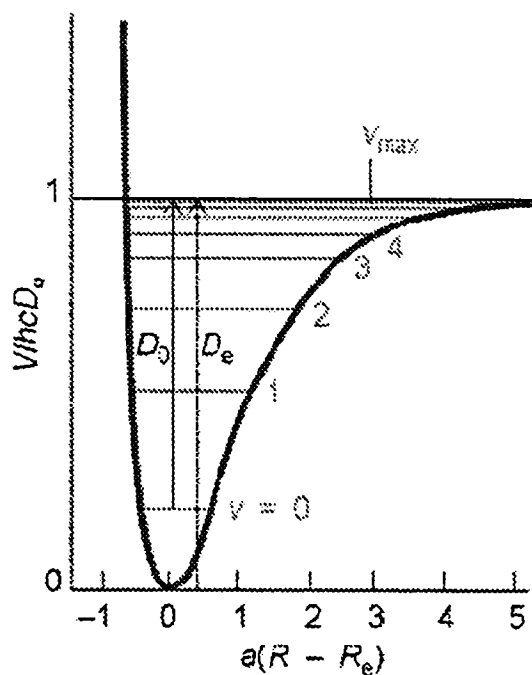


Fig.4.1. Energy levels of an anharmonic oscillator

Chapter IV

Diatomic molecules do not remain stationary as they undergo vibration; they also rotate through space. The rigid rotor model may be used to approximate the rotational contribution to the IR spectrum of a diatomic molecule. For a rigid rotor, the allowed energy levels may be calculated as:

$$E(J) = \frac{h^2}{8\pi^2 I} J(J+1) \quad (3)$$

where

$$I = \mu r^2, \quad \mu = \frac{m_1 m_2}{m_1 + m_2} \quad (4)$$

where J is the rotational quantum number (with integer values 0, 1, 2, ...), 'h' is Planck's constant, and I is the moment of inertia for the molecule (calculated as shown using the reduced mass, μ , and with $r=r_e$). Adding the vibrational and rotational energy terms gives a first approximation of the value of its energy levels. However, the potential for any real molecular system is anharmonic and also there will be effects of centrifugal stretching, and also interaction between vibration and rotation. Many model potential functions are used to represent real molecular systems [1]. An empirical expression for the energy levels (in wavenumber) for the heteronuclear diatomic molecule undergoing vibration and rotation reads as:

$$G(v, J) = \omega_e \left(v + \frac{1}{2}\right) - \omega_e x_e \left(v + \frac{1}{2}\right)^2 + B_e J(J+1) - D_e J^2(J+1)^2 - \omega_e \left(v + \frac{1}{2}\right) J(J+1) \quad (5)$$

where ω_e is the frequency for the molecule vibrating about the equilibrium bond distance r_e , and

$$B_e = \frac{h}{8\pi^2 I_e c} \quad (6)$$

The difference in energy, and thus the separation between adjacent lines (of the same isotope) in each branch of the IR spectrum, is related to B_e . The first and third terms of the equation (5) for G account for the harmonic oscillator and rigid rotor behavior of the diatomic molecule; the second term accounts for anharmonicity, the fourth term takes into account centrifugal stretching, and the last term accounts for the interaction between vibration and rotation.

4.6 Vibrational overtone excitation of polyatomic molecules in the ground electronic state

In recent years, the attention of many molecular spectroscopists all over the world has turned to the study of the different aspects of higher excited vibrational levels of the ground electronic states of polyatomic molecules containing X-H (X=C, N, O) oscillators [2-5]. The major reasons for this interest are the following; first, it is recognized in the study of radiationless electronic transitions that higher excited levels of hydrogen atom based vibrations play a key role in accepting the excited electronic energy [6-8]. Second, the normal mode model, which is found successful in describing the fundamental vibrations of molecules, fails to provide a satisfactory description to the anharmonic overtones. Third, an understanding of higher vibrational levels is essential in the development of the theory of multiphoton photochemistry as well as bond selective chemistry [9]. The spectroscopic studies of higher vibrational states are concerned with excitation of bonds to a significant fraction of their bond dissociation energies, and this can provide a link between chemical reactivity and spectroscopic properties. As already discussed in the earlier section, the development of instrumentation for NIR region made it possible to record the transitions to higher vibrational levels of molecules. Similarly, the development of more sensitive laser based techniques such as thermal lens and photoacoustic techniques, made it possible to extend the measurement of vibrational overtone transitions of many molecules to visible region where conventional spectrophotometers do not perform up to the requirements.

4.6.1 Theoretical description of higher excited vibrational levels – the Local Mode Model

If motions of molecular groups responsible for absorption on infrared radiation are harmonic, there will be no absorption of radiation at overtone and combination frequencies of fundamental vibrations. However, these molecular motions are more harmonic than other resonant vibrations in nature. The deviation from simple harmonic motion of molecular group increases with the amplitude of oscillations become very large as the amplitude approaches that required for dissociation of group. It is the function of masses and force constant 'k' of the

Chapter IV

atoms involved. Hydrogen being the lightest atom oscillates with large amplitude when undergoing stretching mode. Therefore, its motion deviates appreciably from harmonic. It is said to undergo anharmonic oscillations. The restoring force acting upon the vibrating atom is no longer is a single function of displacement from the equilibrium of the atom, but complex function of many dimensions. The degree of anharmonicity of molecular motion can be determined by measuring the difference between the observed frequencies of overtone vibrations and the simple multiple of the fundamental vibrations.

$$\nu_v = \nu_0(1 - vx) \quad (7)$$

where ν_v is the observed frequency of V^{th} harmonic ν_0 is the frequency of the fundamental vibration and 'x' is positive constant indicate anharmonicity. This simple formula is very useful for prediction or identification of overtone and combination bands.

Overtone and combination bands are observed in the infrared spectra not only because of a mechanical anharmonicity of motion, but also because of an electrical anharmonicity in the variation of displacement with motion. Absorption of infrared radiation occurs only when the displacement changes during the course of resonant vibrations with asymmetry that corresponding to a transition of the molecule [10].

Considerable interest had been focused on the success of the Local Mode (LM) model for describing higher excited vibrational levels [11-26]. Henry and Siebrand introduced this model in their attempt to model radiationless electronic transitions in polyatomic molecules [6, 27, 28]. They found that Franck – Condon factors for $T_1 \rightarrow S_0$ and $S_1 \rightarrow S_0$ transitions are governed by the anharmonicity of the CH stretching modes. They also found semi quantitative agreement between the anharmonicity parameter in the Franck – Condon factors and the known anharmonicity of the CH molecule. This led them to find a relation between the CH anharmonicity constant in the CH molecule and that in a hydrocarbon molecule. The Local Mode model is the outcome of these investigations.

The concept of local modes is complementary to that of normal modes. Normal modes arise from the analysis of vibrational motions for infinitesimal amplitudes, where the molecule is considered as $3N-6(5)$ uncoupled harmonic

Chapter IV

oscillators. Normal mode description is useful in understanding the fundamental and to some extent the lower overtones spectra of polyatomic molecules [1]. Continued pumping of energy into the vibrational modes of a molecule leads to dissociation which is a non-harmonic behavior.

Henry and co-workers used these Local Mode ideas to obtain normal mode anharmonicity constants and thus describe the overtone spectra of molecules like NH_3 , C_6H_6 , CH_2Cl_2 etc. in terms of the components of normal mode anharmonicity constants. From these studies, they concluded that higher vibrational levels of X-H ($\text{X}=\text{C}, \text{N}, \text{O}$) containing molecules cannot be described in terms of a set of symmetry allowed normal mode components, but instead by a relatively small number of most anharmonic motions namely localized excitations of bond modes [10, 29].

A quantum mechanical description of the one dimensional (single bond based) appearance of CH overtone spectra with particular application to benzene has been given by Swofford *et al* [30] in their study of the fifth overtones spectra of benzene and its deuterated analogues using thermal lens techniques. This theory forms the basis of the local mode treatment of any molecule.

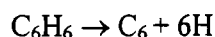
If one uses the conventional normal mode description, the number of symmetry allowed states increases with quantum number. The total number of vibrational levels increases much more rapidly with quantum number. This is given by Bose statistics by which there are ${}^{V+N-1}C_V$ ways of distributing V quanta over N sites. Thus there are 462 CH based levels at $V=6$. Of these, 150 states are allowed. These are 75 doubly degenerate states with E_1 symmetry. However, experimental observations show only a single broad peak in the aryl $\Delta V=6$ region for benzene, deuterated benzene and substituted benzenes. This clearly demonstrates the success of the Local Mode model of uncoupled anharmonic oscillators localized on individual CH bonds.

The local mode concepts and normal mode concepts are complementary. In normal modes the molecules are considered as $3N-6(5)$ uncoupled harmonic oscillators, which vibrates in infinitesimal amplitudes. This model is found to be successful in explaining the fundamental and lower overtone spectra of polyatomic molecules. Continuous pumping of energy into the vibrational modes of a molecule leads to dissociation, which is of non-harmonic in nature. Here the

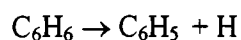
Chapter IV

molecule violates the normal mode concepts by following a low energy pathway leading to dissociation.

Consider the CH stretching vibrations of benzene. There are six identical CH bonds and hence six CH stretching vibrations [31]. These belong to various symmetry species. If we estimate the molecule with sufficiently high energy it will eventually dissociate losing six hydrogen atoms in the process



The dissociation in above equation requires almost six times the CH bond dissociation energy. But the process actually happen is



The difficulty here is that no normal vibration of benzene leads to CH stretching being localized in only one bond. These considerations together with a very early observation of up to eight quanta of CH stretching in benzene led to the concept of local mode of vibration.

For diatomic molecules the relation between anharmonicity constant X and dissociation energy D is clear from the relation

$$X = -\frac{\omega^2}{4D} \quad (8)$$

When a diatomic molecule is concerned there exist much ambiguity in the relation between normal mode anharmonicity constants X_{kk} bond dissociation energies D_i and normal mode dissociation energy D_k . Since in normal modes the vibrational energy is evenly distributed among a number of equivalent chemical bonds. The dissociation energy D_k will be the sum of all bond energies D_i

$$D_k = \sum_i D_i \quad (9)$$

This implies a large value of D_k and hence a small value for diagonal normal mode anharmonicity constants. Physically dissociation means rapture of a single chemical bond. The vibration associate with this rapture is not a normal mode but it is a local mode and $D_i \ll D_k$. thus the corresponding anharmonicity constants X_{ii} will be much larger than X_{kk} . Thus it can be inferred that for higher vibrational levels, the vibrational energy becomes increasingly more diagonal in a local mode

Chapter IV

representation than in a normal mode representation. That is the molecule will oscillate in a pattern closer to a local mode rather than a normal mode.

As early as 1928, Ellis had given the empirical evidence [32-34] for the one dimensional anharmonic oscillator in the overtone spectrum of benzene. The energy levels of a one dimensional anharmonic oscillator given by the perturbation theory as [35]

$$\Delta E_{v,0} = -\frac{1}{2}\left(X_1 + \frac{1}{2}X_2\right) + \left(V + \frac{1}{2}\right)X_1 + \left(V + \frac{1}{2}\right)^2 X_2 \quad (10)$$

Ellis fitted the observed overtone bands to the equation

$$\Delta E_{v,0} = AV + BV^2 \quad (11)$$

where A and B are constants and v is the overtone level.

The empirical constants, A and B in equation. (11) are related to equation (10) as $X_1 = A - B$ (mechanical frequency) and $X_2 = B$ (anharmonicity). X_1 and X_2 are related to conventional spectroscopic parameters through $X_1 = \omega_e$ and $X_2 = \omega_e X_e$. A plot of $\Delta E/V$ versus V (Birge-Sponer plot) for the observed bands from $V=1 - 8$ [30] yielded $A = 3095 \text{ cm}^{-1}$ and $B = -58.4 \text{ cm}^{-1}$.

The Local Mode model predicts a unique single state excitation at all V. The spectroscopic energies of these single state excitations are given by equation (1). The experimental observations are thus in agreement with the predictions of Local Mode model. Fig.4.1 shows the schematic diagram of the $0 \rightarrow V$ overtone transition. The success of the Local Mode model has again been demonstrated by comparing the $\Delta V=6$ overtone spectra of benzene and benzene d_5 . No significant difference in band shape or peak energy are observed for the two molecules in contrast to the predictions to the strongly coupled normal mode model. On the other hand, the Local Mode model predicts the similarity in the observed spectra.

The Local Mode model had been widely used to interpret the overtone spectra of a wide variety of molecules [11-26]. It is found that in addition to the pure overtones, there are combination peaks also. These combination bands arise from the excitation of more than one local mode (local-local combinations) or excitation of low frequency vibrations of the molecules along with a pure local mode (local-normal combinations). The appearance of combination bands in overtone spectra implies the presence of non-zero couplings between local

Chapter IV

modes and between local and normal modes. The magnitudes of these couplings are found to be much smaller than the diagonal Local Mode anharmonicity values. This allows the Local Mode description to be used as a good zero order picture to start within the calculations of higher vibrational spectra. Henry and co-workers [10, 29] have stated the following empirical rules to overtone spectra

- 1) Local Mode overtones involving high frequency oscillators are most intense but fall off in intensity with increasing vibrational quantum number
- 2) Local – local and local – normal combinations occur generally with much lesser intensity than pure local mode overtones
- 3) Combination bands fall off more quickly in intensity than do the pure overtones with increase in quantum number.

4.6.2 Refinements in local mode model

Many workers suggested refinements by inclusion of the terms neglected in the zero order local mode model. Sage and Jortner [36-39] used Morse oscillator function to model the CH bond potential and included the Wilson G matrix cross terms involving CH bending and stretching vibrations in the Hamiltonian.

The local mode picture uses the local mode model as the starting point and considers the interaction between the equivalent local modes and can thus be used to interpret the entire spectra at least down to first overtone level. The general form of the coupled local mode Hamiltonian used for an XH_n system is [40-43]

$$H = \omega \sum_i V_i + \omega_x \sum_i (V_i + V_i^2) + \frac{\omega}{2} \sum_{i=1}^n \sum_{j=1}^n \gamma (a_i^+ - a_i)(a_j^+ - a_j) + \frac{\omega}{2} \sum_{i=1}^n \sum_{j=1}^n \phi (a_i^+ + a_i)(a_j^+ + a_j) \quad (12)$$

Here the first two terms represent the unperturbed local mode energy and the last two terms represent the harmonic coupling between the local modes. ω and ω_x are respectively the mechanical frequency (X_1) and anharmonicity ($-X_2$) of the XH bonds, V_i and V_j are the quantum numbers for the i^{th} and j^{th} X-H bond respectively. The parameter γ characterizes the kinetic energy coupling between the different XH oscillators and ϕ the corresponding potential energy coupling. These coupling parameters are related to Wilson G and F matrix elements respectively.

$$\gamma = -\frac{1}{2} \frac{G_{ij}}{G_{ii}} \quad (13)$$

$$\varphi = \frac{1}{2} \frac{F_{ij}}{F_{ii}} \quad (14)$$

The operators a^+ and a are related to the normalized momentum coordinate variables through

$$p = (a^+ - a) \quad (15)$$

$$q = (a^+ + a) \quad (16)$$

and the usual raising and lowering properties in the harmonic oscillator limit [44]

$$\langle V+1 | a^+ | V \rangle = (V+1)^{1/2} \quad (17)$$

$$\langle V-1 | a | V \rangle = V^{1/2} \quad (18)$$

These properties are shown to be valid to a good approximation even for Morse oscillators [38]. This is called ladder approximation. Since manifolds corresponding to different values of total quantum number $(\sum_i V_i)$ are well separated in energy, inter manifold coupling are neglected.

4.7 Molecular structural details studied by overtone spectroscopy-a survey

Vibrational overtone spectroscopy has recently become a key source of information about molecular structure and the strengths of chemical bonds. The development of high sensitive spectrophotometers in the NIR region and development of ultra sensitive photothermal detection techniques like thermal lensing and photo acoustics allowed the extension of vibrational spectroscopy into Near IR and visible regions. In these spectral regions, the optical excitations are principally into high vibrational overtones of stretching vibrations involving hydrogen (C-H, N-H, O-H etc).

As already explained earlier, the overtone absorption peaks generally fit into the one dimensional equation for an anharmonic oscillator

Chapter IV

$$\Delta E_{0-v} = AV + BV^2 \quad (19)$$

where ΔE is the observed energy difference between the V^{th} quantum level and ground state. The empirical parameters of this equation lead directly to the mechanical frequency $X_1 = A/B$ and the anharmonicity $X_2 = B$ of the oscillator. It is noted that the mechanical frequencies are related to the equilibrium force constants, while both X_1 and X_2 are related to the bond dissociation. From the values of A and B found by use of Birge-Sponer equation can be used to calculate an upper bound of the dissociation energy $E_{\text{max}} = -\frac{A^2}{4B}$ of the anharmonic oscillator. In cases where this equation agrees with the experimental measurements of bond dissociation energies, then the Birge-Sponer equation must be valid for energies close to the dissociation limit.

The concept of spectroscopic evidence for the strengths of individual bonds is not a new one. But much of the earlier evidences are circumstantial owing to the complicated mixing and resonance in the usual IR spectrum of the fundamental molecular vibrations. The important spectroscopic evidence for the influence of conformation on individual bond strengths was first clearly demonstrated in the elegant IR studies by McKean and coworkers on nearly fully deuterated compounds. The deuteration of all sites but one almost always removes the spectral complications in the IR absorption, revealing clearly the factors, which influence the individual C-H bond strengths.

The most important application of spectroscopy finds its place in the characterization of CH bonds in organic compounds. This serves as sensitive probe into the structural information in polyatomic molecules. From the IR spectroscopic studies it is difficult to understand the influence of environment on a particular CH oscillator. There are a lot of additional advantages in opting for overtone spectral studies. First is the practical reason that one can avoid the dependence on deuterated samples, which are often not readily available. The overtone bands are quite well resolved, even for very similar X-H oscillators. Second, the stretching frequency parameters obtained from fitting a number of sequential overtones for each LM oscillator promise higher precision than single measurements in IR. The work also gives the anharmonicity of the LM oscillators. In contrast, the IR studies

Chapter IV

give only the frequencies of isolated oscillators, which are related to the equilibrium bond strengths.

The local mode parameters X_1 and X_2 are characteristics of the particular CH oscillator and thus gives rise to distinct absorption peaks corresponding to the distinct non-equivalent CH oscillators in the molecule. The non-equivalence of CH oscillators occurs because of many reasons. It is well known that the aryl and alkyl CH bonds are non-equivalent due to the difference on states of carbon hybridization. In an alkane there exist non-equivalent CH bonds as primary, secondary and tertiary. Non-equivalence of CH bonds can also arise from conformational origin, inter and intramolecular environmental origin etc.

The local mode model in the original and refined forms has been used successfully to interpret and understand X-H stretching overtone spectra of a number of molecules. There is a very sensitive correlation between changes in CH bond lengths and shifts in CH stretching overtone frequencies. Overtone spectra provide the most sensitive experimental method for detecting these bond length changes at the level of accuracy (0.001 Å) currently provided by *ab initio* molecular geometry optimization. A modified Morse potential is used to provide a theoretical basis for this frequency – bond length correlation and to explain other similar relationships for diatomic molecules [45].

The length of a chemical bond is associated with its strength and by implication, with its chemical reactivity. Local mode model and overtone spectroscopy can be used to determine change in X-H bond lengths and to investigate molecular conformations. In particular, C-H bond length changes that occur upon chemical substitution can be detected with an accuracy of 0.001 Å, i.e., at the same level as *ab initio* approaches [4].

Information about structurally nonequivalent X-H bond lengths can be obtained from the fundamental IR spectra only by selective deuteration method. The X-H oscillators in such selectively deuterated molecules can be thought of as chemically produced local modes. Changes in this isolated stretching fundamental frequency for different molecules correlate remarkably well with the changes in X-H bond lengths. For an isolated C-H oscillator, a shift of 10 cm^{-1} in the fundamental region corresponds to a bond length change of 0.001 Å. Overtone shifts are an extremely sensitive to such small changes in C-H bond length. At

Chapter IV

$\Delta V=6$, a bond length change of 0.001 Å corresponds to a frequency shift of 69 cm^{-1} [46]. These overtone spectral studies are convenient for such structural investigations in the sense that the difficult synthetic procedures involved with the selective deuteration process are not required.

Mizugai *et al* [47] and Gough and Henry [48, 49], in their study of substituted benzenes, noted a correlation between shift in CH overtone frequencies and change in CH bond lengths with respect to benzene. The bond length- overtone shift correlation can conveniently be used [48] to determine the CH bond lengths in substituted benzenes from that in benzene (1.084 Å), and the overtone frequency shift relative to benzene $\Delta\bar{\nu}$ for a given overtone ΔV_{CH} . Clearly the overtone method gives a means of determining change in CH bond length rather than the absolute values [50]. The correlation between the two reads as:

$$r_{\text{CH}}^{\text{LM}}(\text{Å}) = 1.084 - \left(\frac{\Delta\bar{\nu}}{11\Delta V_{\text{CH}}} \right) 0.001 \quad (20)$$

This relation is used to determine CH bond lengths from the CH bond length in benzene and the overtone frequency shift $\Delta\bar{\nu}(\text{cm}^{-1})$ from benzene for a given overtone ΔV_{CH} .

In the spectrum of p-fluorotoluene, the aryl overtone region consists of a clear doublet with peaks of equal intensity [49]. These peaks are associated with two types of nonequivalent CH bonds. Their splitting increases with overtone level in accordance with equation (20). The higher Frequency peaks corresponds to the CH bonds ortho to the fluorine substituent. The combined effect of σ - electron withdrawal and π - electron donation by fluorine substituents cause aryl CH bonds to shorten. A remarkably consistent correlation exists between frequency shifts of overtone peaks associated with nonequivalent CH bonds and *ab initio* predicted bond length changes. In fact, overtone spectra provide the best currently available experimental tool for determining the difference in CH bond lengths at the level of accuracy provided by the *ab initio* molecular orbital theories [4].

Kjaergaard *et al* [51] carried out the overtone spectral investigation on the difference in C-H bond length values in pyridine. They used both intracavity laser photoacoustic spectroscopy (ICL-PAS) and conventional near infrared absorption

Chapter IV

spectroscopy to measure the room temperature C-H stretching overtone spectra of pyridine in both liquid and vapor phase. The peaks corresponding to three nonequivalent CH stretching local modes are assigned in the vapor phase overtone spectra. Absolute oscillator strengths are obtained from the conventional spectra and the relative oscillator strengths between observed peaks within a given overtone from the photoacoustic spectra. Oscillator strengths are calculated with an anharmonic oscillator local mode model and *ab initio* dipole moment functions.

A theoretical basis for the correlation between bond length and local mode frequency is reported by Swanton *et al* [52]. They constructed a modified Morse potential, which allows obtaining equations, which relate the equilibrium internuclear distance in a Morse oscillator ' r_e ' to the experimental quantities ω_e and $\omega_e X_e$.

An important aspect of LM picture of independent X-H oscillators is that the conformationally nonequivalent hydrogen among otherwise "chemically equivalent" moieties should show distinct transition frequencies and anharmonicities in the absorption spectrum. The essentially instantaneous optical absorption resolves the distinct absorption energies even in the cases of relatively low (0.5–1 kcal/mol) barriers to internal rotations. This work demonstrates this conformational sensitivity for methyl groups. The sensitivity of the overtones to small conformational influences may make overtone spectroscopy an important tool for conformational studies.

The first application of local mode model and overtone spectroscopy to the investigation of molecular conformation occurred in the studies of the liquid phase spectra of hexamethylbenzene [53] and the cyclic alkanes [54]. In these studies, the spectral structure was explained on the basis of contributions from non-equivalent C-H bonds, where the corresponding overtone peaks are well resolved [46, 48, 49]. The significance of these experiments is that overtone spectra could give information about conformational features that is totally inaccessible to techniques like N M R.

In *o*-fluorotoluene and *o*-xylene, two peaks are observed in methyl region with an area ratio of 2:1. The studies on *o*-fluorotoluene [55] and *o*-xylene [56] revealed that the most stable conformer is planar one where methyl groups have

Chapter IV

one CH bond in ring plane and the two at 60° . The in-plane CH bond is to be shorter than the two out of plane at 60° , and from spectral splitting; this difference amounts to 0.003 Å. These results are found to agree with ab initio calculations.

The vibrational overtones of C-H oscillators, in liquid phase diethyl ether and dimethoxyethane, measured by conventional and thermal lensing spectroscopy and those in gas phase dimethyl ether, dimethoxyethane, diethyl ether, dimethyl sulphide, trimethylamine, methyl formamide and acetaldehyde measured by photoacoustic spectroscopy are reported by Fang *et al* [15, 19, 57-59]. New results of gas phase butanone and 2-pentanone are compared with previous measurements of acetone. In all the molecules studied where a methyl group is a conformationally anisotropic environment created by an adjacent hetero atom containing one or two lone pair of electrons (N, O, S), or a carbonyl group, two distinct bands at each overtone are seen which are assigned as the overtones of nonequivalent methyl C-H bonds. The influence of lone pair interactions in vibrational spectra is well documented in earlier IR studies [60, 61] also. Bellami and Mayo [60] provide an extensive discussion of lone pairs of electron effects and suggests that the effect originates from the donation of electron density from the lone pair into the antibonding orbital of a C-H situated trans with respect to the lone pair. This phenomenon is known as lone pair trans effect. The sensitivity of the overtones of methyl C-H stretching vibrations to differences in conformational environment is thus well demonstrated in the work of Fang *et al*.

Kuriakose *et al* [62] studied the overtone spectrum of formamide in the near infrared region and observed the inhibition of lone pair effect in this molecule. Vijayan *et al* studied the overtone spectrum of cinnamaldehyde in the NIR region and observed the presence of the indirect lone pair trans effect [63].

Ahmed *et al* [22] reported a local mode analysis of the overtone spectra of some monosubstituted cyclopropanes. The room temperature, liquid phase overtone spectra of $\Delta V_{\text{CH}}=2-6$ and $\Delta V_{\text{NH}}=2-6$ of cyclopropyl bromide, cyclopropyl cyanide, cyclopropyl amine, cyclopropyl methyl ketone and chloromethyl cyclopropane are recorded, and the local mode parameters are calculated.

Chapter IV

Inequivalent C-H oscillators in alkanes and alkenes are studied using gas phase laser photoacoustic overtone spectroscopy by Wong *et al* [46]. The overtone spectra of the C-H stretching vibrations of several gaseous alkanes and alkenes were observed using a laser photoacoustic spectroscopy. Resolvable peaks are observed for each chemically or sterically equivalent C-H bond and were assigned using local mode model.

The gas phase overtone spectra of the fluorobenzenes provided very sensitive information about the non-equivalent aryl CH bond lengths. These bond length changes correlate remarkably well with changes predicted by *ab initio* MO theories. These spectra can be used to obtain information about molecular conformations. The gas phase spectrum of 1,3-difluorobenzene at $\Delta V_{CH} = 3, 4$ and 5 consists of three unresolved peaks [49] which can be decomposed into three component Lorentzians with appropriate area ratios of 1:2:1 and the peaks can be identified with three nonequivalent C-H bonds, where the center peak of greatest intensity corresponds to H(4) and H(6). The combined effect of σ electron withdrawal and π electron donation by fluorine substituent causes the aryl CH bonds to shorten (frequency to increase – electron withdrawing).

The gas phase overtone spectra of toluene and xylenes at $\Delta V_{CH} = 3$ and 4 show two well resolved series of peaks [49] one set corresponding to aryl CH bonds and the other to methyl CH bonds. In these molecules, methyl substitution causes the aryl CH bond lengths to increase (the overtone frequency to decrease) with respect to benzene, resulting from the electron donating nature of the methyl group. For toluene also, there are two aryl peaks one at a lower frequency and the other at the same frequency as the corresponding peak in benzene. The frequency separation between these aryl peaks corresponds to a bond length difference of 0.002 \AA . The higher frequency aryl peaks in toluene correspond to meta and para CH and the lower frequency peaks to CH bonds.

In the intracavity dye laser photoacoustic spectra of *o*-, *m*-, and *p*-fluorotoluenes, two sets of peaks are evident. At $\Delta V=5$, centered around $14,000 \text{ cm}^{-1}$ corresponding to aryl CH bonds and around $13,000 \text{ cm}^{-1}$ corresponding to methyl CH overtones. The methyl CH overtones display a structure (splitting) that occurs due to conformationally nonequivalent methyl CH bonds [4].

Chapter IV

A study of temperature dependence of vibrational overtones in gas phase ethanol is carried out by Fang *et al* [64]. The vibrational overtone spectra for ethanol vapor in the region 10150–19900 cm^{-1} is measured by ICL-PAS technique. The OH overtones are composed of two sub bands, which are assigned as the transitions of two conformers of OH bond in the *trans* or *gauche* position with respect to the methyl group. From the temperature dependence of the OH overtone intensity, the enthalpy difference between the conformers is determined to be 0.7 kcal/mole.

A five dimensional local mode Fermi resonance model for overtone spectra of ammonia has been constructed by Kauppi *et al* [65]. The model Hamiltonian is expressed in terms of curvilinear internal valence coordinates and it includes three stretching vibrations and the doubly degenerate bending vibration.

Homogeneous and inhomogeneous structure in the vibrational overtone spectrum of tetramethyldioxetane is studied by McGinley *et al* [66]. Vibrational overtone photodissociation spectra of tetramethyldioxetane is obtained by monitoring the products of the vibrational overtone initiated unimolecular decomposition. C-H stretching overtone spectra of trimethylene oxide and trimethylene sulphide are reported by Turnbull *et al* [67]. They have recorded the room temperature vapor phase C-H stretching overtone spectra of these compounds in the $\Delta V_{\text{CH}} = 2-7$ region using conventional spectrophotometer and intra cavity laser photoacoustic spectroscopy. The spectra are interpreted with local mode model and are assigned in part on the basis of *ab initio* calculated C-H bond lengths.

Temperature and phase effects on the overtone spectra of several adamantanes are reported by Howard *et al* [68]. They reported the overtone spectra of adamantane, 1-chloroadamantane and hexamethylenetetramine recorded in various phases and several temperatures using conventional infrared spectroscopy and intra cavity laser photoacoustic spectroscopy. The phase effects and temperature effects on the overtone spectra are discussed.

Cavity ring-down overtone spectroscopy of HCN, H^{13}CN and H^{15}CN is done by Romanini *et al* [69]. They reported the results of cavity ring down overtone spectroscopy to extend the study of highly excited vibrational states in HCN and its isotopomers.

Chapter IV

Rotations and local modes in stannane are investigated by Zhan *et al* [70], using photoacoustic overtone spectra recorded with a Ti: Sapphire ring laser. The fifth and seventh stretching vibrational overtone bands of a monoisotopic stannane sample are recorded under Doppler limited resolution, using ICL-PAS. The rotational fine structure of these bands is analyzed. Vibrational overtone transitions of OCS in the near infrared, $10,000 - 14,000 \text{ cm}^{-1}$ are recorded using photoacoustic technique by Yang *et al* [71]. The spectra are analyzed using molecular parameters and Hamiltonians derived for OCS and the observed transitions are well assigned.

The vibrational overtone spectra of gaseous alcohols are reported by Fang *et al* [72]. The overtone absorption spectra of gaseous 1-propanol, 2-propanol and *tert* butyl alcohol are measured with ICL- PAS and FTIR spectroscopy. Prominent features in the spectra are assigned as OH and CH stretching overtones within the local mode model of loosely coupled anharmonic vibrations. Remaining features are assigned as combinations involving a local mode overtone and lower frequency motions of the molecules.

Experimental and *ab initio* investigations for the OH overtone vibration of ethanol are reported by Weibel *et al* [73]. The intracavity dye laser photoacoustic absorption spectra of ethanol, ethanol (1, 1-d₂) and ethanol (2, 2, 2-d₃) are reported for the region $16550 - 16700 \text{ cm}^{-1}$, which contains the OH fourth overtone vibrations. The distinct absorption bands have been assigned to the *trans* and *gauche* conformational isomers. Absorption spectra of gas phase methanol ($10150 - 19900 \text{ cm}^{-1}$) and methanol -d ($10150 - 17600 \text{ cm}^{-1}$) are recorded by intracavity dye laser photoacoustic spectroscopy by Fang *et al* [74]. The prominent features in the spectra are assigned as OH, OD and CH overtones within the local mode model of loosely coupled anharmonic vibrations. Relatively less intense peaks are assigned as combinations involving an LM overtone and lower frequency motions in the molecules.

Overtone spectra of CH and OH stretching vibrations in normal, secondary and tertiary butanol, are reported by Rai *et al* [75]. A large number of combinations and overtone bands along with the fundamentals have been measured and assigned successfully. The vibrational frequency, anharmonicity constant and dissociation energy for the CH and OH stretch motions in respective molecules are obtained. The $\Delta V=3, 4$ and 5 vibrational overtones and conformations of

Chapter IV

hydroxyl group of isobutyl alcohol is reported by Xu *et al* [76]. The OH stretching $\Delta V = 3, 4$ and 5 vibrational overtone spectra of isobutyl alcohol are measured by using cavity ring-down spectroscopy (CRDS), where the observed three bands for OH overtones are assigned to the three kinds of conformations of the hydroxyl group.

Similarly the CRDS of OH stretching overtones in 2-butanol in the $\Delta V=3, 4$ and 5 regions are reported by Xu *et al* [77]. The observed OH stretching bands are assigned to vibrations of different conformations of 2-butanol and further confirmed by density functional theory (DFT) calculations. Intensities for several OH vibrational overtone bands have been measured for vapor phase methanol, ethanol and isopropanol by Phillips *et al* [78]. The trends in intensities as a function of excitation level have been modeled by two empirical approaches, yielding intensity predictions for the higher overtone transitions up to 7ν (OH).

A direct correlation method for OH, NH and CH local modes is described by Fedorov *et al* [79]. The vibrational overtone spectra of gaseous biphenyl, anthracene, isobutanol, 2-chloroethanol and ethylenediamine at the $\Delta V=4$ vibrational overtone region have been recorded by ICL-PAS and assigned using the local mode model. Overtone spectroscopy of the hydroxyl stretch vibration in hydroxylamine (NH_2OH) is recorded in the second ($3\nu_{\text{OH}}$), third ($4\nu_{\text{OH}}$) and fourth ($5\nu_{\text{OH}}$) regions by photoacoustic spectroscopy. Asymmetric rotor simulations of the rovibrational contours provide rotational constants and then estimate of homogenous line width. An internal coordinate Hamiltonian model has been constructed to model torsional motion in the OH stretching vibrational overtone region of methanol (CH_3OH) by Hanninen *et al* [80]. The model includes harmonic couplings between OH and CH stretching vibrations and Fermi resonance interactions between OH stretches and COH bends and between CH stretches and CH_2 bends.

Vibrational overtone spectroscopy is an effective tool in studying inter/intra molecular hydrogen bonding also. The presence of inter/intra molecular hydrogen bond will be well reflected in the mechanical frequency and hence the energy values of the overtone transitions. The presence of intramolecular hydrogen bond in *o*-chlorophenol and *o*-chloroaniline is established by our analysis of CH and NH

Chapter IV

overtone in aniline and chloroanilines [81]. Eappen *et al* analyzed the aryl CH and OH overtone spectrum of α -naphthol and found that there exists intramolecular hydrogen interaction between the hydroxyl group and aromatic nucleus [82].

In the present work we studied the liquid phase NIR overtone spectra of chloroanilines, toluidines and alkyl anilines. The analysis of these spectra has revealed new structural information about these molecular systems. The details are given in chapter V.

Moreover, as already described in chapter II, we successfully used a narrow bandwidth NIR tunable diode laser to record the high resolution, rotationally resolved, second overtone spectra of OH local mode in water vapour and alcohols. This novel method has many advantages over the earlier works.

4.8 Intensity aspects in overtone spectra

Overtone intensity decreases by approximately a factor of 10 at each higher overtone level so the transition became extremely weak. Vibrational fundamental and overtone band intensities of H₂O is calculated by Kjaergaard *et al* [83]. Vibrational intensities are calculated for fundamental and overtone transitions of H₂O up to 18000 cm⁻¹. The intensities are determined from a dipole moment function expanded in the three internal band coordinates. The expansion coefficients are computed *ab initio* at the second order Moller – Plesset level of theory with a 6-31 G* basis set. Vibrational wave functions are calculated from a three-dimensional harmonically coupled anharmonic oscillator (HCAO) model.

Calculations of O-H stretching vibrational intensities of hydrogen peroxide are performed with a harmonically coupled anharmonic local mode model for the O-H stretching vibrational wave functions and *ab initio* calculations to obtain the dipole moment function is reported by Kjaergaard *et al* [84]. Intensities in local mode overtone spectra of propane is reported by Kjaergaard *et al* [85]. The gas phase vibrational overtone spectrum of propane is measured using conventional near infrared spectroscopy for $\Delta V_{CH}=2-5$ regions and intra cavity dye laser photoacoustic spectroscopy for $\Delta V_{CH}=5-6$ regions. The peaks are assigned in terms of the local mode model and the experimental oscillator strengths are compared to calculated values for C-H stretching components of the spectra.

Chapter IV

The relative intensity contributions of axial and equatorial C-H bonds in the local mode overtone spectra of cyclohexane are studied by Kjaergaard *et al* [86]. The vapor phase room temperature overtone spectra of cyclohexane are measured with conventional near infrared spectroscopy for lower overtones $\Delta V_{\text{CH}} = 2 - 4$ and with intracavity dye laser photoacoustic spectroscopy for the higher overtones $\Delta V_{\text{CH}} = 5 - 7$. The relative intensity of the axial to equatorial peak is explained in terms of the local mode model of harmonically coupled anharmonic oscillator. Intensity of C-H and N-H stretching transitions on the overtone spectra of cyclopropylamine is reported by Niefer *et al* [87]. They have recorded both the C-H stretching ($\Delta V_{\text{CH}}=2-7$) and N-H stretching ($\Delta V_{\text{NH}}=2-6$) regions of vapor phase room temperature overtone spectra of cyclopropylamine is measured with conventional absorption spectroscopy for lower overtones and intra cavity laser photoacoustic spectroscopy for higher overtones. The relative intensities of X-H stretching peaks are explained in terms of the local mode model of harmonically coupled anharmonic oscillators. Intensities for several OH vibrational overtone bands have been measured for vapor phase methanol, ethanol and isopropanol by Phillips *et al* [78]. The trends in intensities as a function of excitation level have been modeled by two empirical approaches, yielding intensity predictions for the higher overtone transitions up to 7ν (OH).

References

- [1] G.Herzberg; *"Infrared and Raman spectra of polyatomic molecules"*, Van Nostrand, New York, 1945.
- [2] B.R.Henry, *"Vibrational spectra and structure"*, ed. Durig J R (Elsevier, Amsterdam.) 10 (1981) 269.
- [3] M.S.Child and L.Halonen; *Adv. Chem. Phys.*, 57 (1984) 1.
- [4] B.R.Henry; *Acc. Chem. Res.*, 20 (1987) 429.
- [5] M.Quack; *Ann. Rev. Phys. Chem.*, 41 (1990) 839.
- [6] B.R.Henry and W.Siebrand; *J. Chem. Phys.*, 49 (1968) 5369
- [7] E.W.Schlag, S.Schneider and S.F.Fischer; *Ann. Rev. Phys. Chem.*, 22 (1971) 465.
- [8] T.M.A.Rasheed; *"Laser induced thermal lens and near infrared absorption studies of CH overtones in some organic compounds"*, Ph.D. Thesis, Cochin University of Science and Technology, 1987.
- [9] M.Quack; *Adv. Chem. Phys.*, 50 (1982) 395.
- [10] B.R.Henry; *Acc. Chem. Res.*, 10 (1977) 207
- [11] W.R.A Greenlay and B.R.Henry; *Chem. Phys. Lett.*, 53(2) (1978) 325.
- [12] B.R.Henry and J.A.Thomson; *Chem. Phys. Lett.*, 69 (1980) 275.
- [13] B.R.Henry, M.A.Mohammadi and J.A.Thomson; *J. Chem. Phys.*, 75 (1981) 3165
- [14] R.Nakagaki and I.Hanazaki; *Chem. Phys. Lett.*, 83 (1981) 512
- [15] H.L.Fang and R.L.Swofford; *Appl. Opt.*, 21 (1982) 55
- [16] K.M.Gough and B.R.Henry; *J. Phys. Chem.*, 87 (1983) 3433
- [17] K.M.Gough and B.R.Henry; *J. Phys. Chem.*, 88 (1984) 1298
- [18] A.W.Tarr and B.R.Henry; *Chem. Phys. Lett.*, 112 (1984) 295.
- [19] H.L.Fang, R.L.Swofford, M.McDevitt and A.R.Anderson; *J. Phys. Chem.*, 89 (1985) 225
- [20] M.K.Ahmed, D.J.Swanton and B.R.Henry; *J. Phys. Chem.*, 91 (1987) 293.
- [21] M.K.Ahmed and B.R.Henry; *J. Phys. Chem.*, 91 (1987) 3741
- [22] M.K.Ahmed and B.R.Henry; *J. Phys. Chem.*, 91 (1987) 5194.
- [23] M.G.Sowa, B.R.Henry and Y.Mizugai; *J. Phys. Chem.*, 97 (1993) 809.
- [24] H.G.Kjaergaard and B.R.Henry; *J. Phys. Chem.*, 99 (1995) 899.

Chapter IV

- [25] D.M.Turnbull, M.G.Sowa and B.R.Henry; *J. Phys. Chem.*, 100 (1996) 13433.
- [26] H.G.Kjaergaard, D.M.Turnbull and B.R.Henry; *J. Phys. Chem.*, 101 (1997) 2589.
- [27] W.Siebrand; *J. Chem. Phys.*; 46 (1967) 440; *ibid* 47 (1967) 2411.
- [28] W.Siebrand and D.F.Williams; *J. Chem. Phys.*; 49 (1968) 1860.
- [29] B.R.Henry; *J. Phys. Chem.*, 80 (1976) 2160.
- [30] R.L.Swofford, M.E.Long and A.C.Albrecht; *J. Chem. Phys.*, 65 (1976) 179.
- [31] J.M.Hollas; "*High Resolution Spectroscopy*", II ed. John Wiley & Sons, 1998, p. 250.
- [32] J.W.Ellis; *Trans. Faraday. Soc.*, 25 (1929) 888.
- [33] J.W.Ellis; *Phys. Rev.* 32 (1928) 906.
- [34] J.W.Ellis; *Phys. Rev.* 33 (1929) 27.
- [35] E.B.Wilson, Jr, J.C.Decius and P.C.Gross; *Molecular Vibrations*, Mc Graw Hill New York, 1945.
- [36] M.L.Sage and J.Jortner; *Adv. Chem. Phys.*, 47 (1981) 293.
- [37] M.L.Sage; *Chem. Phys.*, 35 (1978) 375.
- [38] M.L.Sage and J.Jortner; *Chem. Phys. Lett.*, 62 (1979) 451.
- [39] M.L.Sage; *J. Phys. Chem.*, 83 (1979) 1455.
- [40] O.S.Mortensen, B.R.Henry and M.A.Mohammadi; *J. Chem. Phys.*, 75 (1981) 4800.
- [41] M.K.Ahmed and B.R.Henry; *J. Phys. Chem.*, 90 (1986) 1081.
- [42] T.M.A.Rasheed, V.P.N.Nampoori and K.Sathyanandan; *Chem. Phys.*, 108 (1986) 349.
- [43] B.R.Henry, A.W.Tarr, O.S.Mortensen, W.F.Murphy and D.A.C.Compton; *J. Chem. Phys.*, 79 (1983) 2583.
- [44] L.I.Schiff; "*Quantum Mechanics*" 3rd edition McGraw-Hill, 1968 p.182
- [45] B.R.Henry and D.J.Swanton; *J. Mol. Struct. (Theochem)*, 202 (1989) 193.
- [46] J.S.Wong and C.B.Moore; *J. Chem. Phys.*, 77 (1982) 603.
- [47] Y.Mizugai and M.Katayama; *Chem. Phys. Lett.*, 73 (1980) 240.
- [48] K.M.Gough and B.R.Henry; *J. Am. Chem. Soc.*, 106 (1984) 2781.
- [49] K.M.Gough and B.R.Henry; *J. Phys. Chem.*, 88 (1984) 1298.
- [50] B.R.Henry, K.M.Gough and M.G.Sowa; *Int. Rev. Phys. Chem.*, 5 (1986) 133.

Chapter IV

- [51] H.G.Kjaergaard, R.J.Proos, D.M.Turnbull and B.R.Henry; *J. Phys. Chem.*, 100 (1996) 19273.
- [52] D.J.Swanton and B.R.Henry; *J. Chem. Phys.* 86 (1987) 4801.
- [53] B.R.Henry and W.R.A.Greenlay; *J. Chem. Phys.*, 72 (1980) 5516.
- [54] B.R.Henry, I.F.Hung, R.A.MacPhail and H.L.Strauss; *J. Am. Chem. Soc.*, 102 (1980) 515.
- [55] J.Susskind; *J. Chem. Phys.*, 53 (1970) 2492.
- [56] H.D.Rudolph, K.Walzer and I.Krutzik; *J. Mol. Spectrosc.*, 47 (1973) 314.
- [57] H.L.Fang, D.M.Meister and R.L.Swofford; *J. Phys. Chem.*, 88 (1984) 410.
- [58] H.L.Fang, D.M.Meister and R.L.Swofford; *J. Phys. Chem.*, 88 (1984) 405.
- [59] I.A.Findson, H.L.Fang, R.L.Swofford and R.R.Birge; *J. Chem. Phys.*, 84 (1986) 16.
- [60] L.J.Bellamy and D.W.Mayo; *J. Phys. Chem.*, 80 (1976) 1217.
- [61] L.J.Bellamy; *Appl. Spectrosc.*, 33 (1979) 439.
- [62] S.Kuriakose, K.K.Vijayan, S.M.Eapen, S.Shaji, K.P.R.Nair and T.M.A.Rasheed; *Asian. J. Spectrosc.*, 6 (2002) 43.
- [63] K.K.Vijayan, S.Kuriakose, S.Shaji, S.M.Eapen, K.P.R.Nair and T.M.A.Rasheed; *Asian J. Spectrosc.*, 5 (2001) 185.
- [64] H.L.Fang and R.L.Swofford; *Chem. Phys. Lett.*, 105 (1984) 5.
- [65] E.Kauppi and L.Halonen; *J. Chem. Phys.*, 103 (1995) 6861.
- [66] E.S.McGinley and F.F.Crim; *J. Chem. Phys.*, 85 (1986) 5741.
- [67] D.M.Turnbull, M.G.Sowa and B.R.Henry; *J. Phys. Chem.*, 100 (1996) 13433.
- [68] D.L.Howard and B.R.Henry; *J. Phys. Chem.*, 102 (1998) 561.
- [69] D.Romanini and K.K.Lehmann; *J. Chem Phys.* 102 (1995) 633.
- [70] X.Zhan, M.Halonen, L.Halonen, H.Burger and O.Polanz; *J. Chem. Phys.*, 102 (1995) 3911.
- [71] X.Yang and C. Noda; *J. Mol. Spectrosc.*, 183 (1997) 151.
- [72] H.L.Fang and D.A.C.Compton; *J. Phys. Chem.*, 92 (1988) 6518.
- [73] J.D.Weibel, C.F.Jackels and R.L.Swofford; *J. Chem. Phys.*, 117 (2002) 4245.
- [74] H.L.Fang, D.M.Meister and R.L.Swofford; *J. Phys. Chem.*, 88 (1984) 405.
- [75] S.B.Rai and P.K.Srivastava; *Spectrochim. Acta A.*, 55 (1999) 2793.
- [76] S.Xu, Y.Liu, J.Xie, G.Sha and C.Zhang; *J. Phys. Chem. A.*, 105 (2001) 6048.

Chapter IV

- [77] S.Xu, Y.Liu, G.Sha, C.Zhang and J. Xie; *J. Phys. Chem. A.*, 104 (2000) 8671.
- [78] J.A.Phillips, J.J.Orlando, G.S.Tyndall and V.Vaida; *Chem. Phys. Lett.*, 296 (1998) 377.
- [79] A. V. Federov and D.L.Snavely; *Chem. Phys.*, 254 (2000) 169.
- [80] V. Hanninen, M. Horn and L. Halonen; *J. Chem. Phys.*, 111 (1999) 3018.
- [81] S.Shaji and T.M.A.Rasheed; *Spectrochim. Acta. A.*, 57 (2001) 337
- [82] S.M.Eappen, S.Shaji and K.P.R.Nair; *Asian. J. Spectrosc.*, 2 (2001) 89.
- [83] H.G.Kjaergaard, B.R.Henry, H.Wei, S.Lefebvre, T.Carrington Jr., O.S.Mortensen and M.L.Sage; *J. Chem. Phys.*, 100 (1994) 6228.
- [84] H.G.Kjaergaard, J.D.Goddard and B.R.Henry; *J. Chem. Phys.*, 95 (1991) 5556.
- [85] H.G.Kjaergaard, H.Yu, B.J.Schattka, B.R.Henry and A.W.Tarr; *J. Chem. Phys.*, 93 (1990) 6239.
- [86] H.G.Kjaergaard and B.R.Henry; *J. Chem. Phys.*, 96 (1992) 4841.
- [87] B.I.Niefer, H.G.Kjaergaard and B.R.Henry; *J. Chem. Phys.*, 99 (1993) 5682.

Chapter V

**VIBRATIONAL OVERTONE SPECTRAL ANALYSIS OF
CHLOROANILINES, TOLUIDINES AND SOME
ALKYL ANILINES**

	Page
5.1 Introduction.....	107
5.2 Experimental	108
5.3 Results and discussion	109
5.3.1 Analysis of the overtone spectra of aniline and chloroanilines.....	109
5.3.2 Analysis of overtone spectra of toluidines.....	122
5.3.3 Analysis of vibrational overtone spectra of N-methylaniline, N,N- dimethylaniline and N,N-diethylaniline.....	136
References.....	149

Chapter V

VIBRATIONAL OVERTONE SPECTRAL ANALYSIS OF
CHLOROANILINES, TOLUIDINES AND SOME
ALKYL ANILINES

5.1 Introduction

As described in detail in the previous chapter, the local mode model treats the X-H bonds in molecules as loosely coupled anharmonic oscillators. To a first approximation, the overtone transition energies obey the relation

$$\Delta E_{0 \rightarrow v} = AV + BV^2 \quad (1)$$

where V is the quantum level of excitation, $A = X_1$ is the mechanical frequency and $B = X_2$ is the anharmonicity of the X-H bond. The local mode parameters X_1 and X_2 distinguish between both chemically inequivalent X-H oscillators and conformationally inequivalent X-H oscillators and are sensitive to the inter/intramolecular environment in which the X-H oscillator resides. Overtone spectroscopy has thus become an effective tool for the study of molecular structure, inter and intramolecular interactions, conformational aspects and substituent effects in aliphatic and aromatic compounds [1-16].

Aniline and its derivatives are important starting materials in pharmaceutical and other chemical industries. Investigations on the intramolecular interactions, structural details and conformations of these molecules are therefore important in understanding their molecular properties and related chemical reactions. The additional substituents in aniline derivatives are expected to affect the π electron interaction and molecular geometry. The methyl and amino groups are electron-donating substituents in aromatic ring systems. The CH_3 group interacts with the nearby π system via hyperconjugation. In aniline and aromatic amines the lone pair associated with the nitrogen atom gets conjugated with the electron cloud of the benzene ring [17, 18, 19]. The effect of conjugation is the donation of electrons from the N-H bond to the ring C-H oscillator. In substituted anilines the conformational change in the molecules, at low temperature or in a suitable solvent, affect the electronic transitions [20, 21]. Also the properties of

aromatic amine molecules are sensitive to the orientation of NH₂ group [22]. It is well known that the interaction of lone pair with π electrons of the ring can lead to non-radiative process like intersystem crossing. In an attempt to draw conclusions about their structural details, we carried out an overtone spectral study of some of the aniline derivatives.

This chapter describes our analysis of the NIR vibrational overtone spectra of liquid phase aniline, *ortho*, *meta* and *para* isomers of chloroanilines, *ortho*, *meta* and *para* isomers of toluidine and N-methylaniline, N, N-dimethylaniline and N, N-diethylaniline, using local mode model. The analysis confirms the presence of intramolecular hydrogen bonding in *o*-chloroaniline [19], supporting predictions of earlier microwave spectroscopic studies. The analysis confirms the presence steric and electronic effects in *o*-toluidine, supporting results of recent laser induced (LIF) and resonance two photon ionization spectroscopy (R2PI) studies. The effect of molecular conformations in dialkylanilines is reflected in the overtone spectral data.

5.2 Experimental

High purity (>99%) aniline, *o*-chloroaniline, *m*-chloroaniline, *p*-chloroaniline, N-methylaniline, N,N-dimethylaniline and N,N-diethylaniline from Central Drug House Pvt. Ltd, Bombay (India) and *o*-toluidine, *m*-toluidine and *p*-toluidine from Sisco Research Laboratories, Bombay (India) are used for the present experiments. The near infrared spectra (1800-700 nm) are recorded at room temperature ($26 \pm 1^\circ\text{C}$) using a HITACHI Model U-3410 UV-Vis-NIR spectrophotometer, which uses a tungsten lamp as the near infrared source. The spectra of the compounds except *p*-chloroaniline and *p*-toluidine are recorded from pure liquids of 1cm path length with air as reference. *p*-chloroaniline and *p*-toluidine are solids and their absorption spectrum are recorded from a near saturated solution in spectrograde CCl₄.

5.3 Results and discussion

5.3.1 Analysis of the overtone spectra of aniline and chloroanilines

The molecular structures of aniline and chloroanilines are given in figure 5.1.

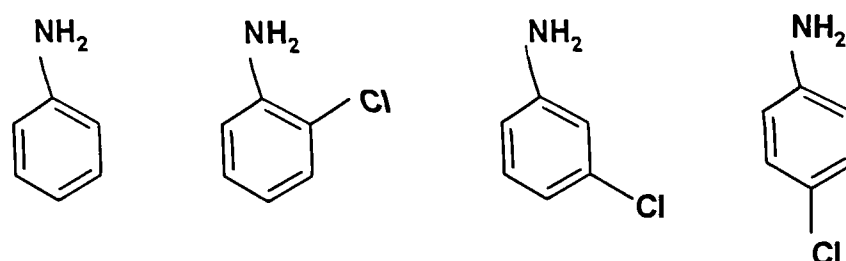


Fig. 5.1 The molecular structures of aniline, *o*-, *m*- and *p*-chloroanilines

The near infrared vibrational overtone spectra of aniline and chloroanilines in the near region 1800-700 nm show bands due to pure overtone transitions of ring CH and NH local mode oscillators and those due to combination transitions involving several vibrational degrees of freedom of these molecules. In the analysis, we will be considering only the pure overtone bands arising from the ring CH and NH oscillators of these molecules. The bands in the $\Delta V = 2-5$ regions of aniline and those in the $\Delta V=2-4$ regions of chloroanilines are shown in figures 5.2 – 5.13. In these figures, the peaks denoted by 'a' represents the aryl CH overtones, 'b' represents NH overtones and 'c' represents combinations. The bands in the $\Delta V = 2$ region show multiple peaks due to the presence of combinations, whereas all higher overtone bands show single overtone peaks. The first overtone peak position in each case is assigned as the one giving the best fit in the Birge - Sponer plot with higher overtone peaks. The Birge-Sponer plots for aryl CH and NH oscillators in aniline and chloroanilines are shown in figures 5.14 – 5.15. The band assignments, transition energies and the local mode parameters of ring CH and NH oscillators are given in Table 5.1. The NH local mode parameters of *p*-chloroaniline are not included since we could record only two NH overtone bands, because the signal to noise ratio is very poor for the spectra below 800 nm.

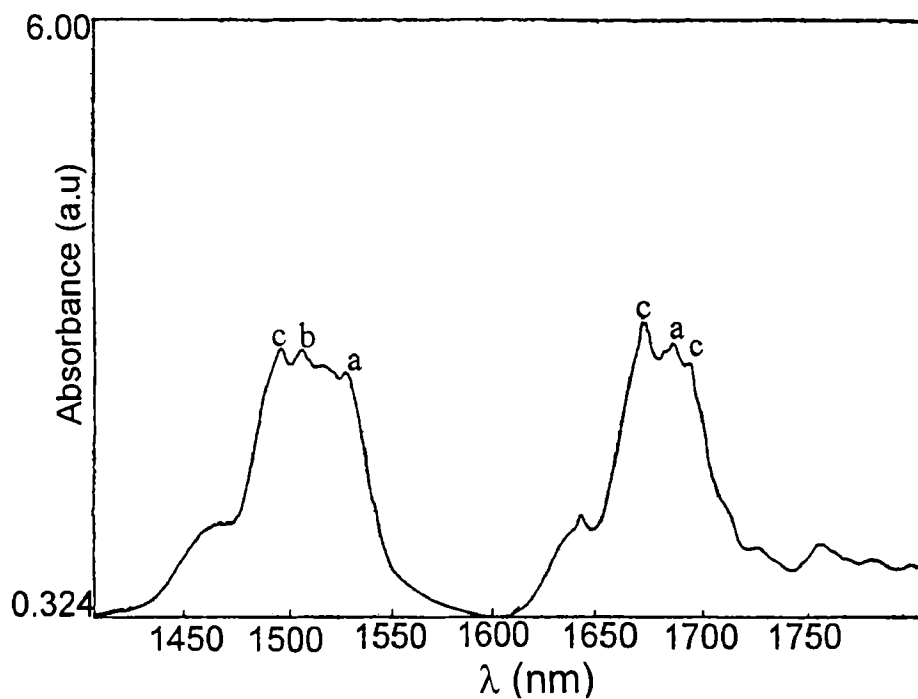


Fig.5.2. The absorption bands of aniline in the $\Delta V = 2$ region

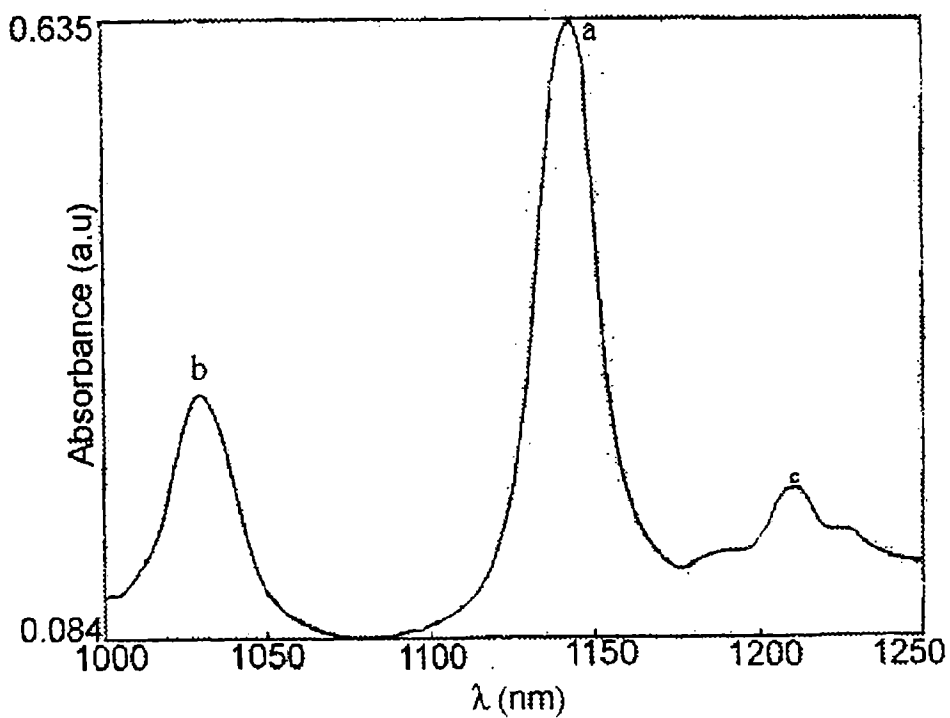


Fig.5.3. The CH and NH overtone bands of aniline in the $\Delta V = 3$ region.

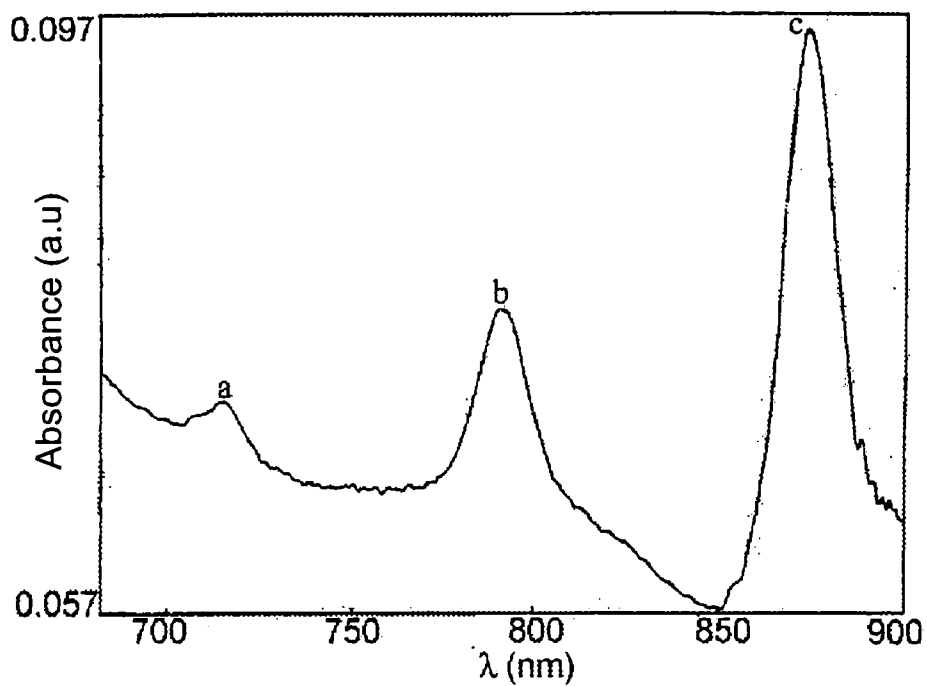


Fig.5.4. The CH ($\Delta V = 4$ and 5) and NH ($\Delta V = 4$) overtone bands of aniline

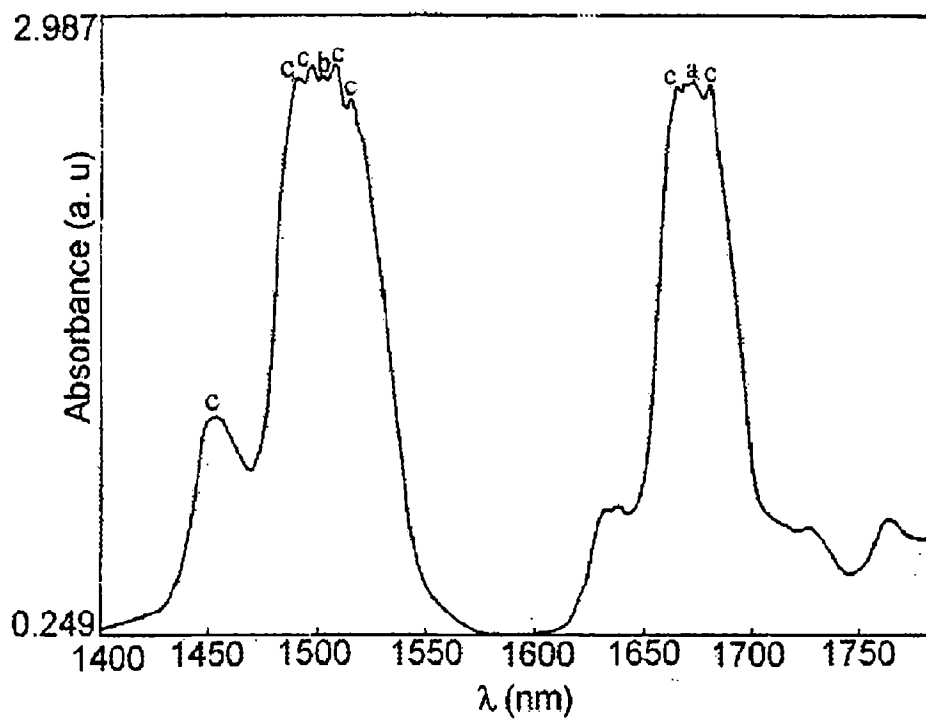


Fig.5.5. The absorption bands of *o*-chloroaniline in the $\Delta V = 2$ region.

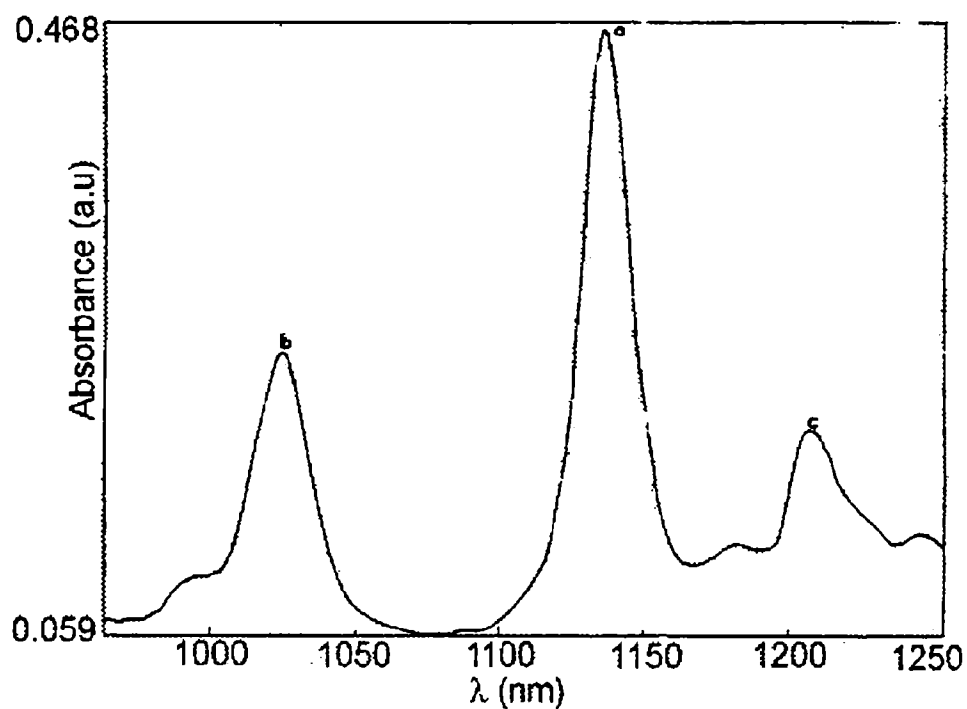


Fig.5.6. The CH and NH overtone bands of *o*-chloroaniline in the $\Delta V = 3$ region.

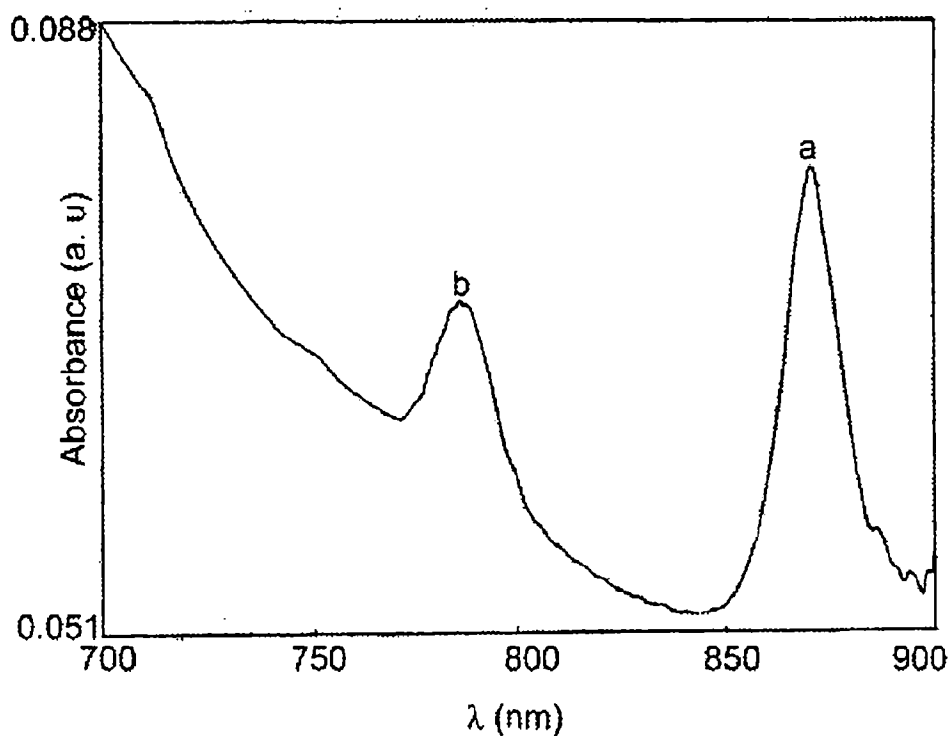


Fig.5.7. The CH and NH overtone bands of *o*-chloroaniline in the $\Delta V = 4$ region

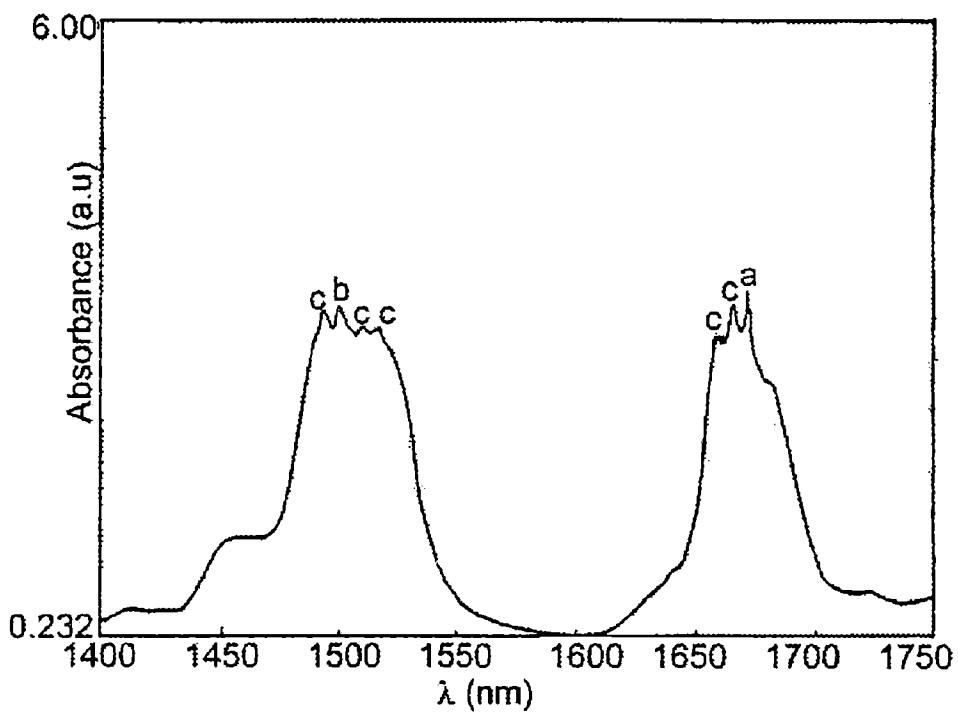


Fig.5.8. The absorption bands of *m*-chloroaniline in the $\Delta V = 2$ region

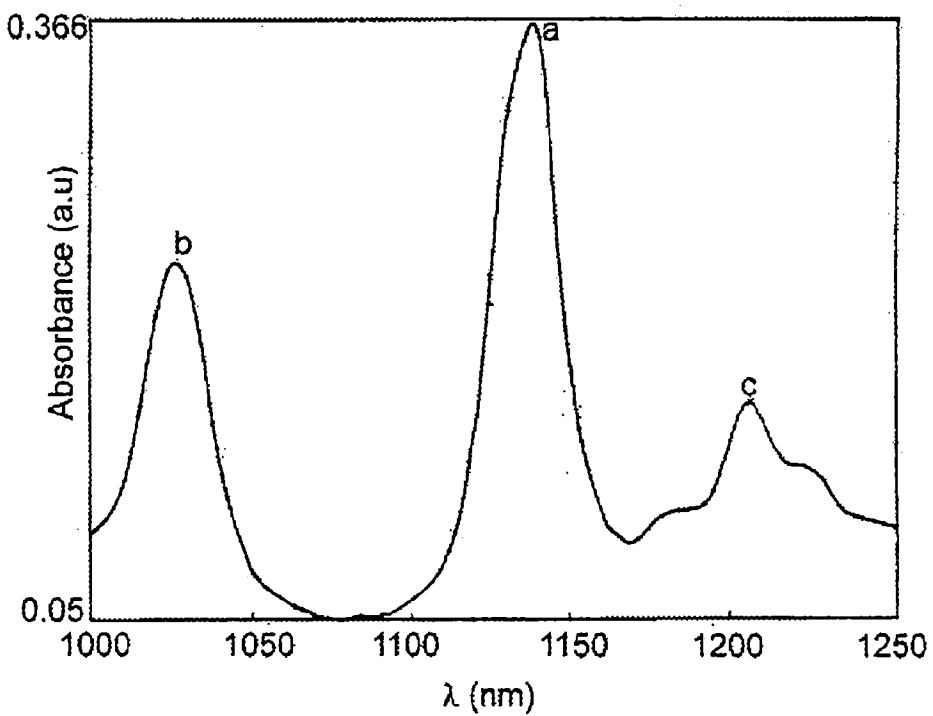


Fig.5.9. The CH and NH overtone bands of *m*-chloroaniline in the $\Delta V = 3$ region.

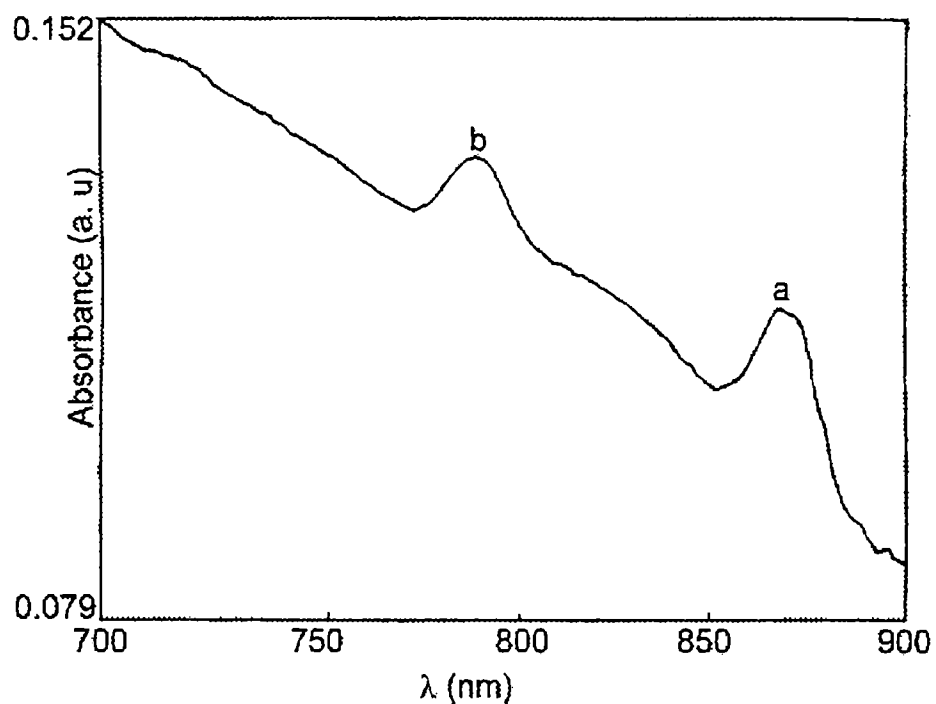


Fig.5.10. The CH and NH overtone bands of *m*-chloroaniline in the $\Delta V = 4$ region.

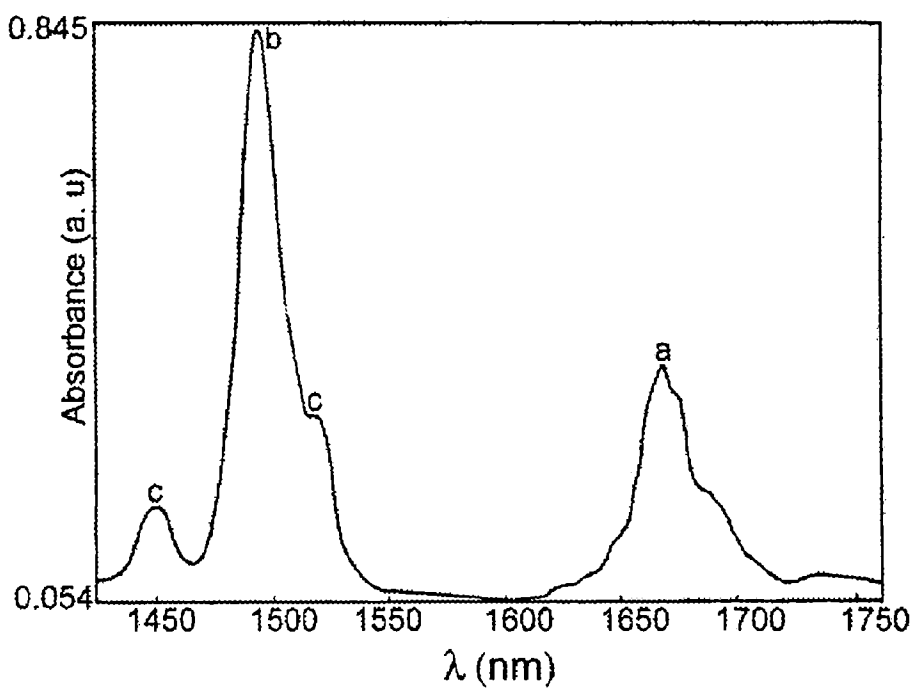


Fig.5.11. The CH and NH overtone bands of *p*-chloroaniline in the $\Delta V = 2$ region

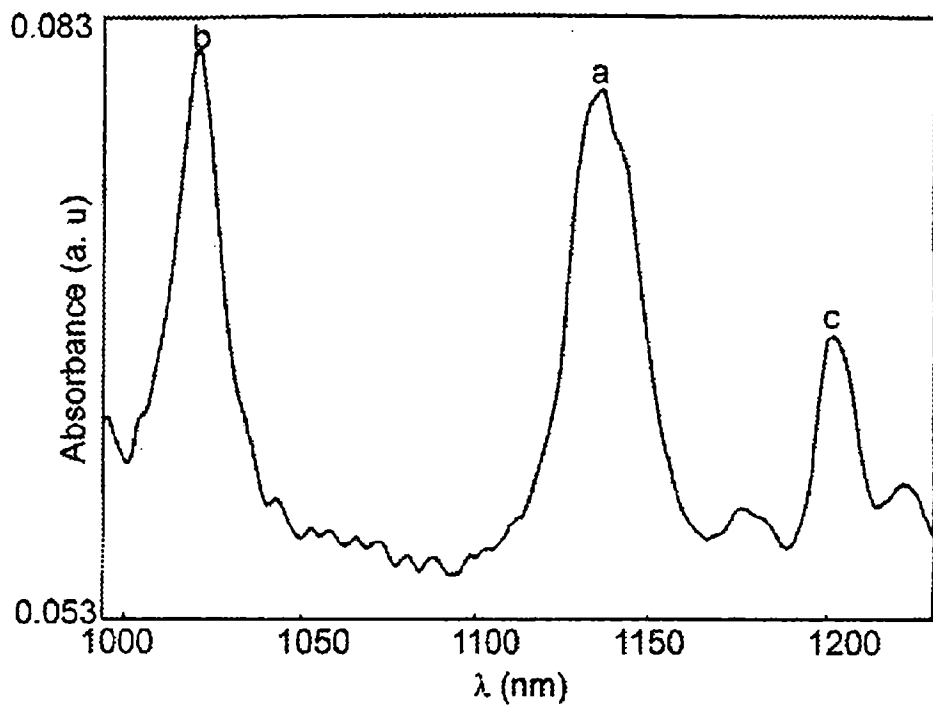


Fig.5.12. The CH and NH overtone bands of *p*-chloroaniline in the $\Delta V = 3$ region.

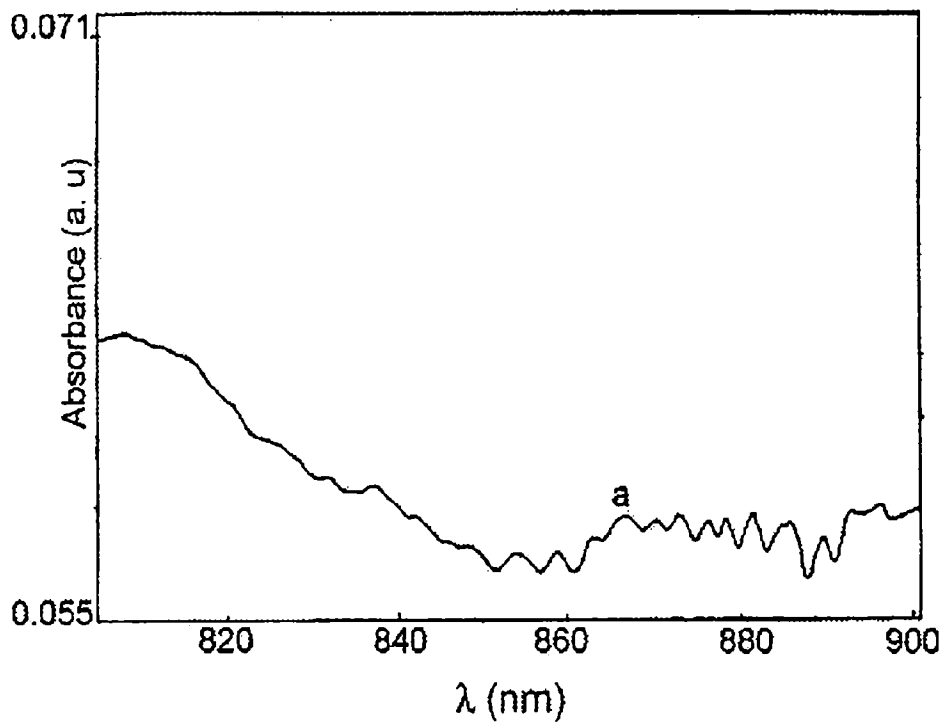


Fig.5.13. The absorption bands of *p*-chloroaniline in the $\Delta V = 4$ region, the pure overtone is denoted by 'a'.

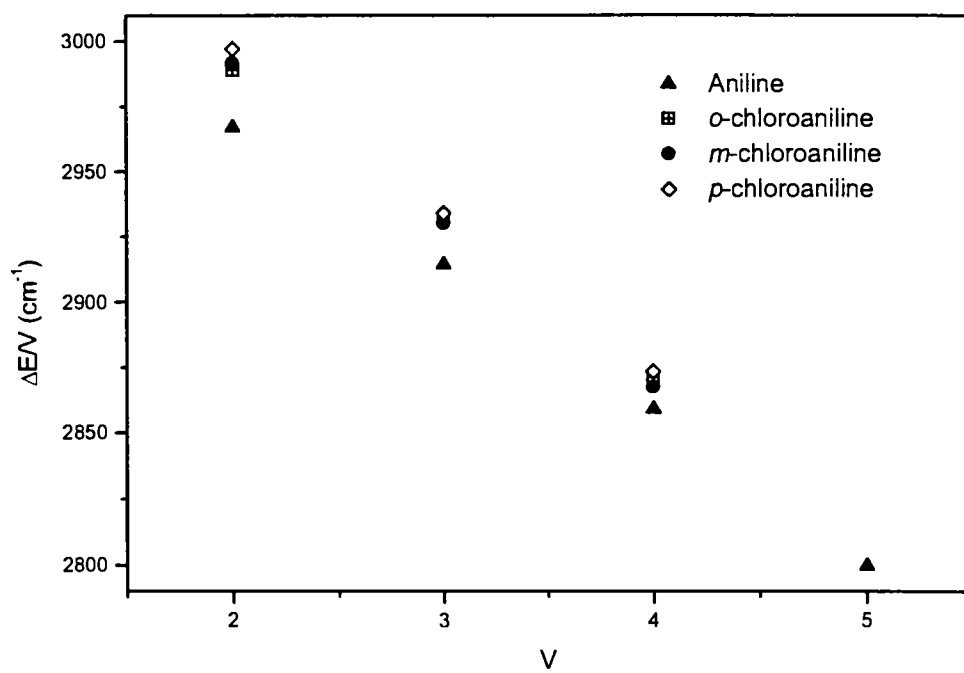


Fig.5.14. Birge-Sponer plots for ring CH overtones in aniline and chloroanilines

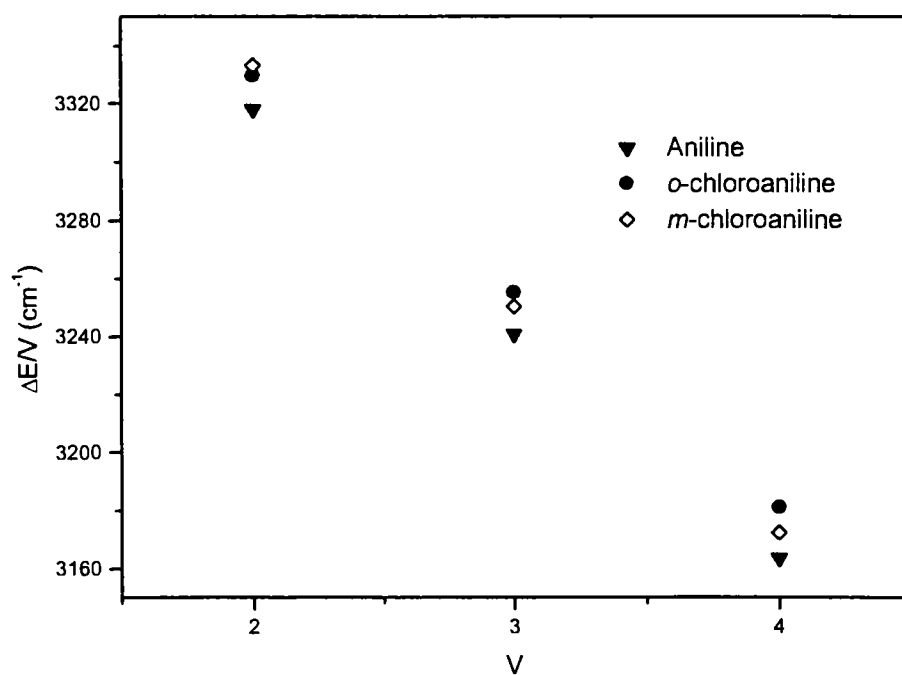


Fig.5.15. Birge-Sponer plots for NH overtones in aniline and chloroanilines

Table 5.1. Band assignments, transition energies and local mode parameters of ring CH and NH oscillators in aniline and chloroanilines.

Sample	Ring CH overtones			NH overtones		
	ΔV	ΔE (cm^{-1})	Local mode parameters and least square coefficient	ΔV	ΔE (cm^{-1})	Local mode parameters and least square coefficient
Aniline	2	5934.37	$X_1 = 3136.33$ $X_2 = -55.83$ $\gamma = -0.99962$	2	6636.14	$X_1 = 3549.56$ $X_2 = -77.16$ $\gamma = -1$
	3	8743.55		3	9722.9	
	4	11436.41		4	12655.02	
	5	13997.76				
<i>o</i> -chloro aniline	2	5978	$X_1 = 3165.77$ $X_2 = -58.71$ $\gamma = -0.9998$	2	6659.56	$X_1 = 3552.22$ $X_2 = -74.16$ $\gamma = -1$
	3	8976.62		3	9766.58	
	4	11486.33		4	12725.88	
<i>m</i> -chloro aniline	2	5983.37	$X_1 = 3178.015$ $X_2 = -62.03$ $\gamma = -0.99998$	2	6666.66	$X_1 = 3573.72$ $X_2 = -80.37$ $\gamma = -0.99988$
	3	8791.21		3	9752.29	
	4	11470.52		4	12690.36	
<i>p</i> -chloro aniline	2	5994.48	$X_1 = 3181.835$ $X_2 = -61.675$ $\gamma = -0.99993$			
	3	8802.82				
	4	11495.57				

An examination of table 5.1 reveals that the local mode mechanical frequencies generally agree with nature of substituents in each case. With the electron-donating nature of the NH_2 group, the donation of lone pair electron density to the ring

reduces the aryl CH mechanical frequency. Hence the aryl CH mechanical frequency in aniline is less than in benzene (by $\sim 12\text{ cm}^{-1}$). On the other hand, halogen atoms are electron-withdrawing groups. Hence the addition of a halogen atom to the phenyl ring of aniline increases the ring CH mechanical frequency with respect to aniline. This effect is generally observed in many substituted benzenes and is well explained by Gough and Henry [23]. The NH local mode mechanical frequency in *o*-chloroaniline is close to that of aniline whereas the corresponding value in *m*-chloroaniline is much larger (by $\sim 24\text{ cm}^{-1}$) than in aniline. The ring CH local mode parameters in all the compounds represent the average value over the various nonequivalent ring CH oscillators, since the observed liquid phase spectra do not show a corresponding resolved structure. As can be seen, there is an increase of $\sim 30\text{ cm}^{-1}$ for the ring CH mechanical frequency in *o*-chloroaniline with respect to aniline, whereas the corresponding increase in *m*-chloroaniline and *p*-chloroaniline are comparable (42 and 46 cm^{-1}) respectively. The increase in ring CH mechanical frequency in all the chloroanilines with respect to aniline is due to the electron withdrawing nature of chlorine atom, and is in agreement with the reported results in substituted benzenes. The important observation here is the appreciable difference in ring CH mechanical frequency of *o*-chloroaniline with respect to *m*-chloroaniline and *p*-chloroaniline.

It is well known [17,18] that in aniline and similar aromatic amines, the lone pair associated with the nitrogen atom gets conjugated with the π electron cloud of benzene ring. One can therefore expect that the electron withdrawing effect exerted by a halogen atom attached to the ring which reduces the electron density at the ring carbon sites, also causes a reduction in electron density at the nitrogen atom. This can cause a net attraction of the electron clouds associated with the NH_2 hydrogen atoms, thus causing an increase in NH force constant which results in an increase in NH mechanical frequency. The increased value of NH mechanical frequency in *m*-chloroaniline with respect to that in aniline agrees with the above mechanism. But the observation that the NH mechanical frequency in *o*-chloroaniline is close to that in aniline shows that the above mechanism of increasing the NH force constant is opposed by some other interaction in this molecule. We propose that the intramolecular hydrogen bonding between chlorine atom and NH_2 hydrogen atoms, which can be expected to be most dominant in *o*-

chloroaniline, is responsible for the opposing effect. The chlorine atom in *o*-chloroaniline involves in intramolecular hydrogen bonding with the NH₂ group that is attached to the adjacent carbon site in the benzene ring causing a reduction in the force constant of the NH bonds. This explains the reduced value of NH oscillator mechanical frequency in *o*-chloroaniline compared to *m*-chloroaniline. A comparison with *p*-chloroaniline could not be made due to the lack of NH overtone data of this compound. The proximity in position of chlorine atom and the hydrogen atoms in amino group in *o*-chloroaniline also favours the possibility of formation of hydrogen bond. The hydrogen bonding interaction in *m*-chloroaniline and *p*-chloroaniline can be expected to be much smaller than that in *o*-chloroaniline, since the intramolecular hydrogen bonding in *o*-chloroaniline “uses” part of the electron withdrawing power of chlorine atom, the net electron withdrawing effect from the benzene ring is expected to be lowered. This clearly causes the average value of ring CH force constant in *o*-chloroaniline to be lower than that in *m*-chloroaniline and *p*-chloroaniline. Hence, these two observations, of reduction in NH mechanical frequency and in ring CH mechanical frequency in *o*-chloroaniline compared to those in *m*-chloroaniline and *p*-chloroaniline, arise from a common origin namely intramolecular hydrogen bonding which will be most dominant in *o*-chloroaniline compared to the *meta* and *para* chloroanilines.

Nonat *et al* [24-27] in a comparative microwave spectroscopic study of *o*-chloroaniline, *m*-chloroaniline and *p*-chloroaniline observed a reduced dihedral angle (angle between the planes of amine group and phenyl ring) and the existence of a torsion around the C-N bond in *o*-chloroaniline, which they attributed as due to the existence of intramolecular hydrogen bond in this compound. Moreover, this intramolecular hydrogen bond is shown to stabilize the conjugation of the nitrogen lone pair with the π electron system of the ring thus favouring a more planar configuration of the molecule. The presence of intramolecular hydrogen bond affects the electron withdrawing/donating nature of the substituents attached to the benzene ring. It is thus clear that in addition to the effect of reduced electron withdrawal from the ring by the chlorine atom due to the intramolecular hydrogen bonding, the increased conjugation of the nitrogen lone pair (an effective electron donation to the ring) will also be contributing to the observed decrease in the ring CH mechanical frequency in *o*-chloroaniline. The present overtone spectral result is thus an

additional support to the conclusions of microwave spectral studies by Nonat *et al*. Thus the presence of intramolecular hydrogen bond is well reflected through the changes in the mechanical frequency values.

The electronic absorption spectra of chloroanilines in cyclohexane/dioxane solutions are reported by Pal *et al* [22]. These authors argue that the intramolecular hydrogen bonding in the ground electronic state of *o*-chloroaniline is insignificant; and if at all originally present, it is replaced by the stronger intermolecular NH...O hydrogen bond between *o*-chloroaniline and dioxane. However, strong intramolecular hydrogen bonding is shown to exist in the excited electronic state of *o*-chloroaniline.

Our observation shows that even the very weak intramolecular hydrogen bonding in the ground electronic state is well reflected in the vibrational overtone spectrum through a change in the CH and NH local mode mechanical frequency values. There are other supporting results when the bond angles and bond lengths in substituted chloroanilines are considered. The presence of intramolecular hydrogen bonding suggests a wider HNH angle in *o*-chloroaniline compared to *meta* and *para* chloroanilines. This trend is predicted in the recently reported classical VFF calculations and semi-empirical quantum chemical MNDO/3 and AM1 calculations [28]. The experimental data [24] available on HNH angles (114.50, 114.32 and 112.99 for *ortho*, *meta* and *para* chloroanilines) also agree well with the existence of intramolecular hydrogen bonding in *o*-chloroaniline. While the difference in the HNH angle of *ortho* compounds with respect to the *meta* and *para* compounds is well exhibited by the classical VFF results, the experimental values of the HNH angles compare better with the AM1 results. The dissymmetry in the intramolecular hydrogen bonding causes a difference between the two NH bond lengths. This behavior is also clearly shown by the results of semi empirical MO calculations [28]. However, our low-resolution liquid phase spectrum does not show a resolved NH overtone band in *o*-chloroaniline corresponding to the nonequivalence NH bonds. The experimental data [24] on NH bond lengths reported (1.002 Å, 1.001 Å and 1.005 Å for *ortho*, *meta* and *para* chloroanilines) also do not show the nonequivalence, probably due to the large value of experimental uncertainty in bond lengths. It is to be pointed out here that a low concentration study of the overtone spectra reported after our work also

revealed the existence of the intramolecular hydrogen bond in *o*-chloroaniline even though there is a minor difference in band assignment in the first NH overtone region [29].

In conclusion, the near infrared overtone absorption spectra of liquid phase aniline and chloroanilines are analysed using local mode model. The analysis of the mechanical frequency values of CH and NH oscillators reveals the existence of intramolecular hydrogen bonding in *o*-chloroaniline, supporting the prediction of microwave spectroscopic study. This illustrates the use of overtone spectroscopy as good diagnostic tool for probing even weak hydrogen bonding interaction in molecules.

5.3.2 Analysis of overtone spectra of toluidines

The molecular structures of aniline and toluidines are shown in figure 5.16.

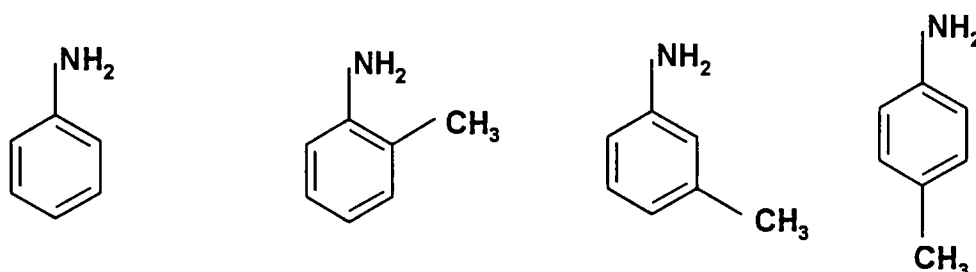


Fig. 5.16. The molecular structures of aniline and ortho, meta and para toluidines

The near infrared vibrational overtone absorption spectra of *o*-toluidine, *m*-toluidine and *p*-toluidine in the region 1800-700 nm show bands due to pure overtone transitions of ring CH, NH and methyl CH local mode oscillators. Combination transitions, involving several vibrational degrees of freedom of the molecule also occur in the NIR region. Only the pure overtone bands arising from the ring CH, methyl CH and NH oscillators are considered for the local mode analysis of the spectra. The bands in the $\Delta V = 2-5$ regions of *o*-toluidine and *m*-toluidine and those in the $\Delta V=2-4$ regions of *p*-toluidine are shown in figures 5.17 – 5.28. In these figures, the peaks denoted by 'a' represents the ring CH overtones, 'b' represents NH overtones and 'c' represents methyl CH overtones and other peaks are combinations. The bands in the $\Delta V = 2$ region shows multiple peaks due to the presence of combinations, whereas all higher overtone bands show single overtone peaks. The first overtone peak position in the case of ring CH, NH and methyl CH is assigned as the one giving the best fit in the Birge - Sponer plot with higher overtone peaks. The Birge-Sponer plots for ring CH, NH and methyl CH overtones for toluidines are shown in figures 5.29 – 5.31. The methyl CH oscillators are nonequivalent and the overtone peaks corresponding to nonequivalent methyl CH oscillators are not distinct in all the regions due to the low resolution of the absorption spectra. The band assignments, transition energies and the local mode parameters of ring CH and NH oscillators are given in Table 5.2.

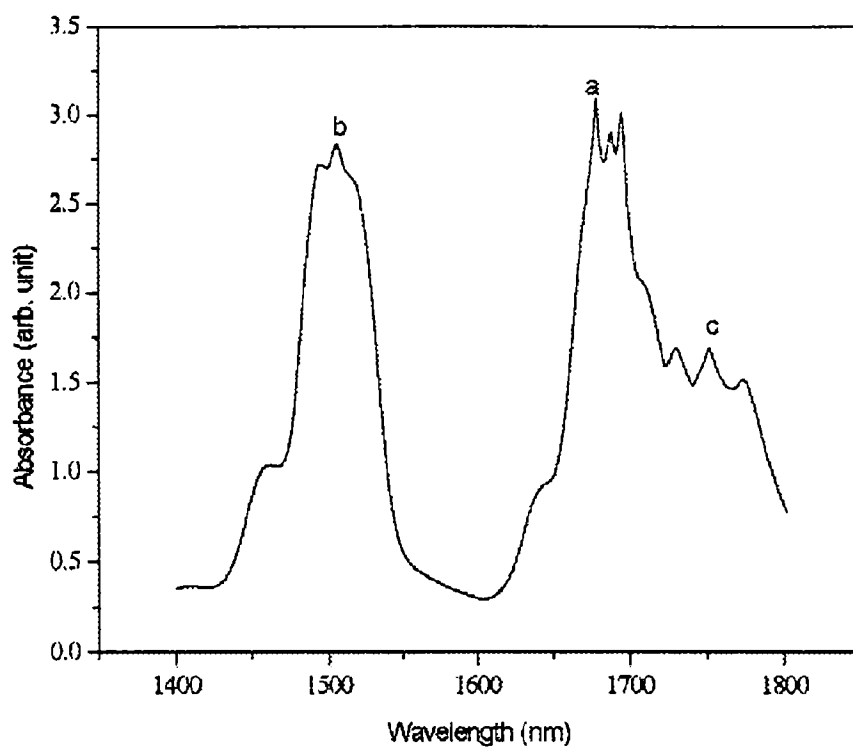


Fig.5.17. The ring CH, NH and methyl CH overtone bands of *o*-toluidine in the $\Delta V = 2$ region

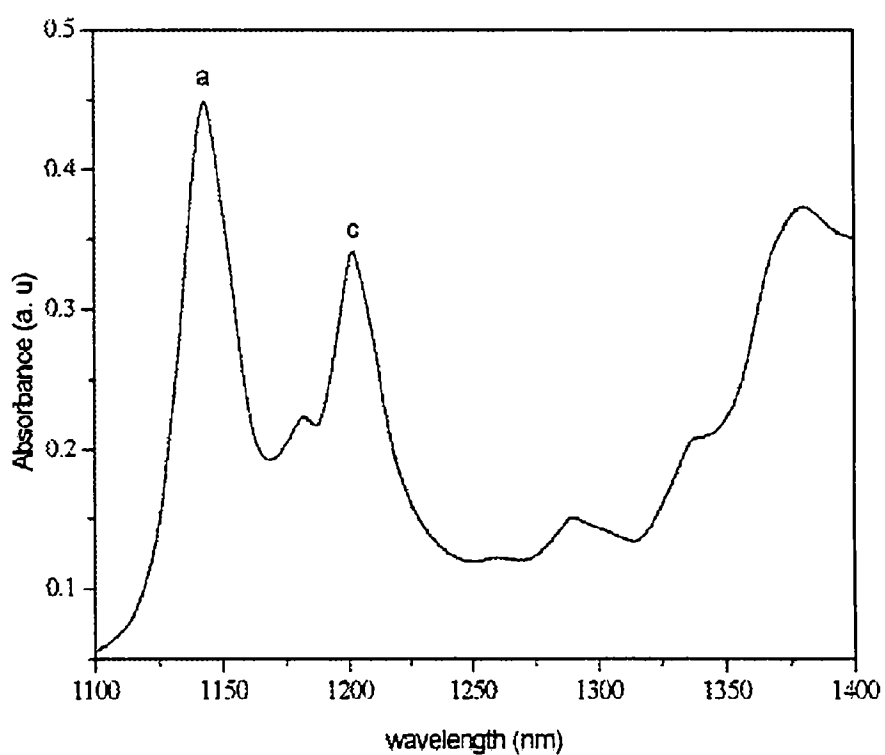


Fig.5.18. The ring CH and methyl CH overtone bands of *o*-toluidine in the $\Delta V = 3$ region

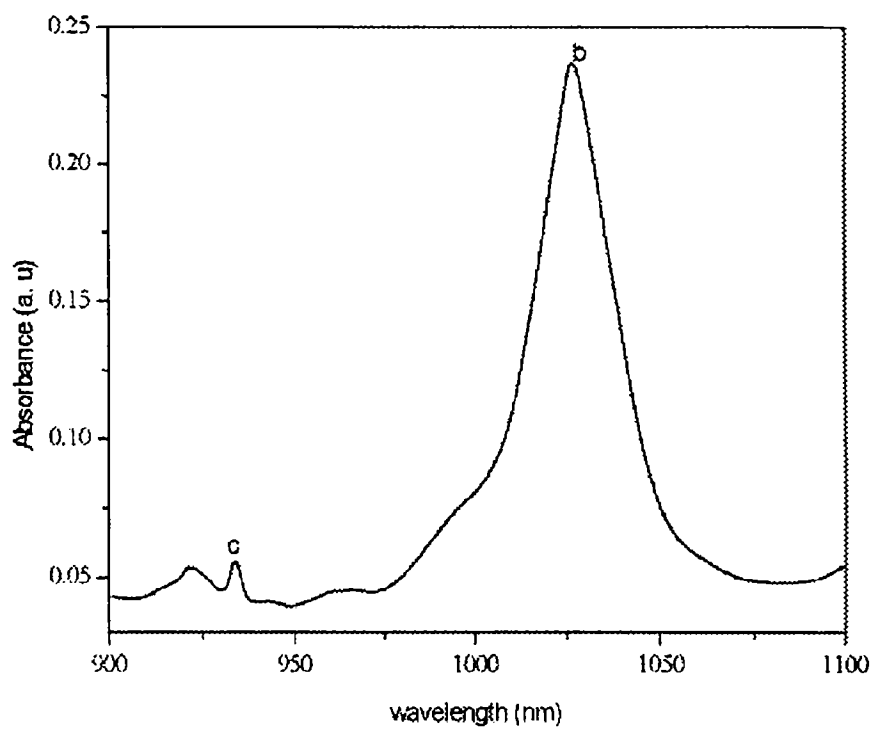


Fig.5.19. The NH ($\Delta V = 3$) and methyl CH ($\Delta V = 4$) overtone bands of *o*-toluidine

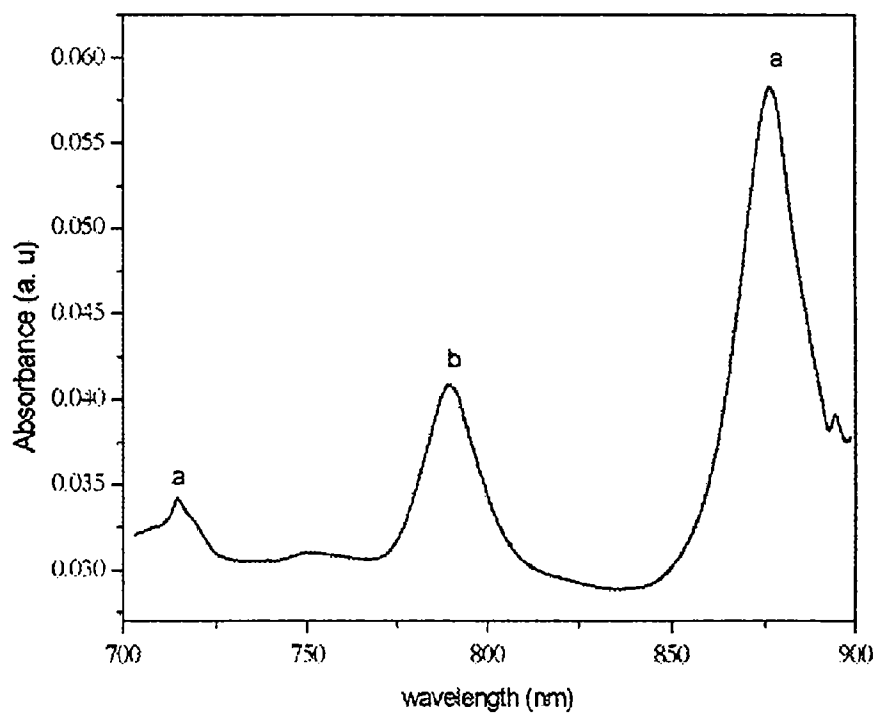


Fig.5.20. The ring CH ($\Delta V = 4$ and 5) and NH ($\Delta V = 4$) overtone bands of *o*-toluidine

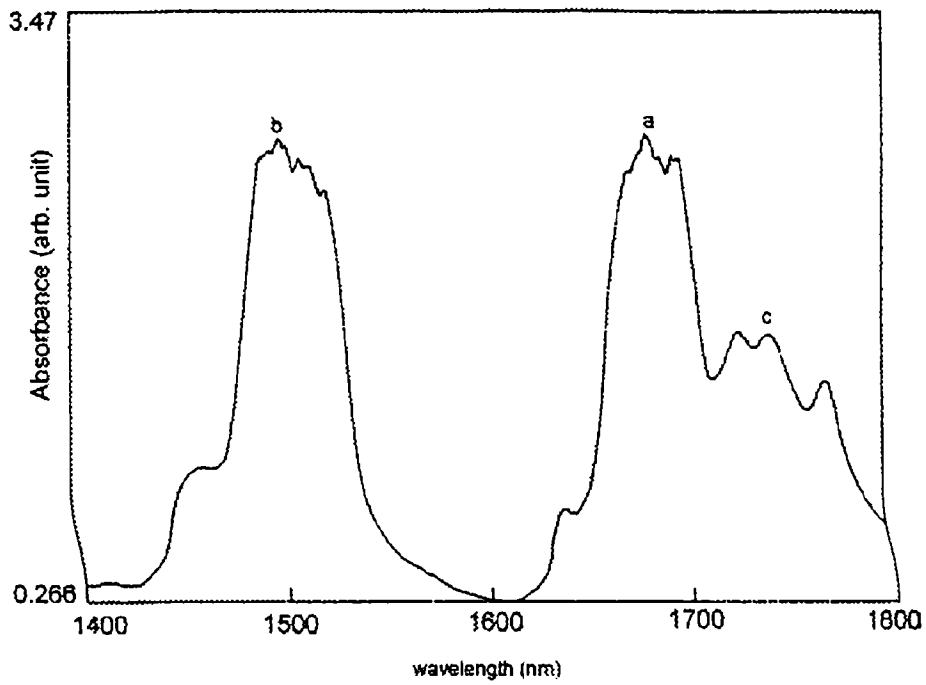


Fig.5.21 The ring CH, NH and methyl CH overtone bands of *m*-toluidine in the $\Delta V = 2$ region

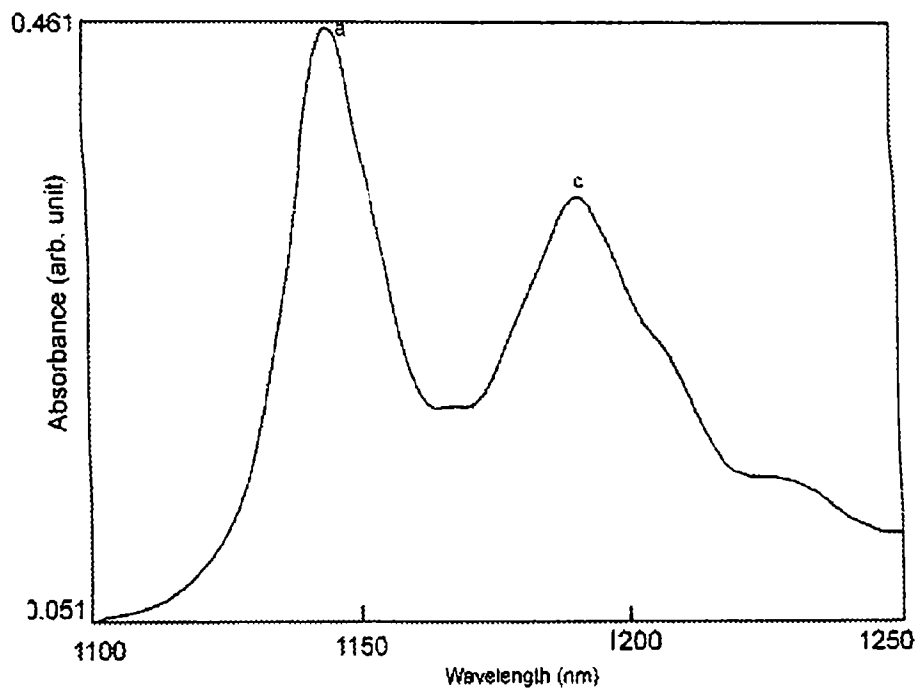


Fig.5.22. The ring CH and methyl CH overtone bands of *m*-toluidine in the $\Delta V = 3$ region

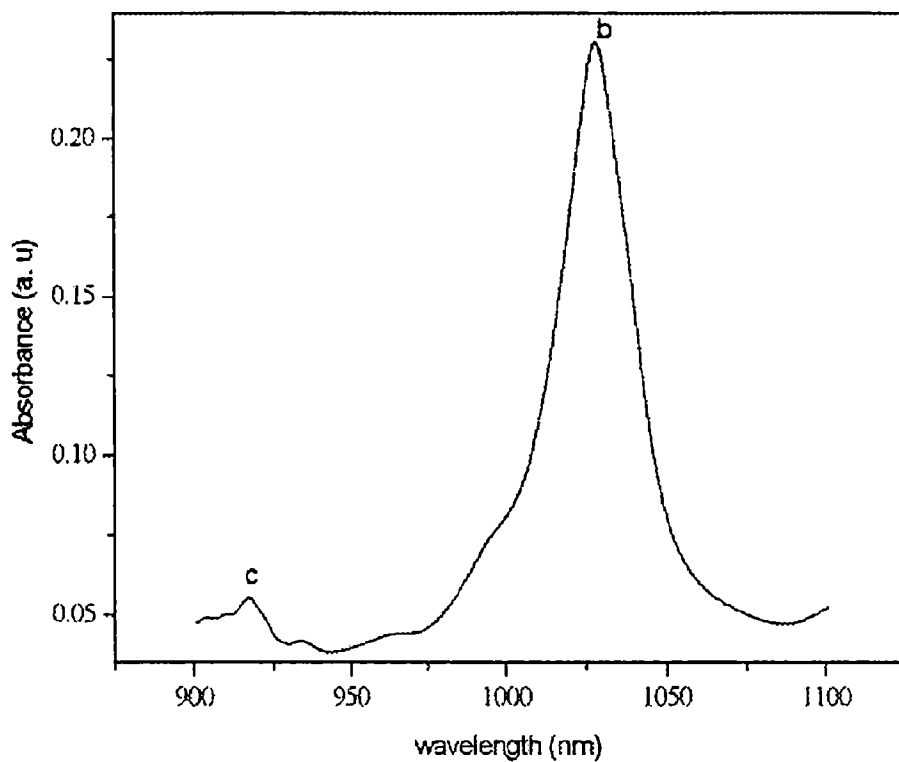


Fig.5.23. The NH ($\Delta V = 3$) and methyl CH ($\Delta V = 4$) overtone bands of *m*-toluidine

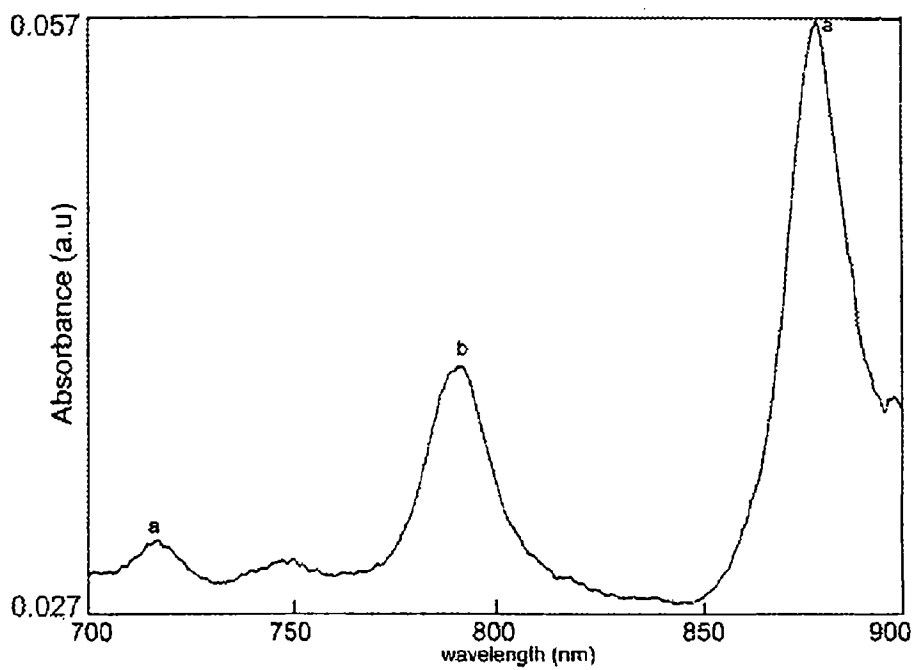


Fig.5.24. The ring CH ($\Delta V = 4$ and 5) and NH ($\Delta V = 4$) overtone bands of *m*-toluidine

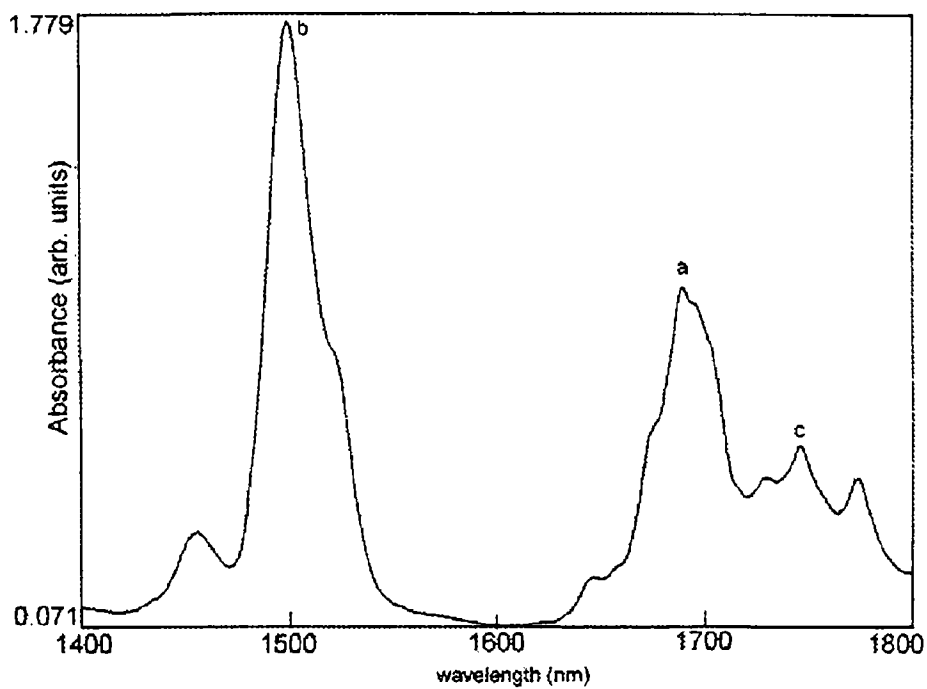


Fig.5.25 The ring CH, NH and methyl CH overtone bands of *p*-toluidine in the $\Delta V = 2$ region

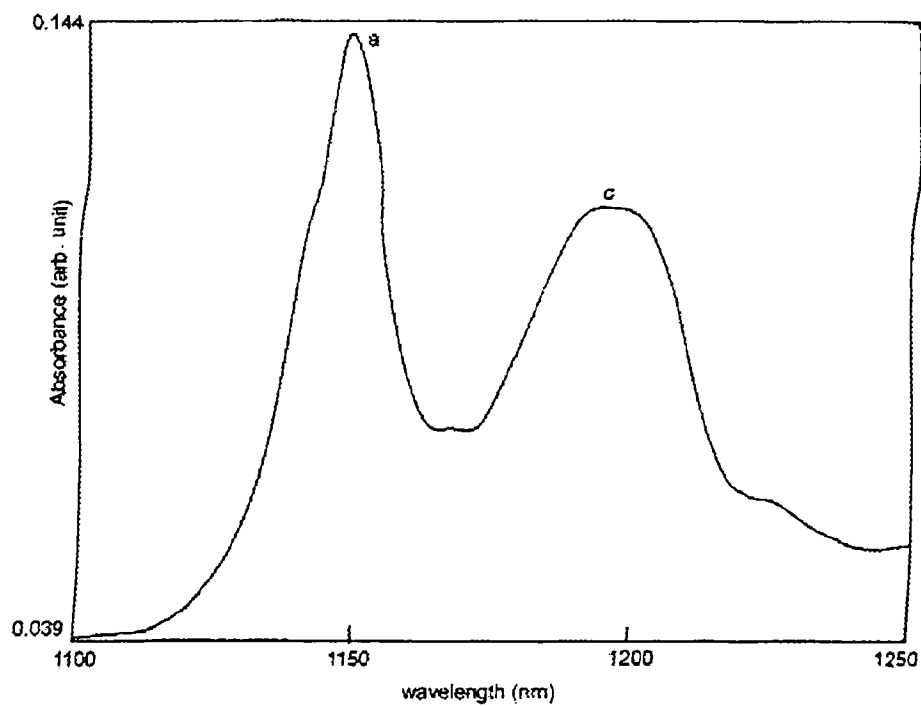


Fig.5.26. The ring CH and methyl CH overtone bands of *p*-toluidine in the $\Delta V = 3$ region

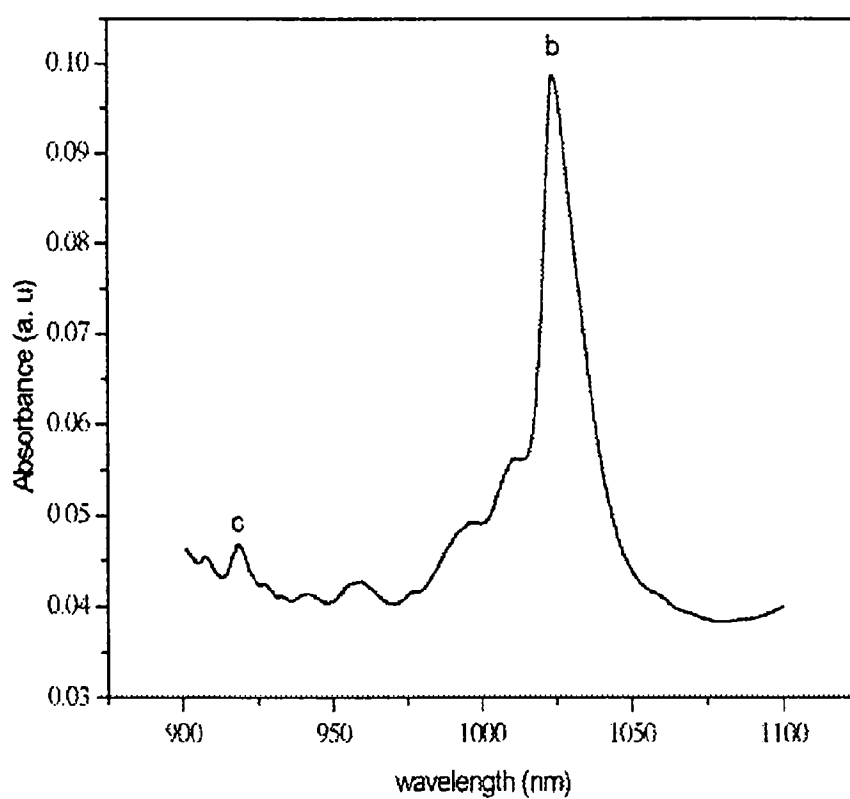


Fig.5.27 The NH ($\Delta V = 3$) and methyl CH ($\Delta V = 4$) overtone bands of *p*-toluidine

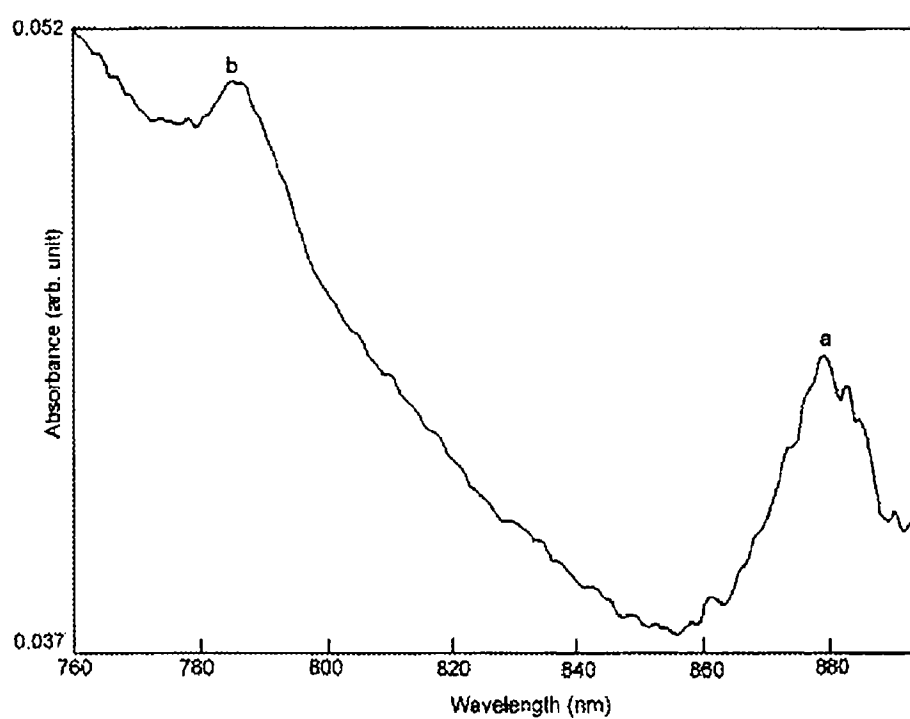


Fig.5.28. The ring CH and NH overtone bands of *p*-toluidine in the $\Delta V = 4$ region

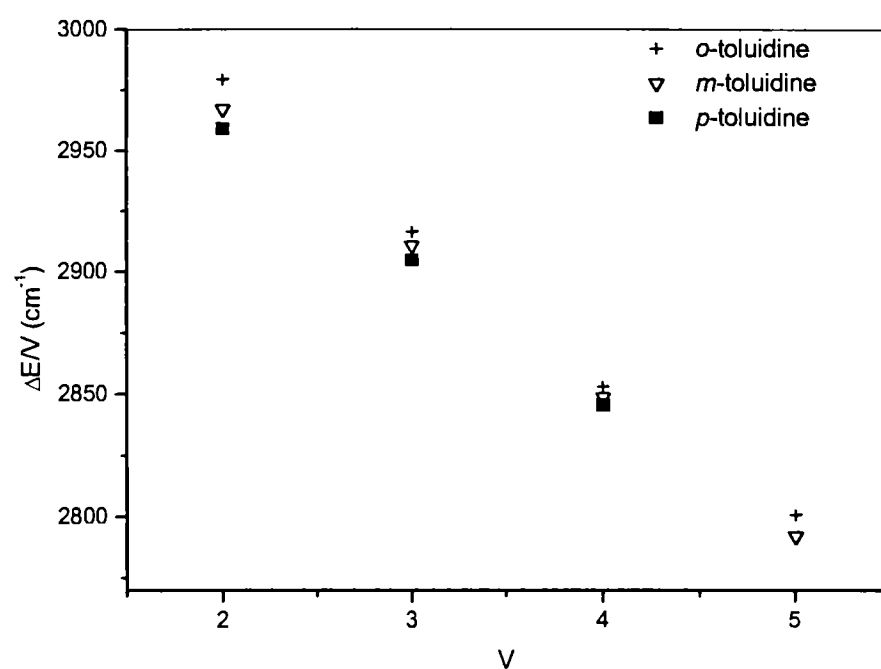


Fig.5.29. Birge-Sponer plots for ring CH overtones in *o*-, *m*- and *p*-toluidine.

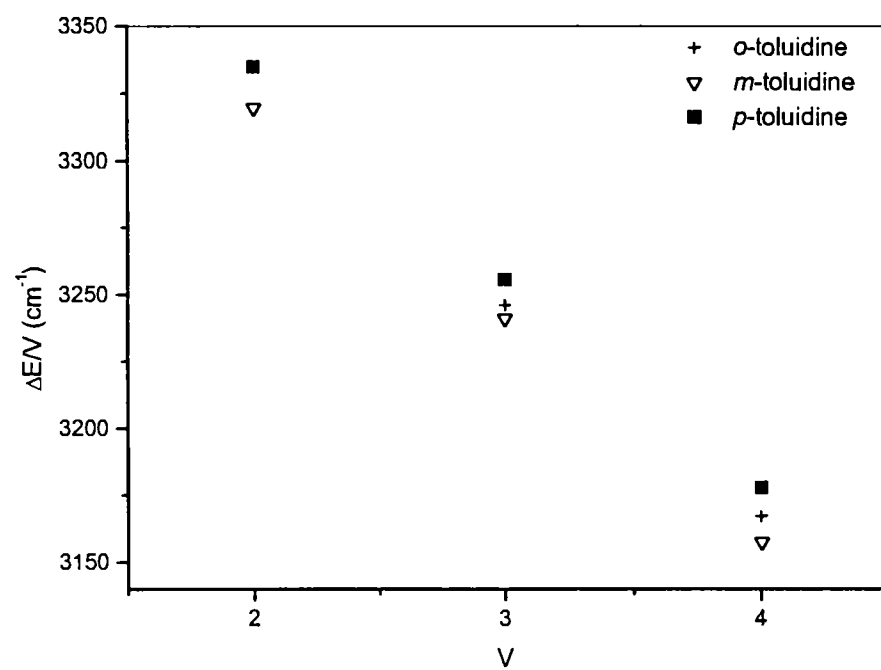


Fig.5.30. Birge-Sponer plots for NH overtones in *o*-, *m*- and *p*-toluidine

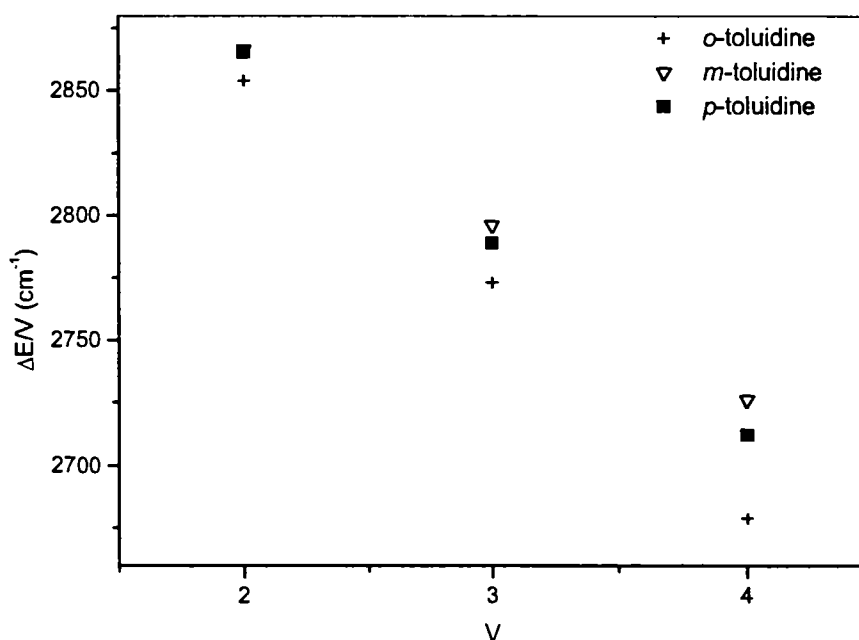


Fig.5.31. Birge-Sponer plots for methyl CH overtones in *o*-, *m*- and *p*-toluidine.

The substitution of an electron-donating group decreases the ring CH mechanical frequency and hence a red shift in overtone energy values. Both the amino group and methyl groups in toluidines are electron-donating groups. As can be seen, there is an increased value for the ring CH mechanical frequency in *o*-toluidine even though both the substituents are electron donating. The same substituents show a decrease in ring CH mechanical frequency values for *m*-toluidine and *p*-toluidine, which are comparable. The increase in ring CH mechanical frequency in *o*-toluidine with respect to aniline is due to the interaction between the amino and methyl substituents, and is in agreement with the reported results that there is through space interaction between amino and methyl groups in *o*-toluidines [20, 30] by laser induced fluorescence and resonance two-photon ionization spectra and no such interaction exists in *m*-toluidine and *p*-toluidine. The important observation here is the appreciable difference in ring CH mechanical frequency of *o*-toluidine with respect to *m*-toluidine and *p*-toluidine due to this interaction existing in *o*-toluidine.

The NH local mode mechanical frequency in *o*-toluidine is close to that of aniline and *o*-chloroaniline [19] whereas the corresponding value in *m*-toluidine and *p*-toluidine are much larger (by $\sim 14 \text{ cm}^{-1}$ and $\sim 21 \text{ cm}^{-1}$) than that in aniline. The ring CH local mode parameters in all the compounds represent the average

value over the various nonequivalent ring CH oscillators, since the observed liquid phase spectra do not show a corresponding resolved structure. The interesting result is that there is an increase of mechanical frequency $\sim 21 \text{ cm}^{-1}$ for ring CH in *o*-toluidine than aniline rather than a decrease even though both amino and methyl substituents are electron donating groups. At the same time, there is a decrease in ring CH mechanical frequency is well observed in *m*-toluidine and *p*-toluidine. The corresponding decrease in ring CH mechanical frequency in *m*-toluidine is $\sim 4 \text{ cm}^{-1}$ with respect to aniline and the decrease in ring CH mechanical frequency for *p*-toluidine is $\sim 6 \text{ cm}^{-1}$ with respect to aniline. The presence of the interaction between amino and methyl groups cause changes in NH mechanical frequency values also. The NH mechanical frequency in *o*-toluidine is close to that of aniline and *o*-chloroaniline, while the NH frequencies in *m*-toluidine and *p*-toluidine are higher than that in aniline and are comparable with that in *m*-chloroaniline. The increased value for ring CH mechanical frequency in *o*-toluidine and the comparable NH mechanical frequency value for *o*-toluidine with aniline are due to the interaction existing between amino and methyl group in *o*-toluidine. Even though we could not obtain well-resolved peaks for non-equivalent methyl CH oscillators, the analysis of the observed methyl CH mechanical frequencies shows a higher value for *o*-toluidine compared to *m*-toluidine and *p*-toluidine. This increase in methyl CH mechanical frequency in *o*-toluidine occurs due to the interaction existing between the amino and methyl groups.

The CH_3 group interacts with the nearby π system via hyperconjugation, while the NH_2 group shares its lone-paired electrons with the p -electrons in the ring. Both mechanisms imply electronic delocalisation. In *o*-toluidine (also known as 2-methylaniline or *o*-methylaniline), a repulsive steric interaction between the two substituents attached to the aromatic ring is expected. There are a lot of studies reported in this aspect. Varsanyi [31] describes the ground state normal vibrations of *o*-toluidine based on liquid and solid phase infrared and Raman spectra. The *ab initio* studies of the ground state and first excited singlet states of aniline are reported by Jiang *et al* [32]. Vaschetto *et al* report the density functional studies of aniline and substituted anilines and that also supports an interaction between amino group and ortho substituent [33]. The *ab initio* molecular orbital calculations employing the MP2/6-31 +G* and CIS/6-31+G* methods and the structural details

of *o*-toluidine, *m*-toluidine and *p*-toluidine using laser induced fluorescence are well studied [30, 34-35]. The structures and normal vibrations of *o*-toluidine and *p*-toluidine are well studied using Resonance Two Photon Ionization Spectroscopy (R2PI) by Tzeng et al [20, 21]. The structures and vibrations of *ortho*, *meta* and *para* fluoroanilines in the ground and first excited state are studied using *ab initio* quantum chemical methods and Resonant two-photon ionization spectroscopy by Tzeng *et al* [36].

The ground state of *o*-toluidine, *m*-toluidine and *p*-toluidines are found to be non-planar with no other symmetry elements except the identity in these studies. The amino part has a somewhat sp^3 hybridization like character due to the presence of lone-paired electrons in nitrogen atom. The methyl group has not much influence on the interaction between ring and amino group in *m*-toluidine and *p*-toluidine. The calculated values of the angle between the ring plane and NH_2 plane in *m*-toluidine and *p*-toluidine are very close to that in aniline and *o*-fluoroaniline. This fact strongly supports that the influence of the methyl group on the amino group is negligible in *m*-toluidine and *p*-toluidine.

The through space interactions between the NH_2 and CH_3 groups are expected to exist in *o*-toluidine due to the proximity of the two substituent groups [20, 30]. Such an interaction behavior is found in studies of substituted anilines by Vaschetto *et al* [33]. While considering the angles between the N-H bonds and the plane of the aromatic ring, the one closer to the methyl group has larger angle. In addition, one of the methyl CH bonds is tilted away by an angle of 3.8° with respect to the ring plane. These findings may result from (1) the repulsion between the hydrogen atoms of the two substituent groups; and (2) the attraction between the lone-paired electrons in the NH_2 part and hydrogen atoms of the CH_3 group (this can reduce the electron donation to the ring) in addition to the ring-substituent interactions. It follows that the rotation of the CH_3 group is slightly hindered by the NH_2 group at the ortho position of the aromatic ring. Considering the C-C bond length, the C_1-C_2 and C_2-C_3 bonds of *o*-toluidine are longer, where as C_6-C_1 bond of *o*-toluidine is shorter than the corresponding bonds in aniline. The angles $C_6C_1C_2$ and $C_1C_2C_3$ are found to be 119.6° and 118.5° respectively resulting from the steric and electronic interaction in *o*-toluidine. This indicates that the CH_3 group at the ortho position has some influence on the σ bonding system of the ring

also [20]. Thus the steric and electronic interaction in *o*-toluidine is well observed in the change in bond length values and bond angles.

In the laser induced fluorescence studies of *o*-toluidine by Ballesteros *et al* [30], it is found that the endocyclic angles in the substituted C atoms and in the C₄ are slightly smaller than 120° where as the angles closer to the substituted C atoms are larger than 120°. Compared to aniline, the largest differences are in the substituted C atoms, due to the presence of methyl and amino groups. The C-C calculated distances in the ring of *o*-toluidine are very similar to aniline except for the C₁-C₂ distance in substituted C atoms, due to the steric and electronic effects of methyl and amino groups in *o*-toluidine. This shows the interaction of the methyl group in the ortho position with the electronic density of the ring of the aniline molecule. This is not observed in *m*-methylaniline and *p*-methylaniline [34, 35] because all the calculated C-C distances are similar to those in aniline. C₁C₂C₇ angle is 120°, but C₃C₂C₇ is 121.4°. This shows that methyl group is tilted away to the amino group, in the same way NC₁C₂ angle is 119.7° and the NC₁C₆ angle is 120.6° so the amino group is also tilted away to methyl group. Both groups are becoming closer due to the attractive interaction between the lone pair of electrons in nitrogen atom of amino group and the hydrogen atom in methyl group.

In *o*-toluidine, the angle between NH bond close to methyl group and the plane of aromatic ring is 34.5° and the angle between other N-H bond and the ring is 21.1°. This shows that the amino group is turned to avoid proximity, due to the steric repulsion by the H atoms in the methyl group, and the methyl group is also turned to avoid proximity, due to this steric repulsion. The calculated angle between the ring plane and NH₂ plane is 42.4° in *o*-toluidine while it is 42.6° in *p*-toluidine and 44.2° in *m*-toluidine. These changes in the angles and C-C bondlengths support the interaction existing between methyl group and amino group in *o*-toluidine. As a result of this interaction between the two substituent groups, the rotation of the CH₃ group is slightly hindered by the NH₂ group in *o*-toluidine.

In conclusion, the near infrared overtone absorption spectra of liquid phase *o*-toluidine, *m*-toluidine and *p*-toluidine is analyzed using local mode model. The existence of steric and electronic interaction between amino and methyl groups in ground state of *o*-toluidine is well reflected in the vibrational overtone spectra

Chapter V

through a change in the CH and NH local mode mechanical frequency values. The vibrational structural studies using LIF and R2PI as well as *ab initio* calculations reported support this result. This illustrates the use of overtone spectroscopy as good diagnostic tool for probing even weak interactions in molecules and molecular conformations.

Table 5.2

Molecule	$\Delta V=2$	$\Delta V=3$	$\Delta V=4$	$\Delta V=5$	X_1	X_2	γ
<i>o</i>-toluidine							
Ring CH	5958.77	8749.68	11411.62	14003.64	3157.22	59.962	-0.999
NH	6639.23	8459.52	12669.45		3548.83	76.12	-0.9998
Methyl CH	5708.09	8319.47	10715.82		3118.9	87.55	-0.999
<i>m</i>-toluidine							
Ring CH	5920.32	8732.1	11394.71	13960.63	3132.9	56.61	-0.999
NH	6639.23	9722.9	12629.45		3563.8	81.1	-0.9998
Methyl CH	5733.29	8388.56	10903.94		3077.59	70.33	-1
<i>p</i>-toluidine							
Ring CH	5918.21	8714.6	11381.74		3130.47	56.84	-0.9997
NH	6669.78	9766.58	12711.33		3570.2	78.53	-0.9999
Methyl CH	5730.66	8367.5	10849.52		3094.86	76.48	-1
Aniline [19]							
Ring CH					3136.33		
NH					3549.56		

Observed overtone transition energies (cm^{-1}), mechanical frequencies X_1 (cm^{-1}), and anharmonicities X_2 (cm^{-1}) of aryl CH, NH and methyl CH in *o*-toluidine, *m*-toluidine and *p*-toluidine. The least square correlation coefficients (γ) are also given

5.3.3 Analysis of vibrational overtone spectra of N-methylaniline, N,N-dimethylaniline and N,N-diethylaniline

The molecular structures of N-methylaniline, N,N-dimethylaniline and N,N-diethylaniline are shown in fig. 5.32

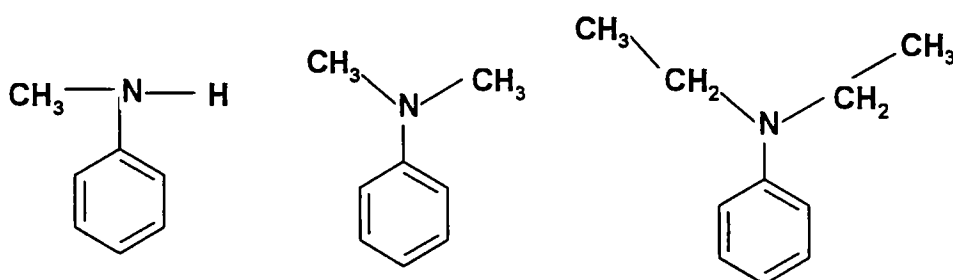


Fig. 5.32 The molecular structures of N-methylaniline, N, N-dimethylaniline and N, N-diethylaniline

The overtone spectra of aryl CH, NH and alkyl CH local mode oscillators of these compounds are shown in figures 5.33 – 5.41. In these figures, the peaks denoted by 'a' represents aryl CH overtones, 'b' represents alkyl CH overtones, 'c' represents NH overtones and others are combination peaks. The first overtone peak position in each case is assigned as the one giving best fit in the Birge-Sponer Plot with higher overtone peaks that are given in figures 5.42 – 5.44. The absorption frequencies satisfying Birge-Sponer Plot, the mechanical frequency and anharmonicity values obtained for the aryl CH, NH and alkyl CH oscillators for each molecule are given in Table 5.3. Overtone peaks corresponding to non-equivalent methyl CH oscillators are not distinct due to the low resolution of the liquid phase spectra.

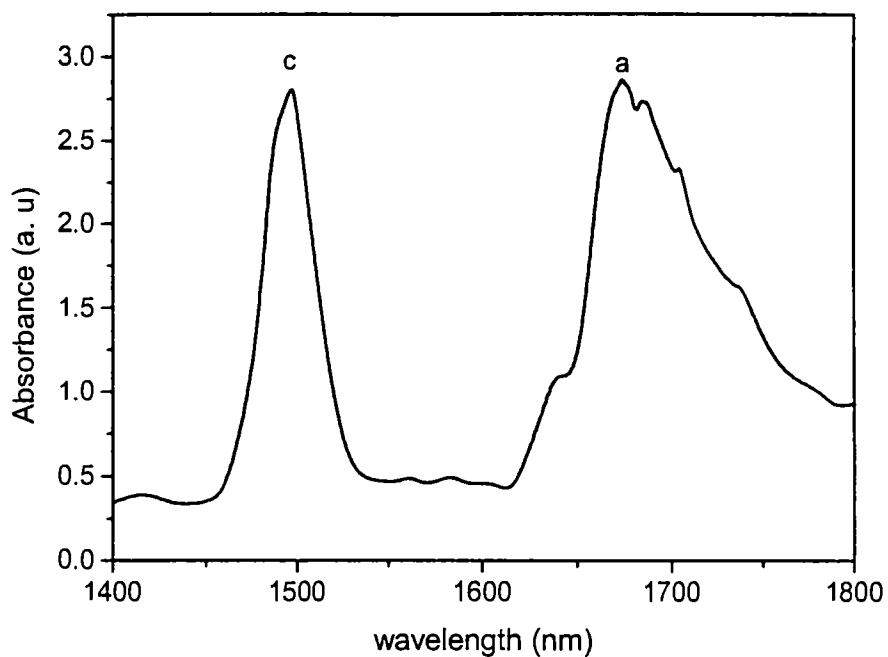


Fig.5.33. The aryl CH and NH overtone bands of *N*-methylaniline in the $\Delta V = 2$ region

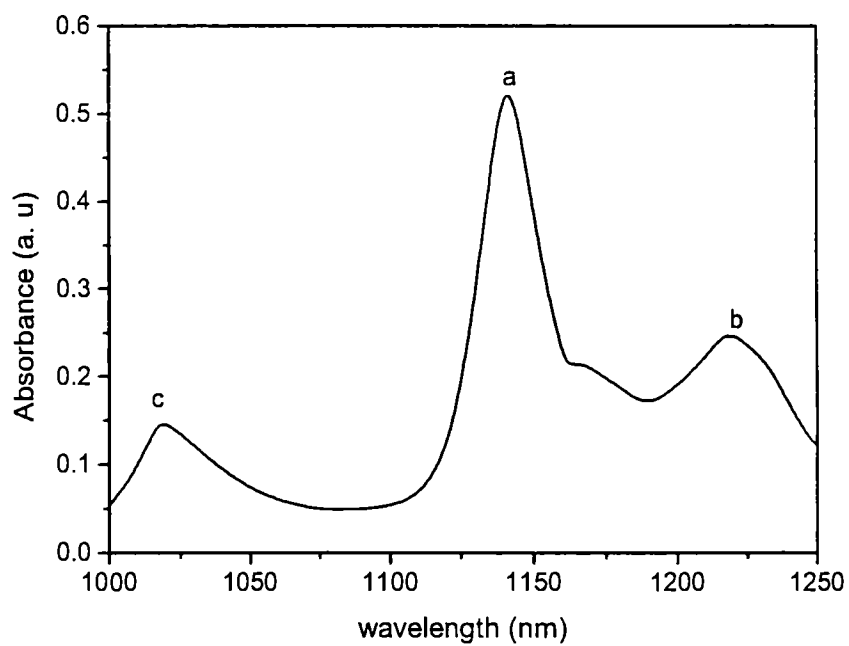


Fig.5.34. The CH (aryl and alkyl) and NH overtone bands of *N*-methylaniline in the $\Delta V = 3$ region

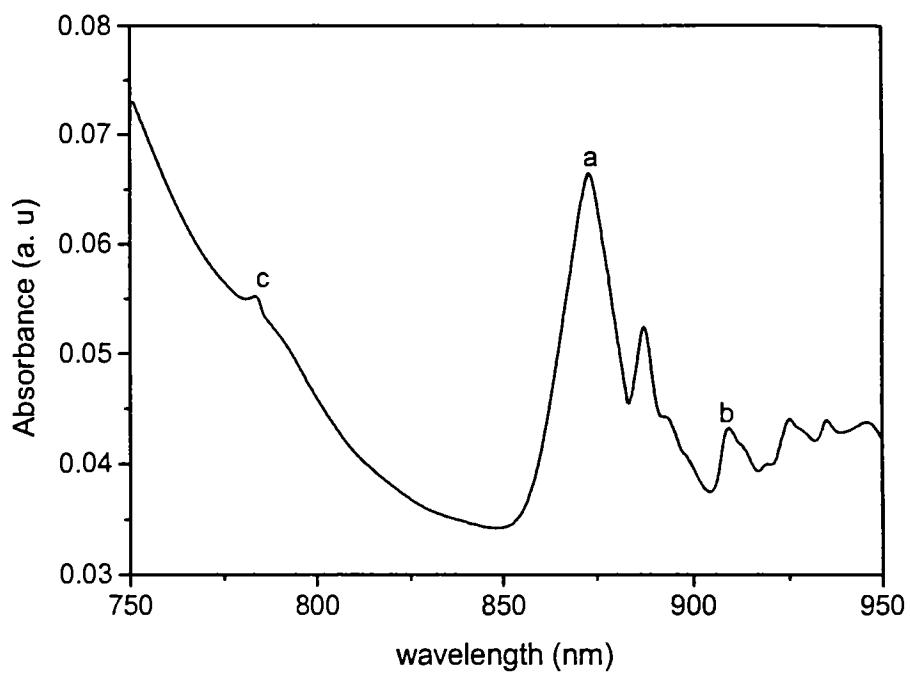


Fig.5.35. The CH (aryl and alkyl) and NH overtone bands of *N*-methylaniline in the $\Delta V = 4$ region

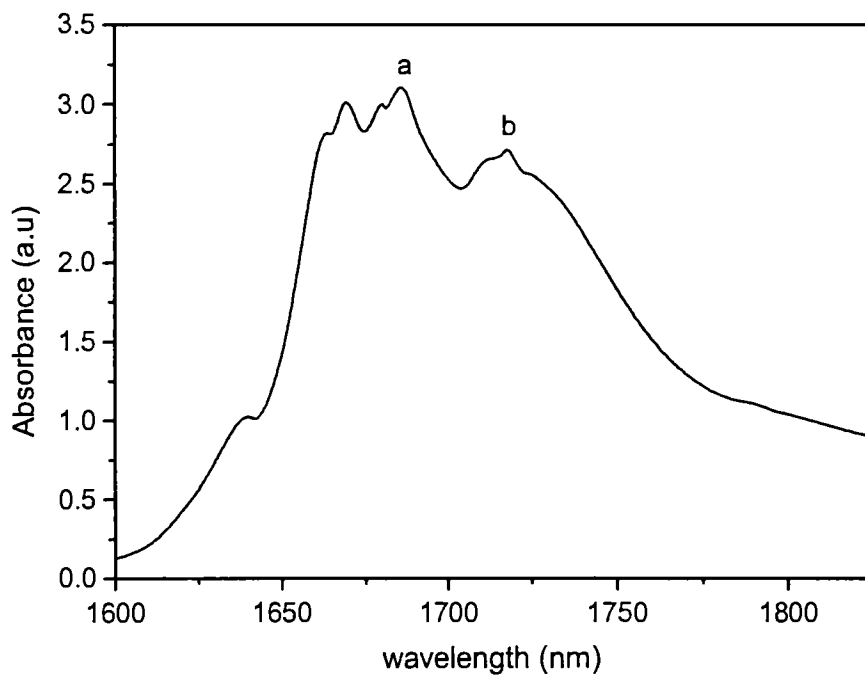


Fig.5.36. The aryl and alkyl CH overtone bands of *N,N*-dimethylaniline in the $\Delta V = 2$ region

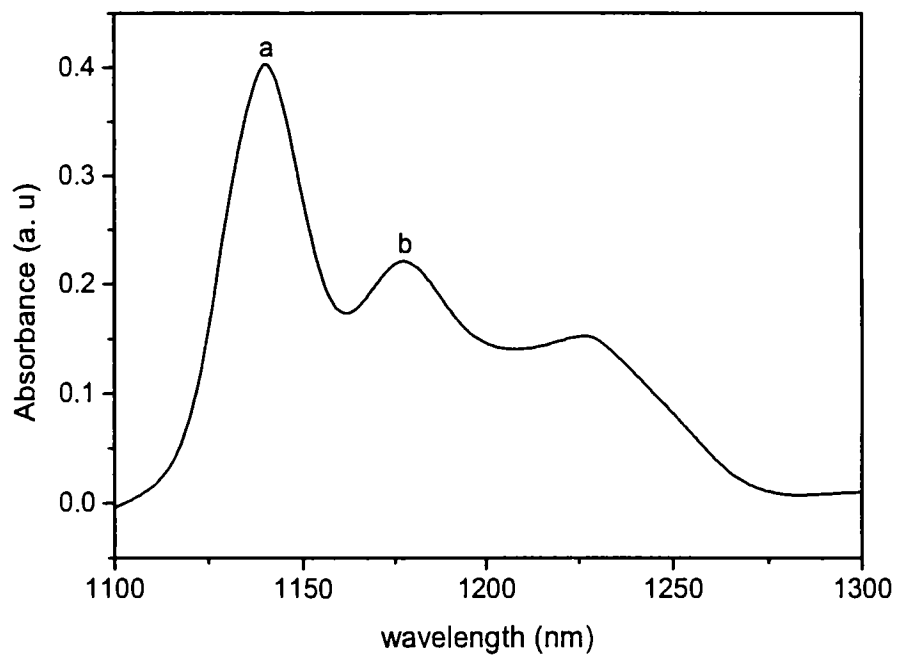


Fig.5.37. The aryl and alkyl CH overtone bands of *N,N*-dimethylaniline in the $\Delta V = 3$ region

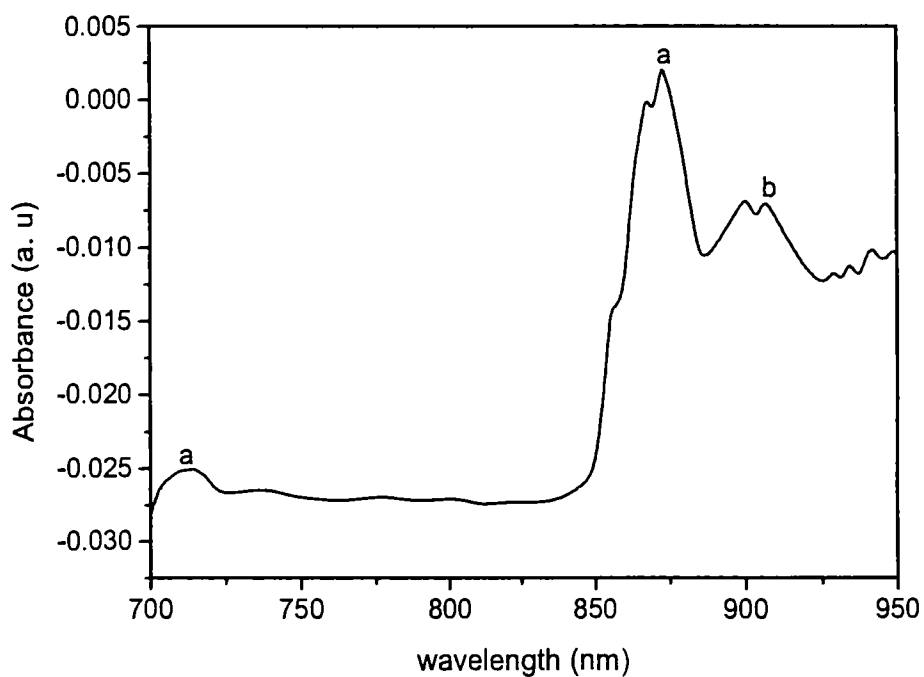


Fig.5.38. The aryl ($\Delta V = 4$ and 5) and alkyl ($\Delta V = 4$) CH overtone bands of *N,N*-dimethylaniline

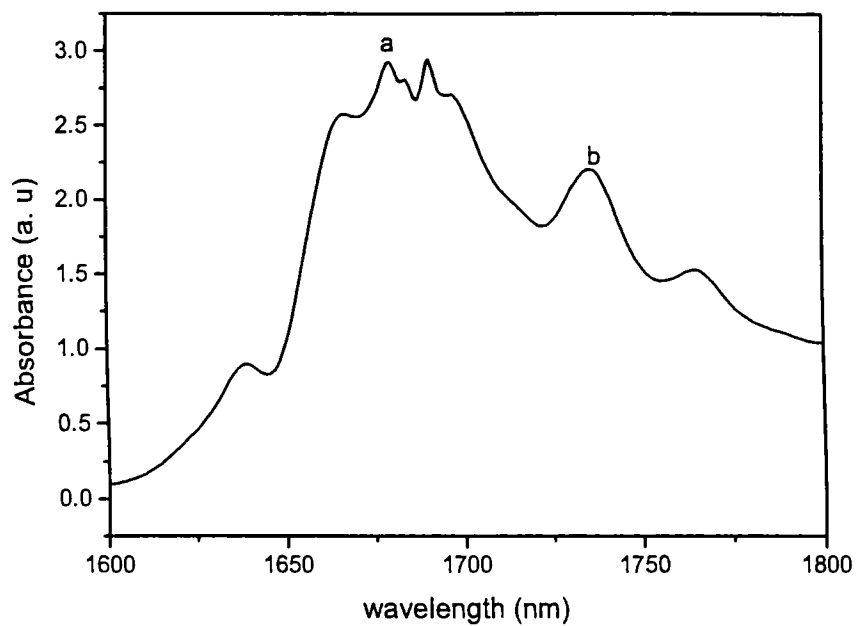


Fig.5.39. The aryl and alkyl CH overtone bands of *N,N*-diethylaniline in the $\Delta V = 2$ region

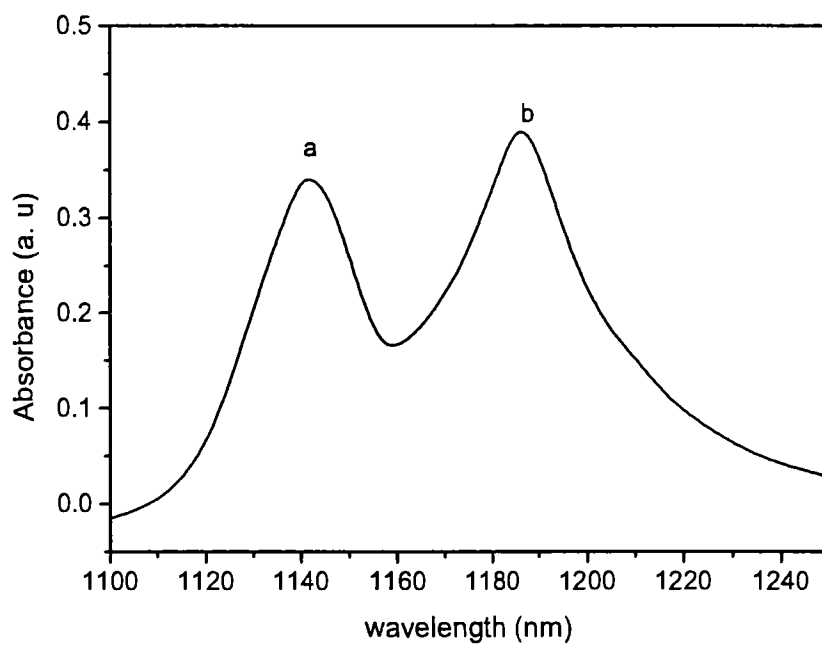


Fig.5.40. The aryl and alkyl CH overtone bands of *N,N*-diethylaniline in the $\Delta V = 3$ region

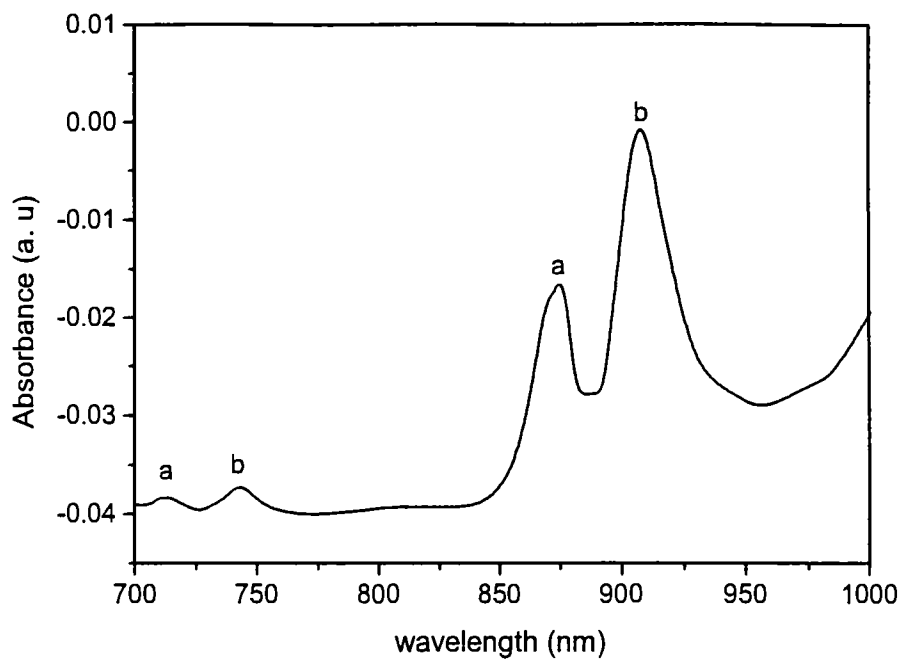


Fig.5.41. The aryl and alkyl CH overtone bands of *N,N*-diethylaniline in the $\Delta V = 4$ and $\Delta V = 5$ region

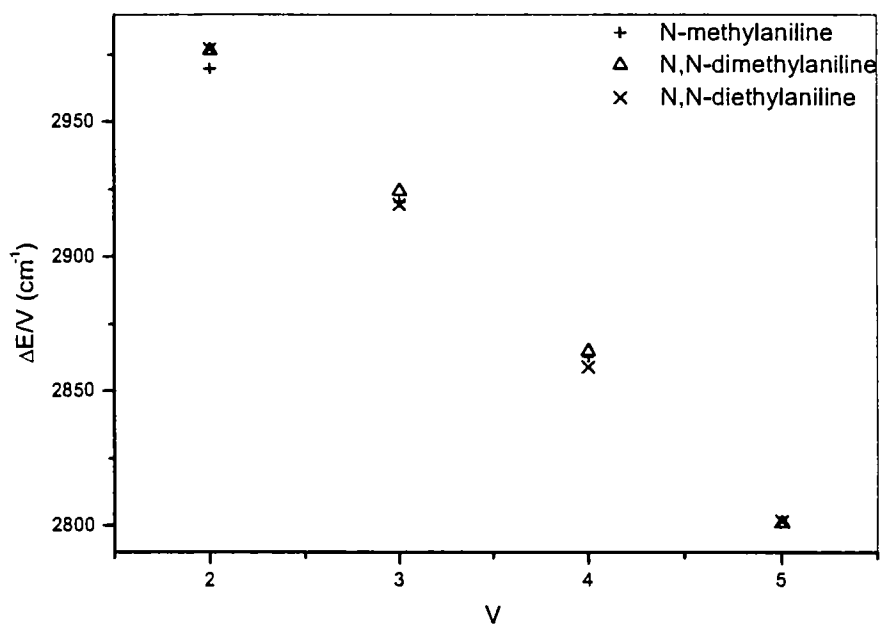


Fig.5.42. Birge-Sponer plots for ring CH overtones of *N*-methylaniline, *N,N*-dimethylaniline and *N,N*-diethylaniline

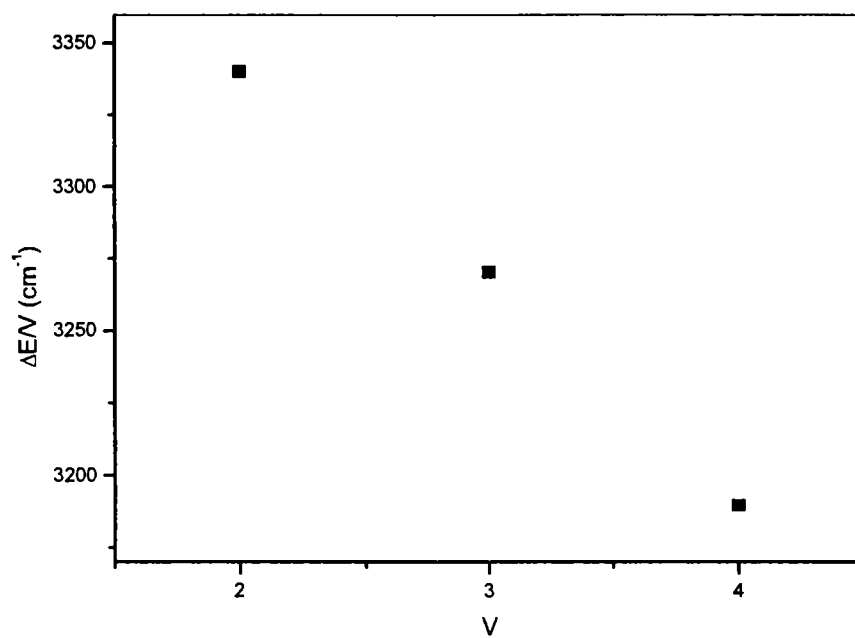


Fig.5.43. Birge-Sponer plots for NH overtone of N-methylaniline

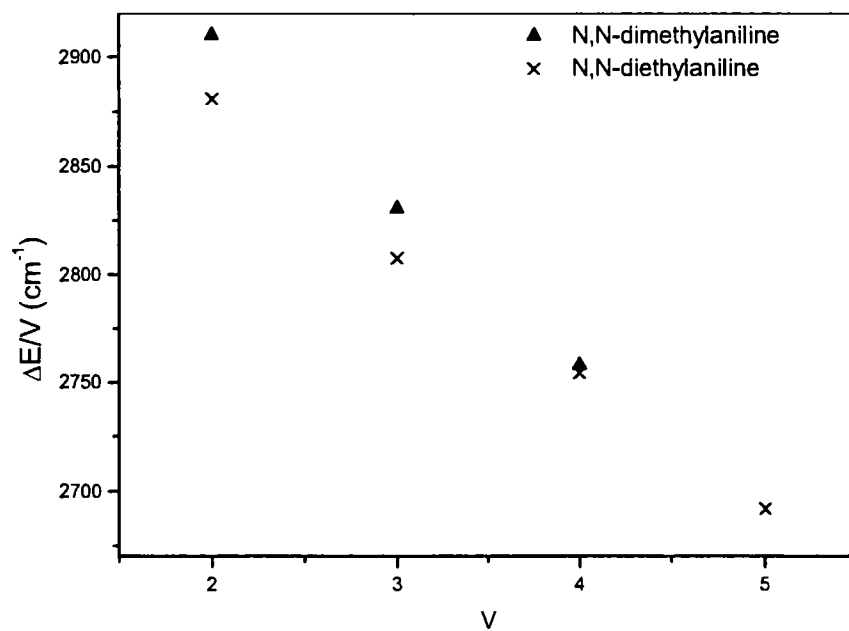


Fig.5.44. Birge-Sponer plots for alkyl CH overtones of N,N-dimethylaniline and N,N-diethylaniline

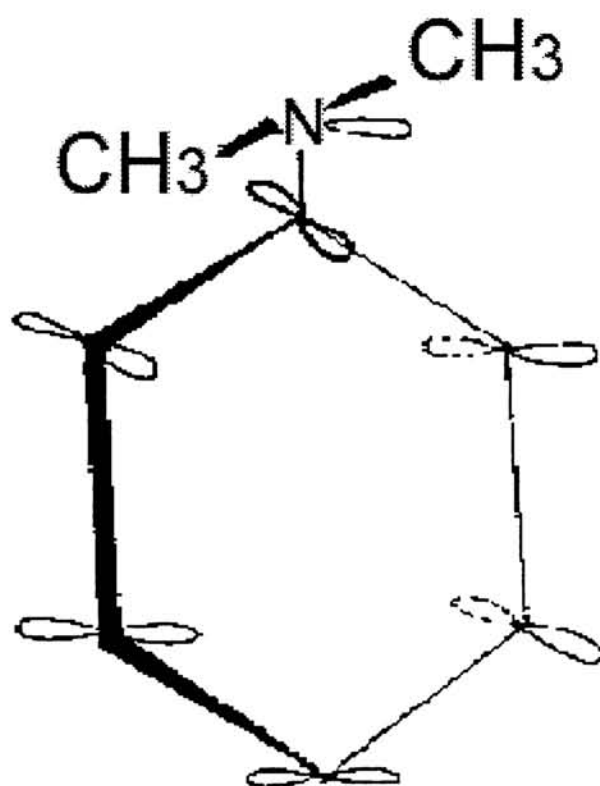


Fig.5.45. Perpendicular configuration of π -electrons in N,N-dimethylaniline

Molecule	$\Delta V=2$ (cm^{-1})	$\Delta V=3$ (cm^{-1})	$\Delta V=4$ (cm^{-1})	$\Delta V=5$ (cm^{-1})	$X_1=A-B$ (cm^{-1})	$X_2=B$ (cm^{-1})	γ
N-methylaniline aryl CH	5939.66	8761.17	11450.8	-	3131.88	-53.56	-0.999
N-methylaniline NH	6680	9810.66	12758.36		3567.45	-75.21	-0.9991
N,N-dimethylaniline aryl CH	5953.44	8773.47	11460	14005.6	3155.67	-58.63	-0.999
N,N-dimethylaniline alkyl CH	5820.38	8492.58	11032.64		3137.12	-76	-0.9997
N,N-diethylaniline aryl CH	5954.51	8758.11	11436.4	14009.5	3153.25	-58.63	-0.9999
N,N-diethylaniline alkyl CH	5762.02	8423.88	11018.08	14810.75	3062.92	-62	-0.998
Benzene [22]					3148		
Aniline[19]					3136.3	-55.83	

Table.5.3 Observed overtone transition energies, mechanical frequencies (X_1) and anharmonicity (X_2) values for aryl CH, NH and alkyl CH overtones in N-methylaniline, N,N-dimethylaniline and N,N-diethylaniline. γ is the least square correlation coefficient.

Table.5.4 A comparison of the mechanical frequencies (X_1) and anharmonicity (X_2) values for aryl CH oscillators in N-methylaniline, N,N-dimethylaniline and N,N-diethylaniline with those of benzene and aniline.

Molecule	X_1 (cm^{-1})	X_2 (cm^{-1})
Benzene [24]	3148	
Aniline	3136.3	-55.83
N-methylaniline	3131.88	-53.56
N,N-dimethylaniline	3155.67	-58.63
N,N-diethylaniline	3153.25	-58.63

It is well established that the aromatic nucleus has a significant effect on the properties of the amino group attached to it. The amino group shares its lone pair of electrons with the ring. The amino group in its turn exerts an influence on the properties of the aromatic ring also. This is a consequence of the conjugation of the lone-paired electron on nitrogen with the mobile π - electrons of the aromatic nucleus [17].

Overtone spectroscopic studies assert that an electron-donating group added to the phenyl ring decreases the mechanical frequency of the ring CH oscillator than that of benzene and an electron-withdrawing group causes an increase in the value than that of benzene [6, 37-41]. The Hammett σ constants which indicate the donating or withdrawing nature of the substituent [42] shows that the $-\text{NH}_2$ group and the $-\text{CH}_3$ group serve as electron donors to the phenyl ring through both inductive and resonance electron donating mechanisms. Hence in effect, both these electron-donating groups reduce the ring CH mechanical frequency. The CH_3 group interacts with the nearby π system via hyperconjugation, while the NH_2 group shares its lone pair electrons with the π electrons in the ring. In all these compounds, the alkyl group is attached to the amino group by removing hydrogen atoms. The mechanical frequencies and anharmonicity constants for the aryl CH, NH and alkyl CH oscillators, obtained for

the three molecules are given in Table 5.3. For aniline the mechanical frequency of aryl CH oscillator is lower ($\sim 12 \text{ cm}^{-1}$) than that of benzene. This is because of the conjugation of the nitrogen lone pair electrons with the π electron cloud of the benzene ring. One can therefore expect an electron donating effect by the amino group, which in turn results in an increased electron density on the ring carbon atom. This causes a decrease in the force constant and hence a corresponding decrease in the mechanical frequency of the ring CH oscillator from that of benzene. The CH_3 group is also electron donating one. Thus ring CH mechanical frequency value for N-methylaniline is 3132 cm^{-1} , which is lower than ($\sim 16 \text{ cm}^{-1}$) benzene. Thus the electron donating nature of both amino and methyl substituents are reflected in the decrease in ring CH mechanical frequency value for N-methylaniline with respect to that of benzene and aniline. The NH mechanical frequency value for N-methylaniline is found to be greater than ($\sim 18 \text{ cm}^{-1}$) that of aniline. There can be an attractive interaction between the lone-paired electrons in nitrogen atom of the amino substituent and the hydrogen atoms of the alkyl substituents in addition to the ring-substituent interaction. This may cause the NH mechanical frequency in N-methylaniline to increase. The effect of the heteroatom on the methyl group is explained as the interaction of lone pair of electrons in the heteroatom with the CH bonds situated trans to the lone pair. The effect is termed lone pair trans effect [43, 44] and it is explained to originate from the donation of the electron density from the lone pair to the antibonding orbitals of CH bonds trans to the lone pair. This also reduces the electron density at the nitrogen atom, which causes the increase in NH mechanical frequency in N-methylaniline. This effect may cause two distinct peaks for methyl overtones at each overtone level. Due to the low resolution of the liquid phase overtone spectra, this effect could not be observed in all the alkyl overtone regions. Even though CH_3 group at this position has not much influence on the σ bonding system of the ring, its interaction with lone pair electrons in nitrogen can exist.

In N,N-dimethylaniline, the aryl CH mechanical frequency obtained is 3156 cm^{-1} and is found to be greater than that of benzene ($\sim 8 \text{ cm}^{-1}$). This increase in ring CH mechanical frequency value than benzene and N-methylaniline indicates that there exists no electron donation or reduced interaction between the lone pair electron on nitrogen and π - electron density on the ring for N,N-

dimethylaniline. This may be because in N,N-dimethylaniline, the CH₃ groups lie in the ring plane and the p-orbital of the free electron on nitrogen is perpendicular to the plane of the ring. This is depicted in fig.5.45. Thus, interaction between the lone pair electrons on nitrogen and π - electrons on the ring become impossible. Hence the donation of the lone pair of electrons in amino group to the ring will not take place and ring CH mechanical frequency will not show a decrease. We propose that, now the inductive effect of the nitrogen here, will act which favors withdrawal of electrons from the ring. As a result the electron density on the ring carbon atom declines and a net positive charge accumulates on the ring carbon. Thus electrostatic interaction between the positive carbon atom and electron cloud of the hydrogen atom increases and hence the CH bond length decreases. This will result in an increased force constant and hence an increased mechanical frequency than that of benzene. The same effect is expected in N,N-diethylaniline also. In N,N-diethylaniline, the aryl CH mechanical frequency obtained is 3153 cm⁻¹ and is found to be greater than that of benzene (~5 cm⁻¹). This increase in ring CH mechanical frequency value for N,N-diethylaniline than benzene and N-methylaniline indicates that there also no electron donation or reduced interaction between the lone pair electron on nitrogen and π - electron density on the ring as observed in N,N-dimethylaniline. In N,N-diethylaniline also the ethyl groups lie in the ring plane and the p-orbital of the free electron on nitrogen is perpendicular to the plane of the ring. Thus, interaction between the lone pair electrons on nitrogen and π - electrons on the ring become impossible. Hence the same effect is the cause for increased value of ring CH mechanical frequency in both these compounds. In N,N-diethylaniline, the mechanical frequency of the CH oscillator is found to be greater than that of benzene (~5 cm⁻¹) and is comparable with that of N,N-dimethylaniline also. So in both these compounds, the alkyl groups lie in the ring plane and the p-orbital of the free electron on nitrogen is perpendicular to the plane of the ring. This orientation of the alkyl groups reduces the interaction between the lone pair electrons on nitrogen and π - electrons on the ring and hence the inductive effect of nitrogen and the electron withdrawal becomes the dominating one and this effect is evident from the increase in the aryl CH mechanical frequency values for both the molecules than that of benzene.

In N-methylaniline the conjugation between the lone pair of electrons in nitrogen and π - electron system of the phenyl ring is possible since their parallel orientation is not disturbed. The mechanical frequency and anharmonicity constant for the CH local oscillators for N-methylaniline, N,N-dimethylaniline and N,N-diethylaniline and a comparison with the same for aniline and benzene are given in Table 5.4. The ring CH mechanical frequency obtained for N-methylaniline is comparable to that of aniline. This indicates that there exists considerable donation of the lone-paired electrons between ring and the amino group. The electron donating nature of methyl group also favors this interaction. The increase in the NH mechanical frequency for N-methylaniline is due to the attraction of the hydrogen atoms in the alkyl group with the lone pair electrons in the nitrogen atom. But this will not hinder the donation mechanism of the amino group to the ring also. Consequently, the mechanical frequency of the ring CH oscillator decreases and that of the NH oscillator increases.

In conclusion, the near infrared vibrational overtone spectra of liquid phase N-methylaniline, N,N-dimethylaniline and N,N-diethylaniline are analyzed using local mode model. The analysis of the mechanical frequency values of CH and NH oscillators reveal the details of molecular conformation of these molecules. This illustrates the use of overtone spectroscopy as an effective tool in molecular structure, conformational aspects and substituent effects.

References

- [1] W.R.A.Greenlay and B.R.Henry; *Chem. Phys. Lett.*, 53(2) (1978) 325.
- [2] B.R.Henry and J.A.Thomson; *Chem. Phys. Lett.*, 69 (1980) 275.
- [3] B.R.Henry, M.A.Mohammadi and J.A.Thomson; *J. Chem. Phys.*, 75 (1981) 3165.
- [4] R.Nakagaki and I.Hanazaki; *Chem. Phys. Lett.*, 83 (1981) 512.
- [5] H.L.Fang and R.L.Swofford; *Appl. Opt.*, 21 (1982) 55.
- [6] K.M.Gough and B.R.Henry; *J. Phys. Chem.*, 87 (1983) 3433.
- [7] K.M.Gough and B.R.Henry; *J. Phys. Chem.*, 88 (1984) 1298.
- [8] A.W.Tarr and B.R.Henry, *Chem. Phys. Lett.*, 112 (1984) 295.
- [9] H.L.Fang, R.L.Swofford, M.McDevitt and A.R.Anderson; *J. Phys. Chem.*, 89 (1985) 225.
- [10] M.K.Ahmed, D.J.Swanton and B.R.Henry; *J. Phys. Chem.*, 91 (1987) 293.
- [11] M.K.Ahmed and B.R.Henry; *J. Phys. Chem.*, 91 (1987) 3741.
- [12] M.K.Ahmed and B.R.Henry; *J. Phys. Chem.*, 91 (1987) 5194.
- [13] M.G.Sowa, B.R.Henry and Y.Mizugai; *J. Phys. Chem.*, 97 (1993) 809.
- [14] H.G.Kjaergaard and B.R.Henry; *J. Phys. Chem.*, 99 (1995) 899.
- [15] D.M.Turnbull, M.G.Sowa and B.R.Henry; *J. Phys. Chem.*, 100 (1996) 13433.
- [16] H.G.Kjaergaard, D.M.Turnbull and B.R.Henry; *J. Phys. Chem.*, 101 (1997) 2589.
- [17] V.M.Potapov; "*Stereochemistry*", Mir Publishers (Moscow), 1978, p.541.
- [18] L.N.Ferguson; "*The modern structural theory of organic chemistry*", Prentice-Hall of India (New Delhi), 1969, p.134.
- [19] S.Shaji and T.M.A.Rasheed; *Spectrochim. Acta. Part A*, 57 (2001) 337.
- [20] W.B.Tzeng, K.Narayanan, J.L.Lin and C.C.Tung; *Spectrochim. Acta. Part A*, 55 (1999) 153.
- [21] W.B.Tzeng and K.Narayanan; *J. Mol. Struct.*, 446 (1998) 93.
- [22] T.K.Pal, G.K.Mallik, S.Laha, K.Chatterjee, T.Ganguly and S.B.Banerjee; *Spectrochim. Acta. A*, 43 (1987) 853.
- [23] K.M.Gough and B.R.Henry; *J. Phys. Chem.*, 87 (1983) 3433.
- [24] G.Roussy, A.Nonat and J.Barriol; *Compy. Rend. Ser.II*, 302 (1986) 935.
- [25] A.Nonat, A.Bouchy and G.Roussy; *J. Mol. Struct.*, 97 (1983) 83.

- [26] A.Nonat, A.Bouchy and G.Roussy; *J. Mol. Spect.*, 108 (1984) 230.
- [27] A.Nonat, A.Bouchy and G.Roussy; *J. Mol. Struct.*, 116 (1984) 227.
- [28] V.E.Borisenko, A.V.Baturin, Przeslawska and A.Koll; *J. Mol. Struct.*, 407 (1997) 53.
- [29] V.K.Rai, S.B.Rai and D.K.Rai, *Spectrochim. Acta. A.*, 59 (2003) 1299.
- [30] B.Ballesteros and L.Santos; *Spectrochim. Acta. A*, 58 (2002) 1069.
- [31] G.Varsanyi; “*Assignments of vibrational spectra of 700 benzene derivatives*”, Wiley (New York), 1974.
- [32] J.C.Jiang and C.E.Lin; *J. Mol. Struct. (Theochem)*, 392 (1997) 181.
- [33] M.E.Vaschetto, B.A.Retamal and A.P.Monkman; *J. Mol. Struct. (Theochem.)*, 468 (1999) 209.
- [34] L.Santos, E.Martinez, B.Ballesteros and J.Sanchez; *Spectrochim. Acta. A*, 56 (2000) 1905.
- [35] B.Ballesteros, E.Martinez, L.Santos and J.Sanchez-Merin; *J. Mol. Struct.*, 605 (2002) 255.
- [36] W.B.Tzeng, K.Narayanan, C.Y.Hsieh and C.C.Tung; *J. Chem. Soc. Faraday Trans.*, 93 (1997) 2981.
- [37] Y.Mizugai and M.Katayama; *J. Am. Chem. Soc.*, 102 (1980) 6424.
- [38] R.Nakagaki and I.Hanazaki; *Spectrochim. Acta A*, 40 (1984) 57.
- [39] T.M.A.Rasheed, K.P.B.Moosad, V.P.N.Nampoori and K.Sathianandan; *J. Phys. Chem.*, 91 (1987) 4228.
- [40] T.M.A.Rasheed and V.P.N.Nampoori; *Pramana.*, 42 (1994) 245.
- [41] T.M.A Rasheed; *Spectrochim. Acta A*, 52 (1996) 1493.
- [42] L.N.Fergusen; “*The modern structural theory of organic chemistry*”, Prentice-Hall of India (New Delhi), 1969, p.421.
- [43] L.J.Bellamy and D.W.Mayo; *J. Phys. Chem.*, 80 (1976) 1217.
- [44] L.J.Bellamy; *Appl. Spectrosc.*, 33 (1979) 439.

Chapter VI

**PULSED LASER INDUCED FLUORESCENCE AND RAMAN
STUDIES OF SOME COMPOUNDS**

	Page
6.1 Introduction.....	152
6.2 Fluorescence and Raman effect	153
6.3.a Molecular structural studies by LIF – a brief survey of recent works	155
6.3.b Molecular structural studies by Laser Raman spectroscopy – a brief survey recent works	156
6.4 Experimental Setup	158
6.5 Experimental considerations	159
6.6 Pulsed laser Raman spectrum of aniline, <i>o</i> -chloroaniline and <i>m</i> - chlorotoluene	162
6.6.1 Pulsed laser Raman spectrum of Aniline	163
6.6.2 Pulsed laser Raman spectrum of <i>o</i> -chloroaniline.....	165
6.6.3 Pulsed laser Raman spectrum of <i>m</i> -chlorotoluene	167
6.7 Conclusions	169
References	170

Chapter VI

PULSED LASER INDUCED FLUORESCENCE AND RAMAN STUDIES OF SOME COMPOUNDS

6.1 Introduction

Both fluorescence and Raman spectroscopy are important spectroscopic tools for studying details of molecular energy levels and structural aspects. As already described in chapter I, the technological advances in lasers provided all the areas of spectroscopy with ideal light sources satisfying the requirements for each, in terms of monochromaticity, tunability, directionality, coherence properties, irradiance and spectral coverage. In the laser era, both laser induced fluorescence (LIF) and Raman spectroscopy have become standard tools for studying molecules and also found widespread diagnostic and analytical applications. Extensive literature is available which reviews these important areas of spectroscopy [1-6].

Pulsed lasers provide additional advantages in both the above areas. With small values of temporal pulsed duration (microseconds to femtoseconds) pulsed laser output generally possesses high peak powers (ratio of pulse energy to pulse duration). While the short duration laser pulses find important applications in time resolved studies of different molecular processes [7], the high peak powers govern the intensities of single shot fluorescence and Raman spectra. The peak intensity of fluorescence emission induced by one photon absorption is proportional to the input irradiance, whereas that induced by two photon absorption is proportional to the square of the incident peak power [8]. Two photon-induced fluorescence provides with a means of studying spectroscopic transitions that are forbidden in one photon absorption. Because of the very small values of absorption cross section for two photon processes, large values of incident intensity are generally required for observing two photon absorption, thus leading to the requirement of pulsed lasers in such experiments, even though some molecular systems undergo two photon transition under CW excitation [9-10]. Like two photon absorption, Raman scattering is also a nonlinear process (the only nonlinear process observed before the development of lasers). Thus excitation by a pulsed laser results in high intensity single shot Raman spectra also.

Recent development of high sensitive solid state detectors called charge coupled devices (CCD), which could be used as electronic analogue of the old photographic plates in spectroscopy, of course with many advantages like high sensitivity, fast response and ease for data processing using a PC, provided scientists with a very convenient method for the detection and analysis of single shot events induced by pulsed lasers [4]. Thus the detection and measurement of single shot fluorescence and Raman spectra, in otherwise difficult or impossible situations due to very low probabilities of the processes, have become a reality. With the combined use of a pulsed laser for excitation and a suitable PC controlled monochromator fitted with a CCD device provides us with a strong tool for spectral analysis.

With the availability of a pulsed Nd:YAG laser and a suitable PC controlled monochromator fitted with CCD device in our department motivated us for examining the fluorescence/Raman scattering of some of the compounds which we investigated by overtone spectroscopy. The present chapter gives the details of the experimental arrangement, the LIF spectra obtained for carbon disulfide and aniline and the Raman spectra obtained for aniline, *o*-chloroaniline, and *m*-chlorotoluene. The observed Raman peaks are assigned successfully and some new low-lying vibrations are also found in these molecules.

6.2 Fluorescence and Raman effect

There are many chemical systems, which are photoluminescent i.e., they can be excited by electromagnetic radiation and as a consequence, re-emit radiation either of the same wavelength or of different wavelength. Fluorescence and phosphorescence are the two important manifestation of photoluminescence. Both fluorescence and phosphorescence constitute possible mechanisms where by electronically excited molecules can lose energy. The two phenomena can be distinguished experimentally by observing the lifetime of the excited states. During the process of excitation, most of the affected molecules acquire vibrational as well as electronic energy. The greatest tendency for them is to drop to lower vibrational states through collisions. If this radiationless process stops at an excited singlet electronic level, the molecule may return directly from there to the ground state by

the radiation of a photon and the phenomenon is known as fluorescence. If they may shift to a metastable triplet state, which is less common, before emitting the radiation and then the radiative emission takes place. This process is known as phosphorescence. The various factors affecting fluorescence and phosphorescence, and their applications are well reviewed [4, 11].

A molecule can be considered as an assembly of positively charged nuclei and negatively charged electrons. When a monochromatic laser beam of high frequency strikes a molecule, it interacts strongly with electrons. The oscillating dipoles of the electrons scatters light in all directions at the incident laser frequency and the process is called Rayleigh scattering. It can be viewed as an elastic collision between the molecule and the light photon. The second type of collision is inelastic collision where the photon either loses or gains energy from the molecule. The energy of the scattered light is $h(\nu_0 - \nu_1)$ or $h(\nu_0 + \nu_1)$, the loss or gain in energy $h\nu_1$ corresponds to the vibrational energy. Thus the energy of the scattered light depends on the frequency of the incident light, but the displacement $h\nu_1$ from Rayleigh line is a constant corresponding to the vibrational level.

A record of the vibrational levels as measured by the displacements from the incident frequency is the Raman spectrum. The Stoke's bands on the low energy side of the Rayleigh line have intensities typically of the order of 10^{-5} of the Rayleigh line. The bands on the high energy side of the Rayleigh line are called Anti-Stoke's lines. The higher intensity of Stoke's line is due to the higher population of molecules in the ground vibrational states compared to those in the excited level.

In measurements of Raman spectra, the laser beam is introduced into the sample cell and the scattered light is usually observed at an angle of 90° to the laser beam. If an analyzer is inserted between the cell and the monochromator slit, the intensity of the Raman bands can be noted and the depolarization ratio (the ratio of the light intensity when the analyzer is perpendicular to that when it is parallel) can be calculated. Vibrations for which depolarization ratio is between 0 – 0.75 are called polarized and are caused by symmetric vibrations; those which it is 0.75 are called depolarized and are caused by totally asymmetric and degenerate vibrations. Measurements of depolarization ratios are useful for assigning bands to

particular vibrational modes and in separation of overlapping bands. The theory and application of Raman spectroscopy are well reviewed [12, 13].

6.3.a Molecular structural studies by LIF – a brief survey of recent works

The application of laser induced fluorescence to high temperature plasmas with principles of LIF, tunable lasers and LIF, calibration of optical systems and plasma measurements are reviewed by Muraoka *et al* [4]. LIF technique is a very important technique in radical detection. Heintxe *et al* [14] has reported the detection of SiH₂ radicals in an a-Si:H deposition plasma by LIF. The LIF detection and kinetics of SiH₂ radical in Ar/H₂/SiH₄ radio frequency discharges is reported by Hertl *et al* [15]. LIF spectroscopy of the jet-cooled methyl thio radical (CH₃S) is reported by Misra *et al* [16]. NO₃ radical is studied using LIF by Kim *et al* [17]. They have reported the fluorescence emission spectra of NO₃ excited at 14742, 15109, 15882, 16053 and 16555 cm⁻¹ and the observed are assigned on the basis of the fundamentals, overtones and combinations of five vibrational frequencies of NO₃.

LIF excitation spectrum of jet-cooled 4-(9-anthryl) aniline helps in observing two weakly coupled electronic states. The LIF excitation spectra and vibrational studies are reported by Lee *et al* [18]. The laser induced dispersed fluorescence experiment offers new possibilities when applied to vibration – rotation states within ground electronic states. This technique as a new tool to study the molecular states is reported by Metsaalaa *et al* [19].

LIF method has been used to study the highly excited vibrational overtones in acetylene. The laser induced vibration – rotation fluorescence and infrared forbidden transitions in acetylene is reported by Jungner *et al* [20]. Collision induced vibration – rotation fluorescence spectra and rovibrational symmetry changes in acetylene are studied by Saarinen *et al* [21]. LIF method has been used to investigate collision-induced processes in the hydrogen stretching vibrational overtone region of the ground electronic state of acetylene.

LIF spectroscopy for phenol and intermediate products in aqueous solutions degraded by pulsed corona discharges above water is done by Hayashi *et al* [22]. They have introduced LIF spectroscopy as an '*in-situ*' diagnostic for phenol and diagnostic products in an aqueous solution degrading. *In-situ* measurements of

subsurface contaminants with a multi-channel LIF system is reported by Pepper *et al* [23].

LIF measurements of formaldehyde in a methane/air diffusion flame is done by Harrington *et al* [24]. This is an important optical measurement in flames of naturally occurring formaldehyde, an important intermediate in the oxidation of hydrocarbons. LIF studies of formaldehyde hot bands in flames is done by Klein-Douwel *et al* [25]. LIF and excitation spectra of formaldehyde in the A-X₄₁⁰ band at 370 nm are recorded in the primary flame front of a Bunsen flame. An examination of the partition functions shows that this excitation can minimize temperature bias for formaldehyde in situ diagnostic measurement.

Vibrational (Infrared) planar laser induced fluorescence (PLIF) imaging technique is used for CO₂ that use a simple, inexpensive, high pulse energy transversely excited atmospheric CO₂ laser to saturate a CO₂ absorption transition at 10.6 μm. This CO₂ imaging with saturated planar laser induced vibrational fluorescence is reported by Kirby *et al* [26]. PLIF imaging of CO using vibrational (IR) transitions is also reported by them [27]. An IR camera collects infrared PLIF, in which a tunable IR source is used to excite vibrational transitions in the IR active molecules and vibrational fluorescence. LIF technique using excitation in the A-X and D-X electronic systems have proven a reliable technique for two dimensional imaging of nitric oxide (NO) concentrations in practical combustion systems. LIF detection of NO in high pressure flames with A-X (0,0), (0,1) and (0,2) excitation is reported by Lee *et al* [28].

Two photon induced fluorescence from the phycoerythrin protein is reported by Chen *et al* [29]. Temporal, spectral and intensity dependant properties of the two photon induced fluorescence emission from phycoerythrin excited by a 1.06 μm laser beam are reported.

6.3.b Molecular structural studies by Laser Raman spectroscopy – a brief survey recent works

Laser Raman spectra and their assignments of a large number of organic and inorganic molecules are described by Brame Jr. *et al* [30] and Nakanishi *et al* [12]. Ito [31] has described the fundamental of Raman spectra and the earlier works done by him on laser Raman spectroscopy. A description of the applications

of resonance Raman spectroscopy in heme proteins is done by Spiro [5]. Applications of Raman spectroscopy in high pressure research are reviewed by Jayaraman *et al* [6]. Interference enhanced Raman spectroscopy of ultra thin crystalline germanium (Ge) films is reported by Kanakaraju *et al* [32]. Resonance Raman spectroscopy is normally used to study the excited state structure and dynamics of various photochemical and photophysical processes. The various applications of resonance Raman spectroscopy in ultrafast chemical dynamics is reported by Biswas *et al* [33].

The Raman spectrum of 4-fluoroaniline with its theoretical vibrational studies is reported by Town *et al* [34]. The microwave and laser Raman spectroscopy of *o*-chlorotoluene is reported by Nair *et al* [35]. The Raman spectra provides some of the newly observed low lying vibrational modes in *o*-chlorotoluene and a torsional state of methyl group in the molecule. The vibrational spectra and structure of benzophenone and its ^{18}O and d_{10} labelled derivatives are reported by Kolev *et al* [36]. They have done the vibrational analysis using *ab initio* molecular orbital (MO) calculations and experimental study by infrared and Raman spectra. The high resolution Raman study of phonon and vibron bandwidths in isotopically pure and natural benzene crystal is reported by Pinan *et al* [37]. The Raman spectrum of gaseous $^{13}\text{C}_2\text{H}_2$ is recorded with charge coupled device camera detection is reported by Becucci *et al* [38]. They have obtained vibration – rotation bands of fundamentals, overtones and combinations in acetylene. Some Q branches of $^{12}\text{C}^{13}\text{CH}_2$ are also detected. Vibrational Raman spectroscopic study of scytonemin is reported by Edwards *et al* [39].

The measurement of methanol proportion in methanol – gasoline mixtures as an application of fiber optic Raman spectroscopy is reported by Anand *et al* [40]. They have used fiber optic Raman spectrometer for in-situ measurement of percentage of methanol by volume in methanol-gasoline mixture.

Raman spectroscopy has become a preferred technique for online monitoring of dispersion polymerization. A low cost low resolution Raman spectrometer for online monitoring of miniemulsion polymerization of is reported by McCaffery *et al* [41]. The Raman spectra of polypyrrole and polyaniline are reported by Beleze *et al* [42]. They have used the Raman spectra for material

characterization. The structural analysis of poly (*o*-toluidine) using Raman spectra is reported by A.Buzarovska *et al* [43]. da Silva *et al* [44] have studied the redox behavior of crosslinked polyaniline films by *in-situ* Raman spectra. Raman spectra of pure p-terphenyl and tetracene p-terphenyl doped crystals have been examined for different guest concentrations above and below the phase transitions is reported by da Costa *et al* [45].

Raman spectroscopy is used in the vibrational structural analysis of CuInSe₂ thin films prepared by chemical spray pyrolysis is reported by Shirakata *et al* [46]. The Raman spectra of ordered vacancy compounds in the Cu-In-Se system is reported by Nomura *et al* [47]. Raman spectra of cobalt hydroxide [Co(OH)₂] at high pressure is reported by Shieh *et al* [48].

6.4 Experimental Setup

In the present experiment, we used the most common geometry of the perpendicular configuration for recording fluorescence and Raman spectra. In this configuration, the sample is excited with the laser beam and the emissions are collected using a monochromator – detector assembly at a 90° angle. The second harmonic emission of a nanosecond order pulsed Q-switched Nd:YAG laser (Spectra Physics, DCR 150) at 532 nm is used as the laser source. An output power of 500 mW is found suitable the LIF emission for many of the organic compounds for emission in the present region 550 nm - 700 nm that we have used. The Q-switched pulsed output from the Nd:YAG laser is allowed to fall on the liquid samples taken in a quartz cuvette. The samples used for the experiment are of high purity (Extra pure AR grade, 99.9 % from Sisco Research Laboratories, India). The quartz cuvette containing the liquid samples is kept in a sample compartment, which is free from ambient light. The sample compartment can be attached to the entrance slit of the monochromator – detector assembly. A cutoff filter at 532 nm is used to prevent the scattered laser beam from the sample cell. The emitted radiations are allowed to fall on a grating monochromator (TRIAX 320) through an entrance slit and the wavelength of emissions separated are allowed to fall on CCD (Spectrum One from ISA Jobin Yuon Spex Instruments Inc.) through an exit slit.

The Monochromator – CCD system is interfaced to a PC using GPIB DAQ from NI and the program used is Spectra Max for Windows version 3.0.

The block diagram and the photographs of the experimental arrangement are shown in fig 6.1

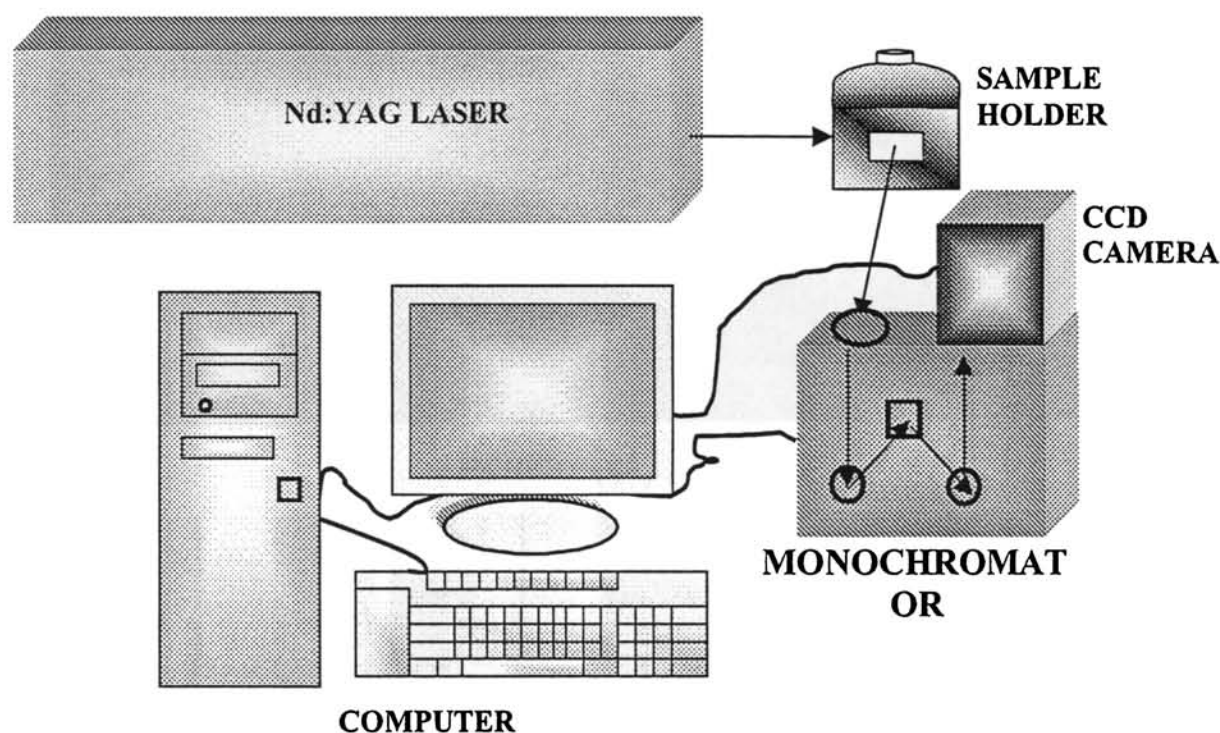
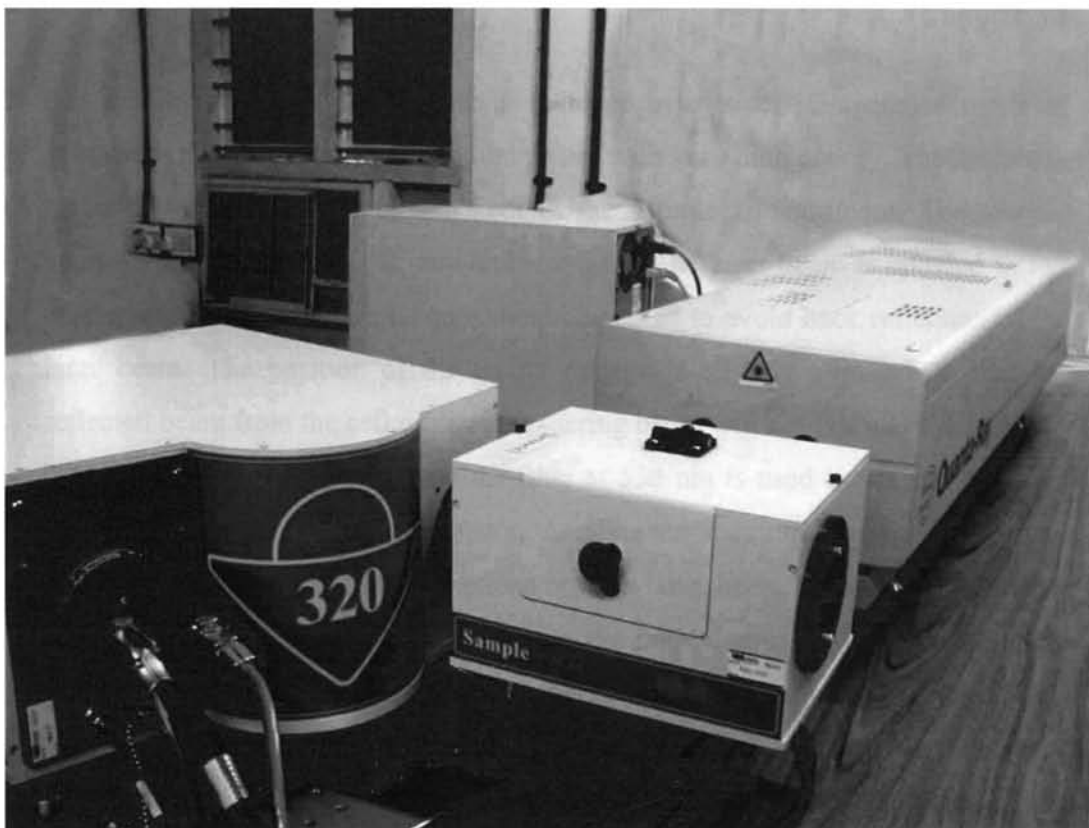


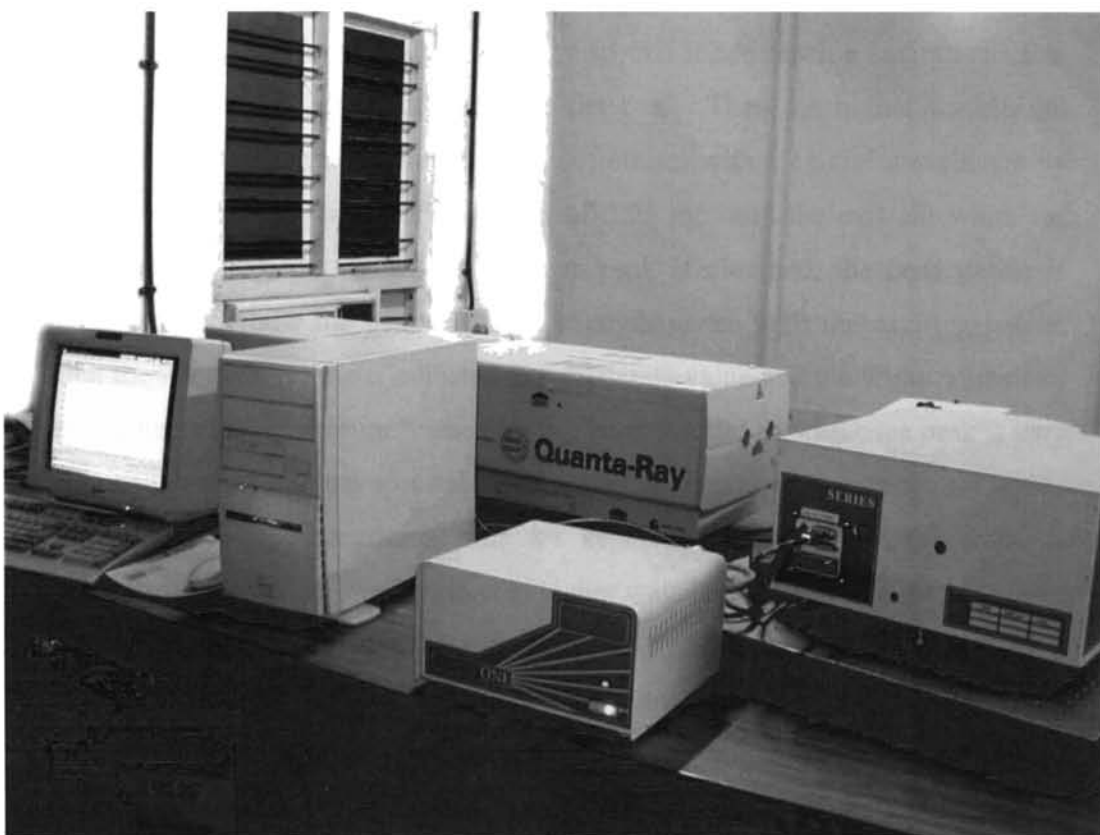
Fig.6.1. The block diagram of the experimental setup used for LIF and laser Raman studies

6.5 Experimental considerations

The LIF spectra are obtained by exciting the sample by second harmonic out of the Q-switched Nd: YAG laser at 532 nm and the emissions from the samples are recorded using the monochromator – detector assembly. There are several experimental factors to be taken care of before recording the spectra. First of all, the output of the laser is to be stable. For that as a first step the flash lamp alone is switched on and the lasing rod is pumped for 15–20 minutes for thermal stability and then the laser is allowed to lase in the microsecond pulse mode for another 15 minutes for the laser power to be stable. Then after making the flashing



(a)



(b)

Experimental setup for LIF & Laser Raman Spectral Studies

Chapter VI

rate a minimum energy, the laser is switched over to the Q-switched mode of operation in which we get nanosecond pulses with very high energy. The sample is taken in the quartz cuvette and kept in the sample compartment. The sample compartment is made free of any ambient light. The laser beam is allowed to fall on the sample cell and special care should be taken to avoid back reflection of the laser beam. The position of the quartz cuvette is slightly adjusted so that the reflected beam from the cell or direct scattering beam will not fall into the entrance slit of the monochromator. A cut off filter at 532 nm is used to prevent the laser beam falling into the monochromator. A reference spectrum can be recorded to check the presence of for any emissions or flash lamp lines. The calibration can be done by recording the laser line and from the known emission lines of the neon lamp or mercury lamp. Once the calibrations are done and the setup is aligned properly, it is ready to start the measurements.

The sample is excited using the laser beam. The power of the laser beam is kept at 450 mW and the emission spectra are recorded at a longer wavelength region than the excitation wavelength. The region including the excitation line is excluded because it is very high in energy so that it can reach a saturation value and the weak emission peaks cannot be detected. Then the higher wavelength region is scanned for a wavelength range of 60 nm with a central wavelength by keeping entrance slit width of the order of 0.05 mm and the exit slit width the minimum of 0.001mm. Once the emission peak is obtained, the laser power is varied to check how the peak emission strength varies with the exciting power. Then the integration time is adjusted to a moderate value and the width of the exit slit is adjusted to a minimum value possible such that the fluorescence peak is very prominent with maximum spectral resolution. The laser power, entrance slit width, exit slit width and integration time are kept constant then and the emission spectrum is recorded in other regions of higher wavelength also. The software used have all the options to set the central wavelength, number of accumulations, integration time, cosmic removal, integration time, entrance and exit slit width, data file name etc. The data file can be exported as Microsoft excel data and the spectra can be plotted using the software Microcal Origin 5.

The LIF spectra obtained for liquid phase carbon disulphide (CS_2) and aniline are given in figures 6.2 and 6.3

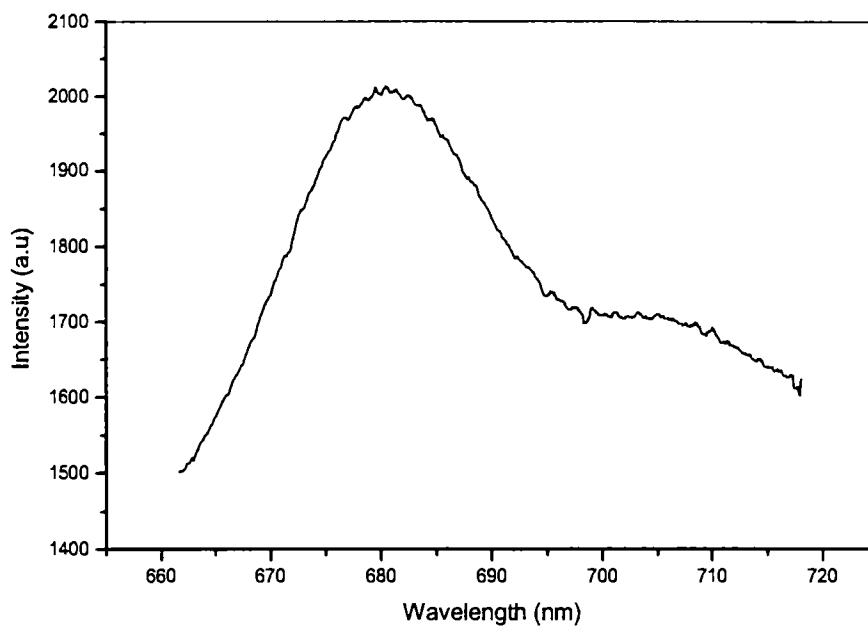


Fig.6.2. Laser induced fluorescence emission spectrum of carbon disulphide (CS_2) when excited by 532 nm

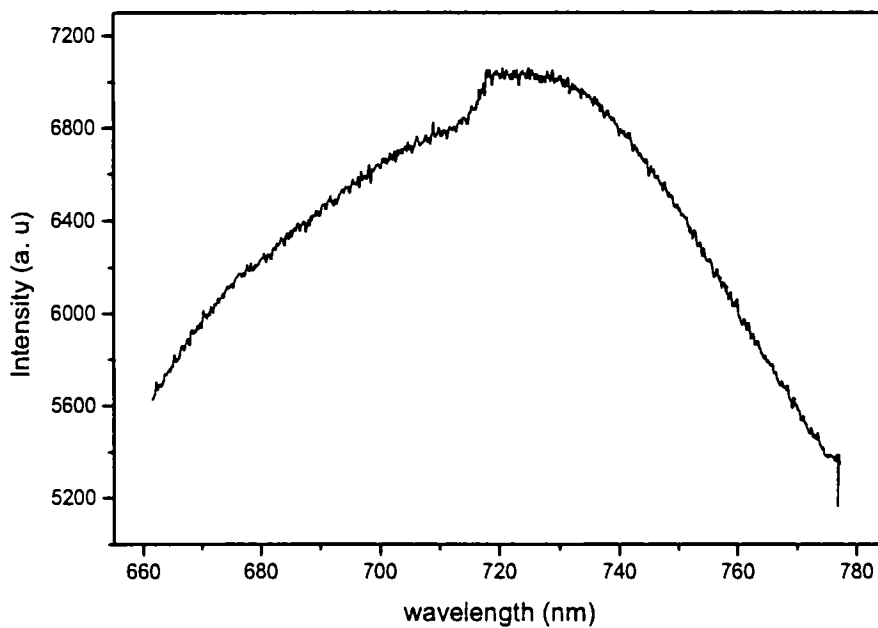


Fig.6.3. Laser induced fluorescence emission spectrum of aniline ($\text{C}_6\text{H}_7\text{N}$) when excited by 532 nm

The fluorescence emission in CS₂ centered at 680 nm. The emission is due to n, π^* transition in CS₂. The fluorescence emission in aniline is centered at 725 nm. The observed emission is due to π , π^* transition in aniline [11].

6.6 Pulsed laser Raman spectrum of aniline, *o*-chloroaniline and *m*-chlorotoluene

The laser Raman spectra of aniline, *o*-chloroaniline and *m*-chlorotoluene are recorded using the nanosecond pulsed Nd:YAG laser, monochromator and CCD system. The high purity sample in liquid phase is taken in a quartz cuvette and is kept in the sample compartment (named "samplemax" which is a compact, state-of-the-art, universal sample compartment). The perpendicular configuration is used for the experiment such that the laser beam falls normally on the sample and the monochromator and CCD is kept perpendicular to the beam direction. The Rayleigh scattered line is also recorded. The Stoke's lines of the spectra observed in higher wavelength region of the Rayleigh line. The data can be obtained in ASCII or Microsoft Excel (*.xls) format. The Raman shift from the Rayleigh line is plotted.

The pulsed laser Raman spectra of extra pure liquid phase aniline, *o*-chloroaniline and *m*-chlorotoluene are recorded using the same Nd:YAG laser, monochromator and CCD setup used for LIF studies. The experimental setup is calibrated at by recording the laser Raman spectra of CCl₄ and CS₂. The reported Raman peaks are obtained for both the compounds.

6.6.1 Pulsed laser Raman spectrum of Aniline

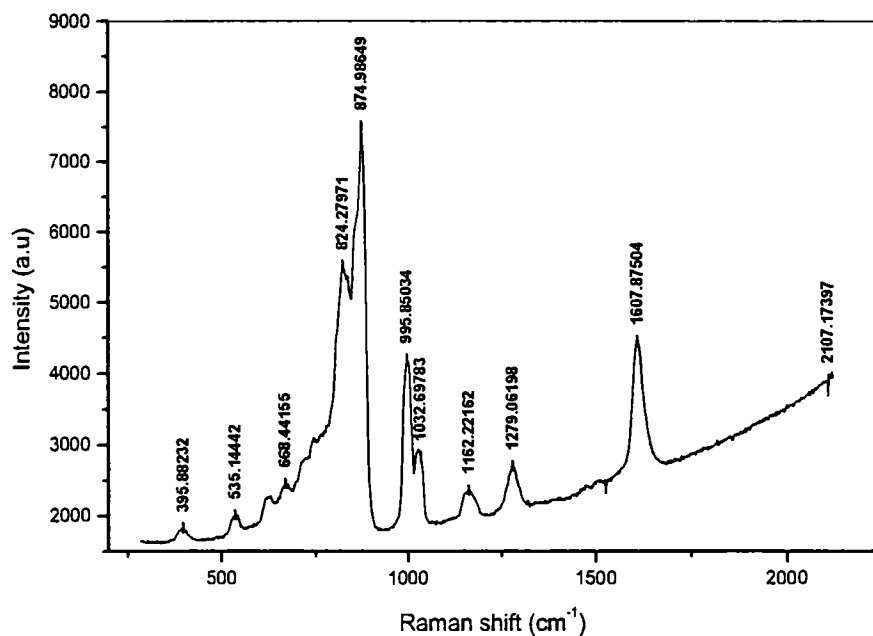


Fig.6.4. Pulsed laser Raman spectrum of aniline in the range 250 – 2600 cm⁻¹

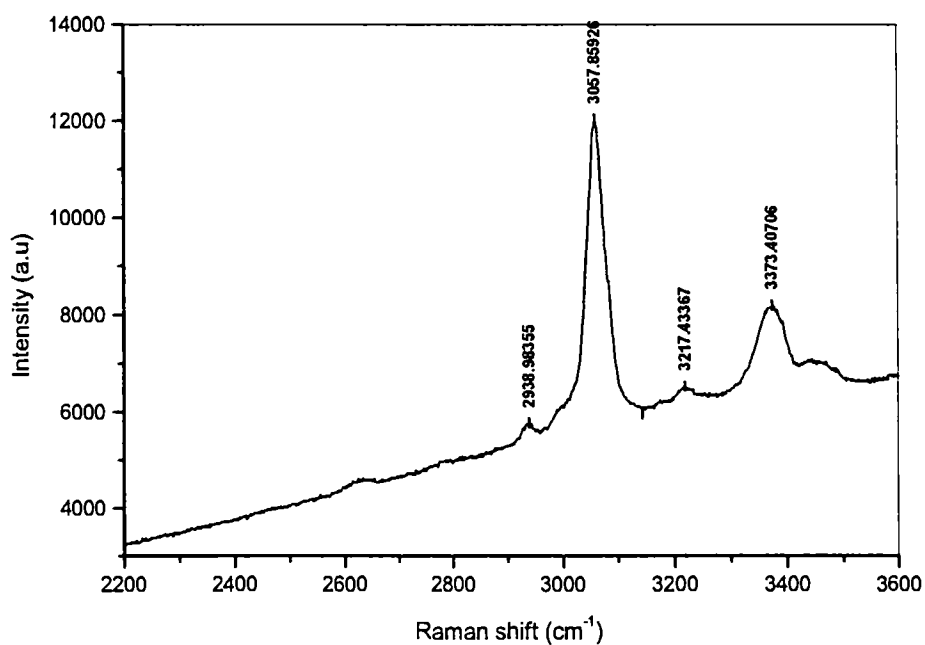


Fig.6.5. Pulsed laser Raman spectrum of aniline in the range 2200 – 3600 cm⁻¹

Observed Raman shifts for aniline and their assignments

Raman shift in cm^{-1}	Assignments
396	
535	C-C-C i.p bending
668	ring deformation mode
824	o.p δ CH
875	o.p δ CH
996	trigonal ring breathing
1033	i.p δ CH
1162	i.p δ CH
1279	i.p δ CH
1608	aromatic ring
2939	combination
3058	aromatic ν_{as} CH
3217	ν_{s} NH
3373	ν_{as} NH

In pulsed laser Raman spectrum of aniline, the NH stretch (3373 cm^{-1}) and aromatic CH stretch (3058 cm^{-1}) are observed. The aromatic ring characteristic peak appeared at 1608 cm^{-1} characteristic of phenyl ring and 996 cm^{-1} , which is the trigonal ring breathing as the strongest peak. Aromatic ring characteristic peaks with in plane CH bending frequencies are observed at 1033 , 1162 and 1279 cm^{-1} [12]. These include the characteristic peaks for substituted benzene. The CH out of plane bending is observed at 824 and 875 cm^{-1} and ring deformation is observed at 668 cm^{-1} and also. The peak at 535 cm^{-1} is the C-C-C in plane bending.

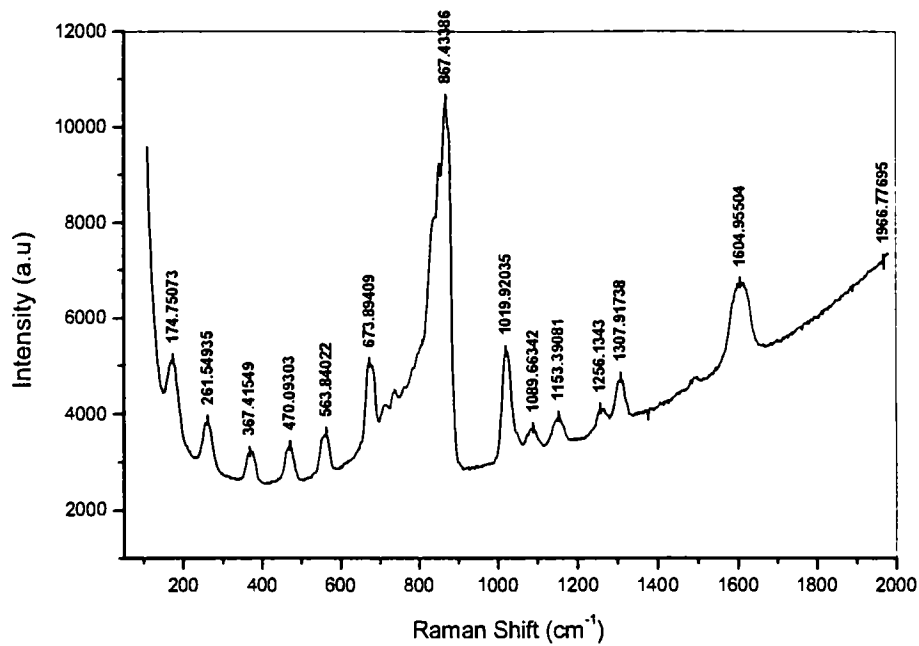
6.6.2 Pulsed laser Raman spectrum of *o*-chloroaniline

Fig.6.6. Pulsed laser Raman spectrum of *o*-chloroaniline in the range 100 – 2000 cm⁻¹

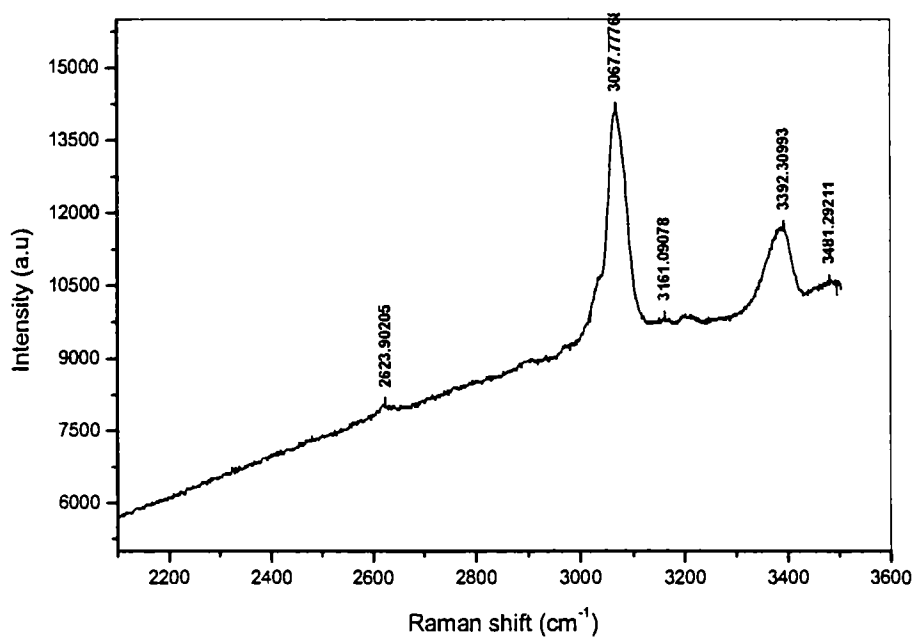


Fig 6.7. Pulsed laser Raman spectrum of *o*-chloroaniline in the range 2100 – 3600 cm⁻¹

Observed Raman shifts for *o*-chloroaniline and their assignments

Raman shift (cm ⁻¹)	Assignments
175	
262	C-C o.p bending
367	C-Cl i.p bending
470	C-C-C i.p bending
564	Characterisitic of <i>o</i> -substituted aromatic ring
674	C -Cl stretch
852	<i>o</i> .p δ CH
867	
1020	trigonal ring breathing
1090	<i>i</i> .p δ CH
1153	<i>i</i> .p δ CH
1256	<i>i</i> .p δ CH
1308	combination
1605	aromatic
2624	combination
3068	aromatic ν_{as} CH
3392	ν_{as} NH

In pulsed laser Raman spectrum of *o*-chloroaniline, the NH stretch (3392 cm⁻¹) and aromatic CH stretch (3068 cm⁻¹) are observed. The aromatic ring characteristic peak appeared at 1605 cm⁻¹ characteristic of phenyl ring and 1020 cm⁻¹ which is the trigonal ring breathing. Aromatic ring characteristic peaks with in plane CH bending frequencies are observed at 1090, 1153 and 1256 cm⁻¹ [12]. These include the characteristic substituted benzene peaks also. CH out of plane bending is observed at 852 cm⁻¹ and C-Cl stretch is observed at 678 cm⁻¹. The peak at 564 cm⁻¹ the characteristic of ortho substituted ring compounds and the peak at 470 cm⁻¹ is the C-C-C in plane bending. The C-Cl in plane bending is observed at 367 cm⁻¹

and C-C out of plane bending is at 262 cm^{-1} [35]. Hence the ring characteristic Raman peaks and peaks due to the substituents are also observed. The observed peaks are well assigned including the low lying vibrational modes.

6.6.3 Pulsed laser Raman spectrum of *m*-chlorotoluene

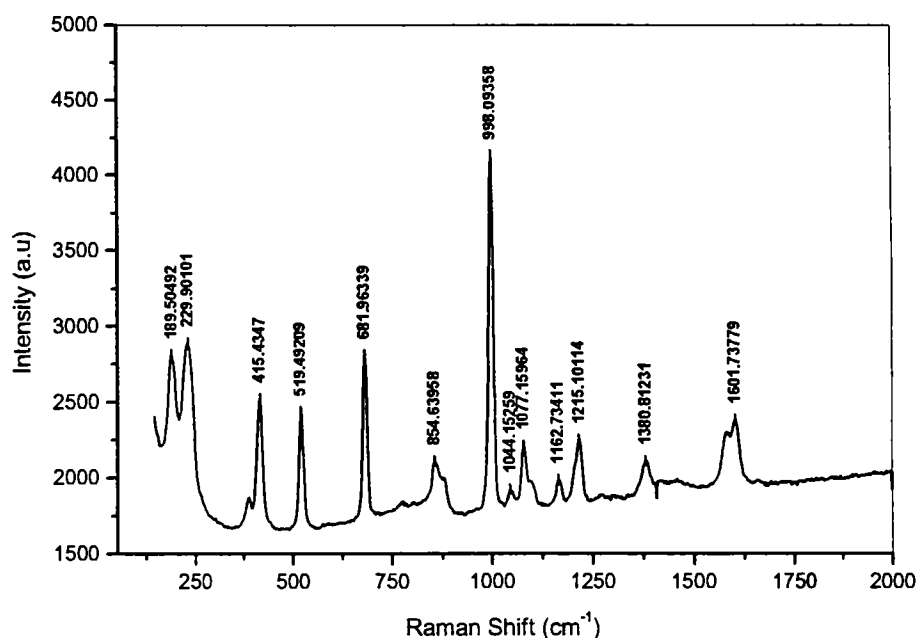


Fig.6.8. Pulsed laser Raman spectrum of *m*-chlorotoluene in the range $100 - 2000\text{ cm}^{-1}$

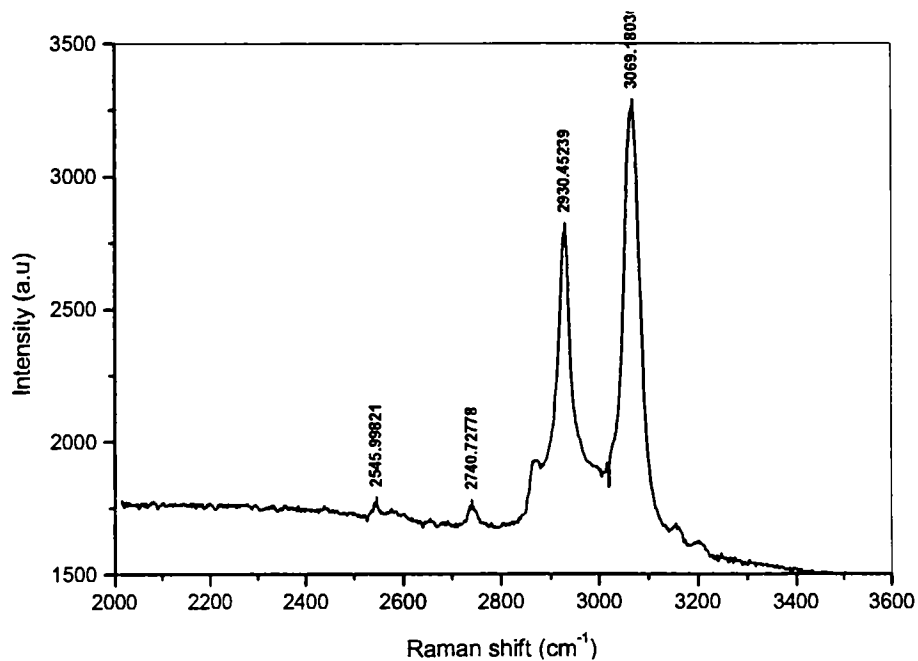


Fig.6.9. Pulsed laser Raman spectrum of *m*-chlorotoluene in the range $2000 - 3500\text{ cm}^{-1}$

Observed Raman shifts for *m*-chlorotoluene and their assignments

Raman shift (cm ⁻¹)	Assignments
189	CH ₃ - torsion
230	C-C o.p (out of plane) bending
415	i.p (in plane) bending
520	C-C-C i.p
682	ring deformation mode
855	o.p δ CH
998	trigonal ring breathing
1044	i.p δ CH, characteristic of <i>m</i> -substitution
1077	i.p δ CH, characteristic of <i>m</i> -substitution
1162	i.p δ CH
1215	i.p δ CH
1381	δ _s CH ₃
1602	aromatic ring
2546	combination
2741	ν _s CH ₃
2931	ν _{as} CH ₃
3069	aromatic ν CH

In *m*-chlorotoluene, the aromatic CH stretch (3069 cm⁻¹) and aliphatic CH stretch (2931 and 2741 cm⁻¹) are observed. The aromatic ring characteristic peak appeared at 1602 cm⁻¹ characteristic of phenyl ring and 998 cm⁻¹, which is the trigonal ring breathing as the strongest peak. Aromatic ring characteristic peaks with in plane CH bending frequencies are observed at 1044, 1077, 1162 and 1215 cm⁻¹ [12]. These include the characteristic *meta* substituted aromatic peaks also. Symmetric bending of methyl group occurred at 1381 cm⁻¹. Ring deformation is observed at 682 cm⁻¹ and out of plane CH bending observed at 855 cm⁻¹ also. The characteristic peak for *meta* substitution at 520 cm⁻¹ is also the C-C-C in plane

bending. The low lying vibrational modes at 190 cm^{-1} is assigned as the torsion of methyl group [35]. The peak at 230 cm^{-1} is C-C out of plane bending. The C-Cl in plane bending is observed at 415 cm^{-1} . Thus the characteristic Raman peaks for aromatic ring, substituted aromatic ring, methyl and chlorine substituents are observed and well assigned. The low-lying vibrational modes observed are also properly assigned.

6.7 Conclusions

The excitation of samples of carbon disulfide, aniline and some substituted anilines resulted in fluorescence emission and/or Raman spectra of these samples. The laser induced fluorescence spectra are assigned as the transitions n, π^* in CS_2 and π, π^* in aniline. The observed pulsed laser Raman spectra for aniline, *o*-chloroaniline and *m*-chlorotoluene are assigned to the vibrational frequencies of these molecules. Some of the new low-lying vibrational modes are also observed and are well assigned. The experiment demonstrates the advantages of pulsed laser-CCD system over conventional setups, for convenient recording and study of fluorescence and Raman spectra.

References

- [1] J.Amorim, G.Baravian and J.Jolly; *J. Phys. D: Appl. Phys.*, 33 (2000) R51.
- [2] C.S.Cooper and N.M.Laurendeau; *Meas. Sci. Technol.*, 11 (2000) 902.
- [3] A.Cessou, U.Meier and D.Stepowski; *Meas. Sci. Technol.*; 11 (2000) 887.
- [4] K.Muraoka and M.Maeda; *Plasma. Phys. Control. Fusion*; 35 (1993) 633.
- [5] T.G.Spiro; *Current Science*, 74 (1998) 304.
- [6] A.Jayaraman and S.K.Sharma; *Current Science.*, 47 (1998) 308.
- [7] W.Demtroder; “*Laser Spectroscopy: Basic concepts and instrumentation*”, Second edition, Springer, 1996.
- [8] B.B.Laud; “*Lasers and non-linear optics*”, second edition, New Age International (P) ltd., New Delhi. 2001.
- [9] M.Reeves, P.V.Farrell and M.P.Musculus; *Meas. Sci. Technol.*, 10 (1999) 285.
- [10] J.Bradshaw and D.D.Davis; *Opt. Lett.*, 7 (1982) 224.
- [11] B.K.Sharma; “*Spectroscopy*”, 11th edition, Goel Publishing House. India., 1995-96.
- [12] K.Nakanishi and P.H.Solomon; “*Infrared absorption spectroscopy*”, Second edition Holden-Day Inc., San Francisco, 1977.
- [13] G.Aruldas; “*Molecular Structure and Spectroscopy*”; Prentice-Hall (India) 2001.
- [14] M.Heintxe and G.H.Bauer; *J. Phys. D: Appl. Phys.*, 28 (1995) 2470.
- [15] M.Hertl and J.Jolly; *J. Phys. D: Appl. Phys.*, 33 (2000) 381.
- [16] P.Misra, X.Zhu and H.L.Bryant Jr.; *Pure Appl. Opt.*, 4 (1995) 587.
- [17] B.Kim, P.L.Hunter and H.S.Johnston; *J. Chem. Phys.*, 96 (1992) 4057.
- [18] S.Lee, K.Arita and O.Kajimoto; *Chem. Phys. Lett.* 265 (1997) 579.
- [19] M. Metsaalaa, M.Nela, S.Yang, O.Vattinen and L.Halonen; *Vib. Spectrosc.*, 29 (2002) 155.
- [20] P.Jungner and L.Halonen; *J. Chem. Phys.*, 107 (1997) 1680.
- [21] M.Saarinen, D.Permogorov and L.Halonen; *J. Chem. Phys.*, 110 (1999) 1424.
- [22] D.Hayashi, W.Hoeben, G.Dooms, E.van Veldhuizen, W.Rutgers and G.Kroesen; *Appl. Opt.*, 40 (2001) 986.
- [23] J.W.Pepper, A.O.Wright and J.E.Kenny; *Spectrochim. Acta. A.*, 58 (2002) 317.
- [24] J.E.Harrington and K.C.Smyth; *Chem. Phys. Lett.*, 202 (1993) 196.

- [25] R.J.H.Klein-Douwel, J.Laque, J.B.Jeffries, G.P.Smith and D.R.Crosley; *Appl. Opt.*, 39 (2000) 3712.
- [26] B.J.Kirby and R.K.Hanson; *Appl. Opt.*, 40 (2001) 6136.
- [27] B.J.Kirby and R.K.Hanson; *Appl. Phys. B.*, 69 (1999) 505.
- [28] T.Lee, D.Shin, J.B.Jeffries and R.K.Hanson; *AIAA* (American Institute of Aeronautics and Astronautics) 2002, 0399, p.1.
- [29] Z.Chen, D.L.Kaplan, K.Yang, J.Kumar, K.A.Marx and S.K.Tripathy; *Appl. Opt.*, 36 (1997) 1655.
- [30] E.G.Brame Jr. and J.G.Grasselli; "*Infrared and Raman Spectroscopy*", Part B; Marcel Dekker Inc., New York, 1977.
- [31] M.Ito; *Current Science.*, 74 (1998) 300.
- [32] S.Kanakaraju, A.K.Sood and S.Mohan; *Current science.*, 74 (1998) 322.
- [33] N.Biswas and S.Umapathy; *Current Science.*, 74 (1998) 328.
- [34] I.L.Town, M.Becucci, G.Pietraperzia, E.Castellucci and J.C.Oero; *J. Mol. Struct.*, 565-566 (2001) 421.
- [35] K.P.R.Nair and S.M.Eappen; *Indian J. Pure. Appl. Phys.*, 39 (2001) 750.
- [36] T.M.Kolev and B.A.Stamboliyska; *Spectrochim. Acta. A.*, 56 (1999) 119.
- [37] J.P.Pinan, R.Quillon, P.Ramson, M.Becucci and S.Califano; *J. Chem. Phys.*, 109 (1998) 5469.
- [38] M.Becucci, E.Castellucci, L.Fusina, G.DiLorenzo and H.W.Schrotter; *J. Raman. Spectrosc.*, 29 (1998) 237.
- [39] H.G.M.Edwards, F.G.Pichel, E.M.Newton and D.D.W.Williams; *Spectrochim. Acta. A.*, 56 (1999) 193.
- [40] K.Anand, V.Asundi and R.Vasudeva; *Paper presented in SAE 2000 World Congress*, Detroit, Michigan, 2000 – 01 – 1336.
- [41] J.R.McCaffery and Y.G.Durant; *J. Appl. Polym. Sci.*, 86 (2002) 1507.
- [42] F.A.Beleze and A.J.G.Zarbin; *J. Braz. Chem. Soc.*, 12 (2001) 542.
- [43] A.Buzarovska, I.Arsova and L.Arsov; *J. Serb. Chem. Soc.*, 66 (2001) 27.
- [44] J.E.P.da Silva, S.I.C.de Torresi and M.L.A.Temperini; *J. Braz. Chem. Soc.*, 11 (2000) 91.
- [45] A.M.A.da Costa, N.Karger, A.M.Amado and M.Becucci; *Solid State Ionics.*, 97 (1997) 115.

Chapter VI

- [46] S.Shirakata, H.Kubo, C.Hamaguchi and S.Isomura; *Jpn. J. Appl. Phys.*, 36 (1997) L1394.
- [47] S.Nomura, S.Ouchi and S.Endo; *Jpn. J. Appl. Phys.*, 36 (1997) L1075.
- [48] S.R.Shieh and T.S.Duffy; *Physical Review B.*, 66 (2002) 134301.

SUMMARY AND CONCLUSIONS

The present work is mainly concentrated on setting up a NIR tunable diode laser absorption (TDLA) spectrometer for high resolution molecular spectroscopic studies. For successfully recording the high resolution tunable diode laser spectrum, various experimental considerations are to be taken into account like the setup should be free from mechanical vibrations, sample should be kept at a low pressure, laser should be in single mode operation etc. The present experimental setup considers all these factors. The TDLA spectrometer uses a commercial near infrared (NIR) tunable diode laser as the laser source, a multipass cell for increasing the pathlength by multiple reflections and hence the absorption of the molecular species is used as sample cell, a vacuum system for the evacuation of the multipass cell to avoid the interference from other species and to operate at low pressure to reduce the pressure broadening of the spectrum. A commercial near infrared photodetector assembly, which can provide balanced detection and autobalanced logoutput is used as the light detector. The experimental components are set on a vibration isolation table to reduce the interference from mechanical vibrations. The TDLA spectrometer is set successfully and its computer interfacing is also done. The high resolution TDLA spectrometer is interfaced to a computer using labVIEW software and necessary hardwares for the computer control, operation, data acquisition and analysis. The experimental setup is calibrated by recording the water vapor lines and the HITRAN database for water vapor. The high resolution OH overtone spectrum of methanol recorded using this setup agrees well with the results already reported. Hence the present TDLA spectrometer is well calibrated and can be used for recording the high resolution spectra of other molecules containing OH group. The high resolution spectrum of –OH group second overtone in ethanol is recorded using the present setup and this gives the well resolved spectral lines corresponding to the two different molecular conformers (*trans* and *gauche*) of ethanol including the P, Q, R branches of the *trans* conformer.

It is to be mentioned here that the setting up of a high resolution NIR TDLA spectrometer is a novel experiment requiring much effort and patience.

Only very few laboratories in India are involved in this emerging area of spectroscopic work. We hope that the present setup would initiate detailed high resolution studies in our laboratory.

The analysis of near infrared (NIR) vibrational overtone spectra of some substituted benzene compounds using local mode model forms another part of the present work. The NIR vibrational overtone spectra of some substituted benzenes from the first through fourth overtones are recorded by conventional spectrophotometric method using a commercial UV-Vis-NIR spectrometer, which uses a tungsten lamp as the light source. The observed NIR spectra of aniline, *ortho*, *meta* and *para* isomers of chloroaniline; *ortho*, *meta* and *para* isomers of toluidine; N-methylaniline, N,N-dimethylaniline and N,N-diethylaniline are analyzed using local mode model. The comparison of the local mode parameters of aniline and *ortho*, *meta* and *para* isomers of chloroaniline shows that intramolecular hydrogen bonding between chlorine and NH₂ group exists in *ortho*-chloroaniline. The ring CH mechanical frequency for *ortho*-chloroaniline is less than (~12 cm⁻¹) that in *meta*-chloroaniline and that of *para*-chloroaniline (~16 cm⁻¹). The NH mechanical frequency in *ortho*-chloroaniline is close to that of aniline while the NH mechanical frequency in *meta*-chloroaniline is higher than (~24 cm⁻¹) that in aniline. This reduction in ring CH mechanical frequency and NH mechanical frequency values is due to the presence of intra-molecular hydrogen bonding in *ortho*-chloroaniline. This is the first report establishing the presence of intramolecular hydrogen bonding in *ortho*-chloroaniline using vibrational overtone spectroscopy. Similarly, the analysis of the overtone spectra of *ortho*, *meta* and *para* isomers of toluidine shows evidence for existence of steric and electronic effects between the amino group and methyl group in the *ortho*-toluidine. The ring CH mechanical frequency in *ortho*-toluidine is higher (~21 cm⁻¹) than that of aniline while the ring CH mechanical frequency in *meta* and *para*-toluidine are close to that of aniline. The NH mechanical frequency for *ortho*-toluidine is close to that of aniline while the same shows an increased value in *meta* and *para*-toluidine. The increased value of ring CH mechanical frequency in *ortho*-toluidine and its almost equal value of NH mechanical frequency to that of aniline are due to the presence of steric and electronic effects existing between the amino and methyl groups in *ortho*-toluidine. The observed higher value for methyl

CH mechanical frequency in *ortho*-toluidine than that for *meta* or *para*-toluidines is also due to the existence of steric and electronic effects in *ortho*-toluidine. Our work shows the first vibrational overtone spectroscopic evidence for the presence of the steric and electronic effects in *ortho*-toluidine. The analysis of the overtone spectra of N-methylaniline, N,N-dimethylaniline and N,N-diethylaniline using the local mode model and the comparison of the mechanical frequency and anharmonicity values of these molecules supports the orientation of the lone pair of electrons in nitrogen atom in these molecules. The ring CH mechanical frequency in N-methylaniline is close to that of aniline while the same in N,N-dimethylaniline and N,N-diethylaniline shows an increase ($\sim 20 \text{ cm}^{-1}$) than aniline. This can be due to the reduced interaction between the lone pair of electrons in nitrogen atom to the ring due to the perpendicular orientation of the lone pair of electrons with respect to the methyl/ethyl groups in these compounds. The effects of the orientation of the lone pair of electrons are well reflected in the mechanical frequency values of these molecules.

An attempt is made to record the pulsed laser induced fluorescence/Raman spectra of some of organic compounds. A Q-switched Nd:YAG laser is used as the excitation source. A TRIAX monochromator and CCD detector is used for the spectral recording. The observed fluorescence emission for carbon disulphide is centered at 680 nm; this is assigned as due to the n, π^* transition. Aniline also shows a broad fluorescence emission centered at 725 nm, which is due to the π, π^* transition. The pulsed laser Raman spectra of some organic compounds are also recorded using the same experimental setup. The calibration of the setup is done using the laser Raman spectra of carbon tetrachloride and carbon disulphide. The observed laser Raman spectra for aniline, *o*-chloroaniline and *m*-chlorotoluene show peaks characteristics of the aromatic ring in common and the characteristics peaks due to the substituent groups. Some new peaks corresponding to low-lying vibrations of these molecules are also assigned.

578880